

Hybrid Molecular Dynamics–Finite Element Simulations of Polystyrene–Silica Nanocomposites

Dissertation

Shengyuan Liu

Darmstadt, 2017 – D 17



TECHNISCHE
UNIVERSITÄT
DARMSTADT



Hybrid Molecular Dynamics–Finite Element Simulations of Polystyrene–Silica Nanocomposites

**Vom Fachbereich Chemie
der Technischen Universität Darmstadt**

zur Erlangung des akademischen Grades eines
Doktor rerum naturalium (Dr. rer. nat.)

genehmigte
Dissertation

vorgelegt von

Shengyuan Liu, M.Eng. of Materials Chemical Engineering
aus Hengyang, V.R. China

Referent:	Prof. Dr. Florian Müller-Plathe
Korreferent:	Prof. Dr. Michael C. Böhm
Tag der Einreichung:	15.12.2016
Tag der mündlichen Prüfung:	30.01.2017

Darmstadt 2017

D 17

DEDICATION

To everyone who supports me,
and to my almae matres where I was ever educated.




TECHNISCHE
UNIVERSITÄT
DARMSTADT



河北理工大学
Hebei Polytechnic University

Shengyuan Liu

Shengyuan Liu



The present Ph.D. work is completed under the supervision of Prof. Florian Müller-Plathe and Prof. Michael C. Böhm. Chapters 2, 3 and 4 of the thesis are based on the following three publications. Specifically, the analytical tool of the uncertainty quantification method (Section 2.4) was developed by the research group of Prof. Jens Lang (Department of Mathematics, Technical University Darmstadt). The Finite Element code of the applied hybrid simulation method was developed by the research group of Prof. Paul Steinmann (Chair of Applied Mechanics, University of Erlangen-Nuremberg).

[1] S.Y. Liu, A. Gerisch, M. Rahimi, J. Lang, M.C. Böhm, F. Müller-Plathe, J. Chem. Phys., 142 (2015) 104105.

[2] S.Y. Liu, M.C. Böhm, F. Müller-Plathe, Mater. Res. Express, 3 (2016) 105301.

[3] S.Y. Liu, S. Pfaller, M. Rahimi, G. Possart, P. Steinmann, M.C. Böhm, F. Müller-Plathe, Comput. Mater. Sci., 129 (2017) 1.

Additionally, S.Y. Liu has also contributed to other two publications during the Ph.D. study.

[4] F. Leroy, S.Y. Liu, J.G. Zhang, J Phys. Chem. Part C, 119 (2015) 28470.

[5] D. Davydov, E. Voyiatzis, G. Chatzigeorgiou, S.Y. Liu, P. Steinmann, M.C. Böhm, F. Müller-Plathe, Soft Materials, 12.sup1 (2014) S142-S151.

Summary

Polymer nanocomposites are manufactured by blending a fraction of nanoparticles into a polymer matrix. A high surface-to-volume ratio of the added nanoparticles leads to a large interphase area in polymer nanocomposites. Structural and dynamic properties of polymer chains in the interphase differ from the bulk behavior because of the polymer-nanoparticle interaction. As a matter of fact, the interphase dimension has a significant influence on the mechanical properties of polymer nanocomposites. The mechanical behavior of polymer nanocomposites during a deformation process is fundamentally associated to changes of the structural characteristics of the polymer chains. Investigations of interphase properties and the mechanical deformation behavior of polymer nanocomposites are helpful to design better materials for industrial applications. Nevertheless, from experimental investigations it is often difficult to understand correlations between microscopic polymer properties and the macroscopic mechanical behavior of nanocomposites, as changes of structural polymer properties during deformation take place at a molecular scale.

Computer simulations have intrinsic advantages to analyze scientific problems of polymer nanocomposites from a microscopic perspective. In collaboration with the group of Prof. Paul Steinmann, our group has developed recently a hybrid molecular dynamics-finite element (MD-FE) method to simulate mechanical deformations of neat polystyrene and polystyrene nanocomposites containing bare silica nanoparticles. In the adopted hybrid framework, an inner particle region that captures microscopic quantities of interest is coupled to a surrounding elastic continuum region that allows the application of external loads to deform the studied materials. A dissipative particle dynamics (DPD) shell separates the inner particle domain from the continuum domain. The convergence properties of the hybrid simulation method have been investigated by recent project contributors (Mohammad Rahimi and Sebastian Pfaller) in simulations of a model polystyrene system. The main aim of the present Ph.D. work is the application of our hybrid MD-FE method to investigate interfacial structures and the mechanical deformation behavior of polymer nanocomposites blended with silica nanoparticles.


The present Ph.D. thesis starts with a background introduction to different hybrid simulation methods and with a description of interphase properties as well as with a description of the mechanical deformation of polymer nanocomposites. Specifically, the introduction is mainly divided into the following sections: (i) review on coupling strategies of computer simulation methods at different time and length scales; (ii) description of the used hybrid MD-FE framework and its applications in the fields of hydromechanics and structural mechanics; (iii) uncertainty quantification (UQ) investigations of input parameters of the hybrid simulation model; (iv) analysis of the interfacial structure and mechanical deformation behavior of polymer nanocomposites.

In the hybrid model, a large number of anchor points (e.g. several thousand) have to be introduced into the so-called handshaking domain to achieve an exchange of simulation information (i.e. forces and displacements) between the MD and FE region. Input parameters related to the anchor points mainly include the force constant between the anchor points and the polymer beads, the distribution and number of the anchor points as well as the thickness of the handshaking domain. Prior to further applications of the hybrid method to polymer nanocomposites, a reasonable combination of the input parameters of the hybrid model has to be determined. For this purpose, in the second chapter of the thesis, the UQ method is used to analyze quantitatively the influence of these input parameters on the robustness of the hybrid method. The UQ analyses have turned out that the hybrid model without the FE domain is robust when the thickness of the surrounding DPD domain and the inner core of the MD domain are both large enough. The MD simulations in the hybrid scheme with the input parameters set in the safe range can reproduce accurately the results of the reference MD calculations for the same system using traditional periodic boundary conditions.

The influence of the interphase area between the polymer matrix and the nanoparticles on global and local properties of polymer chains in nanocomposites has not been investigated quantitatively up to now. In the third chapter, coarse-grained MD simulations have been performed to investigate structural and dynamic properties of polymer chains in polystyrene nanocomposites containing a fraction of silica nanoparticles of different geometrical shapes (i.e. sphere, cube and regular tetrahedron). The structural properties of polymer chains are described

in terms of the chain dimension (i.e. end-to-end distance and radius of gyration) and the chain orientation as a function of the distance from the nanoparticle center of mass. Additionally, the dynamic properties of polymer chains are monitored by the center of mass diffusion of the chains, the decorrelation of chain end-to-end vectors and the escape behavior of polymer chains from the interphase. In addition, possible correlations between the interphase area and mechanical properties of polymer nanocomposites have been investigated, too. The observed results have demonstrated that as an universal factor, the interphase area of nanocomposites influences almost linearly the global chain geometry, chain dynamics as well as the overall elastic properties. Nevertheless, the local chain geometry and dynamics in the interphase region which refers approximately to one chain radius of gyration differ from their global behavior.

In the fourth chapter, both standard MD and hybrid MD-FE simulations are applied to investigate the deformation behavior of polystyrene nanocomposites containing silica nanoparticles as a function of the silica mass fraction, particle size and grafting density. In the hybrid framework, the outer continuum domain solved by the FE method allows external load steps to deform the inner particle domain in which MD simulations are performed to capture structural polymer properties. Material properties of polymer nanocomposites such as the Young's modulus and Poisson's ratio are identified from standard MD simulations. They are then used as material parameters in the hybrid MD-FE simulations. Interfacial properties of polymer nanocomposites are analyzed in terms of the structure and dynamics of the polymer chains. The deformation of individual polymer chains upon elongation is also investigated by a simple geometrical transformation model which assumes that all atoms in the material translate affinely with the deformation of the entire sample. Our simulations have demonstrated that the fraction of high-modulus fillers and their total interfacial area contribute to a general stiffening of the polymer nanocomposites. Smaller nanoparticles have a stronger influence on nanocomposite properties compared with larger ones. The addition of nanoparticles restricts the polymer mobility, so that the polymer conformations deviate more from affine translations than in neat polystyrene.



Last but not least, the main conclusions obtained by the present Ph.D. work as well as an outlook to applications of the hybrid MD-FE method in polymer nanocomposites are summarized in the fifth chapter.

Zusammenfassung

Polymer-Nanokomposite werden durch das Mischen einer bestimmten Menge an Nanoteichen und einer Polymermatrix hergestellt. Durch ein großes Verhältnis zwischen der Nanoteichen-Oberfläche und dem System-Volumen führt die Zugabe von Nanoteichen zu einer großen Interphase in Nanokompositen. Die strukturellen und dynamischen Eigenschaften der Polymermatrix in der Interphase unterscheiden sich aufgrund der Wechselwirkungen zwischen dem Polymer und den Nanoteilchen stark vom Polymerverhalten im Bulk. Die Größe der Interphase zwischen Polymermatrix und Nanoteilchen hat einen starken Einfluss auf die mechanischen Eigenschaften von Polymer-Nanokompositen. Das mechanische Verhalten dieser Systeme wird deutlich von strukturellen Änderungen der Polymerketten während einer Dehnung beeinflusst. Deshalb sind Untersuchungen der Interphase und des mechanischen Verhaltens bei Dehnungen von Polymer-Nanokompositen für die Herstellung von Verbindungen mit verbesserten Eigenschaften für industrielle Anwendungen nützlich. Allein auf Basis experimenteller Untersuchungen ist es schwierig, funktionelle Zusammenhänge zwischen mikroskopischen Polymereigenschaften und dem makroskopischen mechanischen Verhalten dieser Systeme zu verstehen, da sich strukturelle Änderungen des Polymeres während einer Dehnung in einer molekularen Skala abspielen.

Computersimulationen haben nun den großen Vorteil, dass sie eine Analyse von Polymer-Nanokompositen aus einer mikroskopischen Perspektive zulassen. Durch eine Zusammenarbeit mit der Gruppe von Prof. Paul Steinmann gelang uns die Entwicklung einer Molekulardynamik-Finite Element (MD-FE) Hybrid-Methode, um Dehnungen von Polystyrol oder Polystyrol-Nanokompositen angereichert mit Silica-Nanoteilchen zu simulieren. In dieser Hybrid-Methode wird ein inneres Teilchenggebiet, in dem die interessierenden Eigenschaften berechnet werden, an ein umgebendes Kontinuum gekoppelt, das im Rahmen einer elastischen Näherung beschrieben wird. Mit diesem Ansatz werden dann externe Störungen der Systeme durchgeführt und die Materialeigenschaften berechnet. Ein Bereich, in dem die Bewegung der Teilchen im Rahmen einer dissipativen Dynamik (DPD) beschrieben wird, trennt die innere Teilchen-Region vom umgebenden Kontinuum. Das Konvergenz-Verhalten der entwickelten Hybrid-Methode wurde in Arbeiten ehemaliger Mitarbeiter (Mohammad Rahimi und Sebastian Pfaller) in Simulationen


von einem Polystyrol-Modellsystem untersucht. Ziel der vorliegenden Doktorarbeit ist die Anwendung dieser MD-FE-Hybrid-Methode, um Grenzflächen-Strukturen sowie die mechanischen Eigenschaften von Polymer-Nanokompositen mit Silika-Teilchen bei einer Deformation zu untersuchen.

Die vorliegende Arbeit gibt zunächst einen Überblick über Hybrid-Simulationen, über die Eigenschaften der Interphase und über das Deformations-Verhalten von Polymer-Nanokompositen. Diese Einleitung ist in folgende Abschnitte aufgeteilt: (i) Beschreibung von Kopplungs-Strategien bei Simulationsmethoden in verschiedenen Zeit- und Längenskalen. (ii) Anwendung des MD-FE Verfahrens in der Hydromechanik sowie der strukturellen Mechanik. (iii) Parameter-Analyse des MD-FE Modells durch die Quantifizierung von Unsicherheiten (i.e. Uncertainty Quantification, UQ). (iv) Studium von Grenzflächen-Strukturen und dem Verhalten von Polymer-Nanokompositen bei einer mechanischen Deformation.

Unser Hybrid-Modell erfordert die Einführung einer bestimmten Anzahl von Ankerpunkten im MD-FE-Kopplungsbereich zum Austausch von Informationen (i.e. Kräften und Auslenkungen) zwischen den getrennten MD und FE Gebieten während einer Simulation. Eingabe-Parameter, die den Ankerpunkten zugeordnet sind, umfassen die Kraftkonstanten zwischen den Ankerpunkten und Polymer-Teilchen, die Verteilung und Anzahl der Ankerpunkte sowie die Dicke des MD-FE-Kopplungsgebietes. Vor weiteren Anwendungen der Hybrid-Methode auf Polymer-Nanokomposite ist es notwendig, sinnvolle Kombinationen der erwähnten Eingabe-Parameter zu bestimmen. Zu diesem Zweck wird im zweiten Kapitel dieser Doktorarbeit die UQ-Methode beschrieben, um quantitativ den Einfluss von Eingabe-Parametern auf die Qualität der Hybrid-Ergebnisse zu untersuchen. UQ Analysen haben gezeigt, dass unser Hybrid-Modell unter Nichtberücksichtigung des FE Gebietes stabil ist, wenn die Dicke der umgebenden DPD Region und des inneren MD Bereichs groß genug ist. Rechnungen mit dem MD Baustein unseres Hybrid-Verfahrens liefern Ergebnisse, die denen entsprechen, die mit konventionellen MD Simulationen unter periodischen Randbedingungen erhalten werden, wenn Eingabe-Parameter in einem „sicheren Bereich“ verwendet werden.

Der Einfluss der Interphase, i.e. der Grenzfläche zwischen den Nanoteilchen und der Polymermatrix, auf globale und lokale Eigenschaften von Nanokompositen wurde bisher nicht quantitativ untersucht. Im dritten Kapitel werden vergrößerte, i.e. coarse grained (CG), Simulationen beschrieben, in denen strukturelle und dynamische Eigenschaften von Polymerketten in Polymer-Nanokompositen mit Silica-Nanoteilchen verschiedener Geometrien (z.B. Kugeln, Würfel, Tetraeder) untersucht werden. Strukturelle Charakteristiken der Polymerketten werden sowohl durch Längenparameter (Kettenenden-Vektor, Gyrationradius) als auch durch einen Orientierungsparameter als Funktion des Abstands zwischen der Oberfläche eines Nanoteilchen und dem Polymer-Massenschwerpunkt beschrieben. Das dynamische Verhalten der Polymerketten wird auf Basis des Diffusionskoeffizienten des Massenschwerpunkts von Polymerketten, der Dekorrelation des Kettenenden-Vektors und der Zeit für das Verlassen der Interphase beschrieben. Zusätzlich werden mögliche Abhängigkeiten zwischen der Größe der Interphase und den mechanischen Eigenschaften von Polymer-Nanokompositen untersucht. Die erhaltenen Resultate haben gezeigt, daß die Größe der Interphase in Nanokompositen als universeller Parameter betrachtet werden kann, der linear die globale Geometrie der Ketten, ihre Dynamik und ihre elastischen Eigenschaften bestimmt. Die lokale Geometrie der Ketten in der Interphase sowie ihre Dynamik in diesem Bereich unterscheidet sich jedoch von dem globalen Verhalten. Die Ausdehnung der Interphase entspricht in etwa dem Polymer-Gyrationradius.

Im vierten Kapitel werden sowohl reine MD-Rechnungen als auch MD-FE Hybrid-Simulationen beschrieben, die sich mit dem Deformationsverhalten von Polystyrol-Nanokompositen mit Silica-Nanoteilchen als Funktion der Silica-Konzentration, der Größe der Nanoteilchen und der Oberflächen-Beladung beschäftigen. Der Finite-Element-Bereich in der Hybrid-Methode erlaubt eine einfache Beschreibung externer Deformationen, die zu einer Änderung der Polymerstruktur im inneren Kern der Simulationszelle führen. Material-Parameter der Nanokomposite wie das Elastizitätsmodul oder die Poisson-Zahl werden auf Basis von Standard-MD-Simulationen berechnet und dienen dann als Eingabeparameter in den Hybrid-Simulationen. Die Grenzflächeneigenschaften der Polymer-Nanokomposite werden auf Basis struktureller und dynamischer Eigenschaften der Polymerketten analysiert. Die Deformation einzelner Polymerketten während einer Dehnung wird auch durch ein einfaches geometrisches Modell untersucht. Dieses Verfahren nimmt an, dass die Translation der Teilchen affin mit der Deformation der



gesamten Probe verläuft. Unsere Simulationen haben gezeigt, daß die Füllmaterialien mit ihrem hohen Elastizitätsmodul und ihrem Grenzflächen zu einer Versteifung von Polymer-Nanokompositen führen. Kleinere Nanoteichen haben einen stärkeren Einfluss auf die Eigenschaften von Nanomaterialien als große Teichen. Die Zugabe von Nanoteichen limitiert die Mobilität der Polymer-Ketten. Dadurch lassen sich Polymer-Konformationen schlechter auf Basis einer affinen Translation als in reinem Polystyrol.

Schließlich werden die wichtigsten Schlussfolgerungen der vorliegenden Doktorarbeit sowie ein Ausblick auf Anwendungen von Hybrid-Simulationen an Polymer-Nanokompositen in Kapitel fünf präsentiert.

Table of Contents

Summary	1
Zusammenfassung.....	5
Table of Contents.....	9
1. Introduction.....	11
1.1 Hybrid molecular dynamics–finite element methods	11
1.1.1 Basic principles of hybrid molecular dynamics–finite element methods.....	11
1.1.2 Different applications of hybrid molecular dynamics–finite element methods	13
1.1.3 Coupling strategies of hybrid molecular dynamics–finite element methods	14
1.1.4 Further analysis of the used hybrid molecular dynamics–finite element method.....	16
1.2 Interfacial structure and mechanical deformation of polymer nanocomposites	18
1.2.1 Microscopic properties of polymer chains in the interphase of nanocomposites.....	18
1.2.2 Mechanical deformation of polymer nanocomposites under external loads.....	19
1.2.3 Computer simulations of the deformation behavior of polymer nanocomposites	20
1.3 Description of the tasks set in the present dissertation	21
References.....	23
2. Robustness of Hybrid Molecular Dynamics–Finite Element Method for Amorphous Polystyrene Analyzed by Uncertainty Quantification	30
2.1 Abstract.....	30
2.2 Introduction.....	31
2.3 Simulation methods and computational details.....	34
2.4 Uncertainty quantification analysis methodology.....	38
2.5 Results and discussions.....	43
2.5.1 Force constant for the interaction between anchor points and polymer beads.....	43
2.5.2 Anchor point distribution in the dissipative-particle-dynamics domain	49
2.5.3 Size of dissipative-particle-dynamics domain	52
2.5.4 Comparison with molecular dynamics simulation under periodic boundary condition.....	52
2.6 Summary and conclusions	56
References.....	57
3. Role of Interfacial Area for Structure and Dynamics in Polymer Nanocomposites: Molecular Dynamics Simulations of Polystyrene with Silica Nanoparticles of Different Geometries.....	59
3.1 Abstract.....	60
3.2 Introduction.....	61

3.3 Simulation systems and computational details	65
3.3.1 Polystyrene blended with silica nanoparticles of different geometrical shapes	65
3.3.2 Computational details of molecular dynamics simulations.....	67
3.4 Results and discussion	69
3.4.1 Structural properties of polymer chains in nanocomposites	69
3.4.2 Dynamic properties of polymer chains and nanoparticles	74
3.4.3 Relation between mechanical properties of nanocomposites and the interphase area	84
3.5 Summary and conclusions	86
References.....	89
4. Uniaxial Deformation of Polystyrene–Silica Nanocomposites Studied by Hybrid Molecular Dynamics– Finite Element Simulations.....	93
4.1 Abstract.....	94
4.2 Introduction.....	95
4.3 Simulation method and computational details	98
4.3.1 Hybrid molecular dynamics-finite element method.....	98
4.3.2 Details on the coarse-grained nanocomposite systems	102
4.3.3 Geometrical transformation model	104
4.4 Results and discussion	105
4.4.1 Parameter identification from periodic MD simulations.....	105
4.4.2 Influence of nanoparticles on microscopic structural and dynamic properties of polymer chains as derived by periodic MD simulations	108
4.4.3 Hybrid MD-FE simulations	113
4.5 Conclusions.....	121
References.....	124
Supporting Information.....	128
5. Concluding Remarks and Outlook.....	131
Simulation Tools and Supercomputing Resources	138
Publications.....	139
Financial Support.....	140
Acknowledgments.....	141
Curriculum Vita	143
Erklärung	144
Eidesstattliche Erklärung	145

1. Introduction

Polymer nanocomposites¹ are prepared by mixing a fraction of nanoparticles into a polymer matrix. In recent decades they have been extensively used in different industrial fields. In general, polymer nanocomposites are consisted of three different phases, namely the polymer matrix, the nanoparticles and the interphase^{2,3}. A high surface-to-volume ratio of the nanoparticles leads to a large interphase area of nanocomposites. Due to the polymer-nanoparticle interaction, the properties of polymer chains in the interphase of nanocomposites differ from those in the bulk. The addition of the nanoparticles (and hence the generation of an interphase) changes the properties of polymer nanocomposites. For instance, the characteristics⁴ of nanoparticles (i.e. curvature, grafting state and dispersion) have a significant influence on structural and dynamic properties of polymer chains. Additionally, the presence of the interphase improves the mechanical strength of nanocomposites and suppresses the formation of crazes and cavitations in nanocomposites at large strains⁵. It is of practical and theoretical relevance to investigate correlations between the interphase and the mechanical properties of polymer nanocomposites. Experimental techniques are often not helpful to investigate properly molecular details of the interphase. Computer simulation methods at different scales have been widely applied to address different problems in the nanocomposite systems. Hybrid particle-continuum simulation methods⁶ have intrinsic advantages to investigate relations between the interphase structure and the macroscopic deformation behavior of nanocomposites. By collaboration with the group of Prof. Paul Steinmann, a hybrid molecular dynamics-finite element (MD-FE) method⁷ has been developed by our former colleague (Mohammad Rahimi) to simulate the deformation behavior of neat polymers and nanocomposites containing a single nanoparticle. In the present thesis, this hybrid method is further applied to investigate the microscopic interphase structure and the macroscopic deformation behavior of nanocomposites under external loads.

1.1 Hybrid molecular dynamics-finite element methods

1.1.1 Basic principles of hybrid molecular dynamics-finite element methods

In the past decades computer simulations have become a powerful technique to address scientific problems at different time and length scales⁸⁻¹⁰. The computational capacity of supercomputers

has obtained a tremendous development, whereas the difference between intended simulation accuracy and computational efficiency still restricts their applicability¹¹. Finite element (FE)^{12–19} methods solve macroscale problems by discretizing the studied systems as meshing units on a basis of continuum mechanics, so that they offer a high computational efficiency. Due to a continuum approximation, FE simulations do not allow accurate predictions of molecular properties of the studied system²⁰. In molecular dynamics (MD) simulations^{21–23}, an atom or a bead coarse-grained from a sub-group (e.g. monomer of polymer chains) is typically treated as the smallest simulation unit. The MD method has been used widely to investigate nanoscale (1~100 nm) problems of different systems such as interfacial structures^{24,4,25,26}, nanoparticle assemblies^{27–30} and biomacromolecular foldings^{31–33}.

To overcome the tradeoff between accuracy and efficiency, the coupling of two simulation methods at different scales, namely coupled MD-FE simulations, opens an access to complicated systems. A central question in the hybrid schemes^{17,34,35} is how to simulate accurately a spatial region of interest (e.g. liquid-solid and solid-solid interphases^{36–38}) embedded in a region with a coarser description where molecular details can be neglected. A hybrid MD-FE method provides a high resolution for simulations of macroscale problems (e.g. fluid flow and material deformation^{12–15,18,26,39,40}) at an affordable computational cost. These hybrid simulation methods have shown their robustness and advantages in investigations of different systems^{41,22,6,42} (e.g. nanocomposites, nanoclusters and nanofluids). More details on the aforementioned hybrid frameworks are introduced in the following sections.

As a numerical methodology, the FE method has been developed originally to solve partial differential equations⁴³ in the context of mechanical problems. Its main purpose is to simplify the considered problems by treating a whole spatial domain as a combination of several smaller correlated sub-domains⁴⁴. Without consideration of molecular details, a continuum description of the studied systems is an efficient way to address many macroscale problems related to hydrodynamic¹⁵ and structural^{45,46} mechanics. In the continuum mechanics scheme^{16,17,47}, simulation objects are simplified to a continuous body that comprises a certain number of infinitesimal elements without molecular structural details. Specifically, each infinitesimal element in the continuous body obeys constitutive rules of the simulation object as a whole body,

namely conservation of mass, momentum and energy flux. In an FE approximation, continuum mechanics problems are solved by partial differential equations that govern the respective macroscale phenomena. According to the physical state of the simulated systems, continuum mechanics is commonly divided into fluid and solid continuum mechanics^{46,48}. The former analyzes the flow behavior of liquids. The latter mainly investigates macroscale properties of solid materials, e.g. dislocations, grain boundaries⁴² and elastic-plastic deformations⁴⁶. As mentioned above, the MD method provides a high simulation accuracy as molecular details are considered. A coupling of the FE and MD simulation methods allows us to investigate accurately macroscale problems (e.g. material deformation) at an affordable computational cost. The present Ph.D. work mainly focuses on the application of the hybrid MD-FE method to polymer nanocomposites under a spatial deformation. The following sections are scheduled to introduce coupled molecular-macroscale (i.e. MD-FE) simulation methods as well as their applications in the fields of hydrodynamic and structural mechanics.

1.1.2 Different applications of hybrid molecular dynamics-finite element methods

Because of a large reduction in the degrees of freedom of the simulated systems, continuum-based simulations have a higher efficiency than particle-based simulations. Nevertheless, continuum mechanics cannot simulate precisely a heterogeneous system where inhomogeneous features and molecular properties of interest influence the system properties. As an example, the flow dynamics of liquids in microchannels (i.e. flows in blood vessels¹⁵) is affected largely by the intermolecular interaction between the fluid and solid wall. Therefore, the intermolecular interaction has to be described reasonably at a molecular resolution. To my knowledge, pioneering work in the coupled MD-FE simulation of complex fluid flows has been contributed by O'Connell et al.⁴⁰. In their simulations, the microchannel flow system is decomposed into a particle region, a hybrid solution interphase (HSI) region and a continuum region. The particle and HSI regions are both studied by an atomistic MD simulation that probes the influence of structural molecular factors in the vicinity of the solid wall on the hydrodynamics in the microchannels. The continuum region is described by a finite volume discretization on the basis of the Navier-Stokes equation¹². The continuity of the mass and momentum flux in the HSI region is achieved by exchanging velocity and other thermodynamic parameters between the particle and continuum region. This hybrid method has been also applied by others (e.g. Bugel et

al.⁶, Yen et al.¹², Cui et al.⁴⁸ and Werder et al.¹⁵) to investigate hydrodynamic problems in different multiphase systems.

In addition to fluid mechanics, the structural mechanics of solid materials is another field in which the hybrid particle-continuum method is applied widely. Macroscopic mechanical properties of multiphase solid materials (e.g. iron-carbon alloys⁴⁹, fiber-reinforced ceramics⁵⁰ and polymer nanocomposites⁵¹) are often determined by their microscopic structure in the so-called interphase between the matrix and the reinforcement phase. Conventional FE methods, such as the representative volume element⁴¹ (RVE) technique, decompose a material into a certain number of continuous elements that share overall properties of the material. In particular, these FE methods cannot describe the influence of the reinforcement phase on certain material properties. Similar to hydrodynamical coupling schemes, hybrid structural mechanics simulations have been applied to investigate material mechanics problems. They couple a particle-based MD region of local molecular details to a continuum-based FE surrounding that is able to reproduce the macroscale deformation behavior of the whole sample. Nevertheless, it should be mentioned that a central problem of these hybrid particle-continuum schemes is, how to transfer system information between the particle and continuum region.

1.1.3 Coupling strategies of hybrid molecular dynamics–finite element methods

According to the different ways to transfer information, hybrid structural mechanics methods are typically divided into two categories, namely sequential^{11,13,39,52,53} and concurrent^{45,46,54} coupling schemes. In the sequential coupling scheme, the MD and FE simulations are not performed simultaneously. Material properties and model parameters derived from the MD simulation are transferred into the subsequent FE computation at a lower resolution in an off-line way. The macroscopic behavior and microscopic structure of materials cannot be captured concurrently by an individual simulation in the sequential coupling framework. The RVE method^{39,53} is a widely used technique to reproduce approximately mean constitutive properties of heterogeneous nanocomposite materials in FE simulations. A RVE is generally defined as the smallest unit volume that reflects statistical averages of material properties. Yang et al.¹⁴ have developed a hybrid micromechanics model for multiscale constitutive simulations of silica/nylon-6 nanocomposites. In their work, interfacial structures between nylon-6 and silica are analyzed

qualitatively by the RVE model. Additionally, by using an equivalent-continuum method based on the RVE approximation, Odegard et al.³⁹ have predicted successfully the influence of the nanotube length, orientation and concentration on mechanical and other properties of polymer/nanotube composites.

In the concurrent coupling scheme, a bridging boundary⁴⁷ or handshaking region is introduced between the particle and continuum region. It contributes to a seamless coupling of potential energies by allowing an information transfer between both sub-regions at different scales in an online way. The overall potential energy in the handshaking region is formulated as a combination of the particle- and continuum-based energy. Their contribution to the total energy depends on chosen numerical rules to evaluate the weighting function. It is worth mentioning that these weighting factors have to be chosen according to details of the specific simulation system. The coupling simulation converges only when the total energy arrives at a global minimum value⁴⁶. The seamless energy combination and the online information exchange between the particle and continuum region enable concurrent coupling methods to capture simultaneously macromechanics and microstructures of materials. The concurrent coupling method has been used widely to investigate the mechanical deformation behavior⁴⁹ of solid crystalline materials such as fracture, dislocation and crack propagation. Due to the perfect periodicity of solid crystalline materials, it is simple to create meshing structures for the continuum and handshaking region in hybrid simulations. To achieve a seamless coupling of the MD and FE region, the position of each FE node in the overlap region is generated by a simple projection of a MD atom to a FE node in a one-to-one relation. Therefore, the displacement of the FE node in the overlap region coincides with the displacement of a MD atom under an application of a scaling procedure when performing the hybrid MD-FE computation⁵⁵.

However, the hybrid MD-FE method is still rarely applied to simulate amorphous polymer materials. This is caused by difficulties of discretizing the overlap region to generate the FE mesh structures for amorphous, non-periodic materials such as polymers or polymer nanocomposites⁵⁶. The Arlequin-based method developed by Ben Dhia et al.³⁵ is a feasible technique to perform simulations of amorphous polymer materials. In the Arlequin framework, the overlap region in a hybrid model is merely constructed according to a purely particle-based

description; it does not require a crystalline description. By collaboration with the group of Prof. Steinmann at Erlangen-Nuremberg University, our group has developed recently a new hybrid MD-FE method^{7,57} based on the Arlequin algorithm. The hybrid framework requires the definition of three different regions, namely the inner MD, the outer FE and the intermediate dissipative particle dynamics (DPD) region. More technical details on the hybrid method are described in Sections 2 and 4. In contrast to the existing hybrid frameworks, our hybrid MD-FE simulations are performed in a staggered way. This means that the particle-based MD region cannot feel the continuum-based FE region when performing FE computations and vice versa. Additionally, it is worth noticing that a large number of anchor points (e.g. several thousand) are introduced into the MD-FE overlapping region of the hybrid simulation space for the following purposes: (i) the transfer of information (i.e. forces and displacements) between the MD and FE region; (ii) they serve as a thermal bath and reduce the probability that polymer beads can leave from the particle region. The robustness of the hybrid method without consideration of the FE part on variations of input parameters related to the anchor points has been analyzed by an uncertainty quantification in simulations of a polystyrene model system⁵⁸.

1.1.4 Further analysis of the used hybrid molecular dynamics–finite element method

Computer simulations aim to gain insight into the behavior or properties of a system being modeled⁵⁹. This goal can be fulfilled by reproducing physical and chemical phenomena of the studied system with a set of input parameters⁶⁰. However, the input parameters in many systems^{61,62} are often uncertain. Reasonable combinations of them for these systems are often not accessible directly by a physical law, as the response of system properties to variations of the input parameters is not always explicitly known^{63,64}. As an example, coarse-grained force fields used in MD simulations often exhibit a poor transferability between various thermodynamic conditions⁶⁵ such as temperature and pressure. Quite generally, these force field models are able to reproduce quantities of interest (QoI) of the studied system within a certain range of thermodynamic conditions, but fail at other ranges. In this sense, the accuracy of the QoI of the simulated system is sensitive to the thermodynamic conditions. To make simulation results more reliable, it is of theoretical and practical relevance to investigate the sensitivity of the QoI or their robustness as a function of uncertainties in the input parameters.

As a statistical analysis technique, uncertainty quantification (UQ)^{66,67} has been used widely to locate uncertainties in the system response and to characterize correlations between the calculated QoI and the chosen input parameters. For instance, based on a random sampling (i.e. Monte Carlo method) of a chosen parameter space, Rouhi et al.^{68,69} have demonstrated by UQ analyses that uncertainties from geometrical and mechanical properties of carbon nanofibers influence largely the calculated elastic properties of thermostat polymer materials. In addition, Jacobson et al.⁶⁵ have employed a generalized polynomial chaos (gPC) technique to reconstruct the analytical surface of system properties of coarse-grained water models as a function of the input parameters. The UQ analyses have indicated that the overall transferability of the coarse-grained water model depends on the targeted output property of the water model. The workflow of the UQ scheme can be summarized as follows:

- (i) Define the conditions of a UQ study by selecting input parameters (i.e. temperature, cutoff of non-bonded interactions, timestep) and quantities of interest (QoI) of a given model (i.e. MD simulation);
- (ii) Define a range of the input parameters and a parameter sampling method (i.e. random sampling method and stochastic collocation method);
- (iii) Generate a set of the input parameters in a given parameter range according to the parameter sampling method and calculate the corresponding value of the QoI of the given model.
- (iv) Identify statistic features (i.e. mean value and standard deviation) of the QoI in the given parameter range based on the results from (iii);
- (v) Analyze the sensitivity of the QoI to a variation of the input parameters and determine the uncertainty sources of the studied model.

In the hybrid MD-FE framework, the impact of several anchor-point-related input parameters on the robustness of the hybrid MD-FE model still has not been analyzed systematically. The relation between input parameters and system properties cannot be interpreted by an explicit physical law. These input parameters mainly include the force constant between anchor points and polymer beads, the number and distribution of anchor points and the thickness of the DPD region. As a matter of fact, they have to be chosen reasonably prior to production runs of the

hybrid simulations. It is therefore necessary to further investigate quantitatively the influence of these input parameters on the performance of the hybrid model. In the present thesis, an investigation of the robustness of the hybrid method as a function of variations of these input parameters by the UQ method is scheduled as the first mission. The algorithm details of the UQ analysis on the hybrid model are described in Section 2.

1.2 Interfacial structure and mechanical deformation of polymer nanocomposites

1.2.1 Microscopic properties of polymer chains in the interphase of nanocomposites

Polymer materials such as polystyrene⁷⁰, polyethylene⁷¹ and polyurethane⁷² have been widely employed as a result of their excellent properties², e.g. light-weight, high ductility and good processability. Compared with conventional metallic and inorganic nonmetallic materials, the low mechanical strength of neat polymer materials restricts the range of their industrial application^{3,73}. Mechanical properties of polymer materials are typically improved by composite manufacturing processes in which a low-modulus polymer matrix is blended with a fraction of high-modulus nanofillers (e.g. silica nanoparticles^{2,74-78}, carbon nanotubes⁷⁹⁻⁸³, layered clay^{1,84,85}). The mechanical strength of polymer nanocomposites is largely determined by the presence of an interphase structure⁸⁶. The interaction between the polymer matrix and the nanoparticles influences the properties of the polymer chains around the nanoparticles^{87,88}. Therefore, the local behavior of the polymer chains in the interphase differs from the one in the bulk. Investigations of local inhomogeneities in the polymer properties as a function of a separation from the nanoparticle surface allow us to understand details of the interfacial structures of polymer nanocomposites.

It is often difficult to obtain molecular details of the interphase by experimental methods. Molecular simulation techniques have intrinsic advantages in investigations of interfacial properties of polymer nanocomposites from a microscopic perspective. By performing either atomistic or coarse-grained MD simulations, our former group members (i.e. Ndoro et al.^{24,89}, Ghanbari et al.⁹⁰⁻⁹² and Voyiatzis et al.⁹³) have investigated structural and dynamic properties of the polymer chains near to the nanoparticle surface in nanocomposite systems containing a single nanoparticle. According to their simulations, polymer chains in the interphase expand their

dimension (i.e. chain end-to-end distance) relative to the bulk and orientate tangentially to the spherical nanoparticle surface⁹⁴⁻⁹⁶. Additionally, the dynamics (i.e. chain center of mass diffusion coefficient) of polymer chains in the interphase is hindered by interfacial adsorption effects⁹⁷⁻⁹⁹. It has also been found that both the curvature and grafting state of nanoparticles have a significant influence on interfacial chain properties in nanocomposites¹⁰⁰. The global and interfacial chain properties¹⁰¹ are also influenced by other nanoparticle properties^{102,103} such as the mass fraction and the geometrical shape of nanoparticles. As the second aim of the present thesis, the influence of the chosen nanoparticle properties (and hence of the interphase area) on the global and local behavior of the polymer chains is investigated by performing coarse-grained MD simulations of polystyrene nanocomposite systems containing silica nanoparticles of different geometrical shapes.

1.2.2 Mechanical deformation of polymer nanocomposites under external loads

Experimental investigations¹⁰⁴⁻¹⁰⁸ have found that the mechanical properties of polymer nanocomposites are improved by an increasing concentration and grafting density of nanoparticles or by reducing the nanoparticle size at a constant nanoparticle concentration. It is of theoretical and practical relevance to investigate from a microscopic perspective, how the mechanical improvement of polymer nanocomposites correlates with nanoparticle characteristics⁵⁰⁻⁵² (i.e. nanoparticle concentration, size, grafting state). Quite generally, the presence of nanoparticles with a massive surface-to-volume ratio leads to a large interphase area between the polymer matrix and the nanofillers^{109,110}. The spatial profiles of structural and dynamic properties of polymer chains in the interphase^{54,57} reflect molecular details of interfacial structures. The interphase^{111,112} has generally a thickness of a few nanometers, and has a significant influence on the mechanical deformation behavior of polymer nanocomposites. It is commonly considered as an interaction zone^{113,114} that leads to an increase in the effective interaction region of the nanoparticles. Liang et al.¹¹⁵ and Rafiee et al.¹¹⁶ have found that the formation and propagation of crazes in polymer nanocomposites at a large strain can be attenuated due to the presence of an interphase region. This can be explained by the fact that a fraction of the polymer chains is strongly adsorbed by the nanoparticle surface¹¹⁷. In addition, Zhang et al.¹¹⁸ have suggested that nanoparticles can act as physical cross-linkers in nanocomposites. The “bridge network” structure¹¹⁹ formed by wrapping long polymer chains

around neighbouring nanoparticles can improve efficiently the mechanical properties of polymer nanocomposites.

Understanding the mechanical deformation behavior of polymer materials under an external load is helpful to design improved polymer materials⁹⁴. Stress-strain relations obtained by experimental measurements² have shown that the deformation of polymer materials can lead to two different phases, namely an elastic¹²⁰ and a plastic one^{121,122}. In the former phase which exists for small strains, the deformation-induced stress increases almost linearly with the strain. Subsequently, the deformed material reaches a yield point^{123,124} from which the linear increase of the stress with the strain is terminated. Beyond the yield point, the stress extends to a plateau where a plastic deformation takes place at larger strains. The deformation behavior of polymer materials is fundamentally connected to the changes of chain structures and conformations as response to the external load^{125,126}. As reported by Hossain et al.¹²⁷, Li et al.¹²⁸ and Shang et al.¹²⁹, an applied external load leads to an expansion and a gradual orientation of polymer chains along the applied stress. In the elastic phase the mechanical work is mostly stored as non-bonded and bonded energies^{130,131}, while it is partially dissipated as thermal energy in the plastic phase. Specifically, elastic and plastic deformations are both accompanied by chain elongations (i.e. angle bending and bond stretching) and mutual chain slips.


1.2.3 Computer simulations of the deformation behavior of polymer nanocomposites

Mechanical deformations of semi-crystalline polymer materials^{132–136} have been studied extensively by various experimental methods. In general, correlations between morphology and micromechanical deformation processes in semicrystalline polymer systems can be analyzed by electron microscopy and X-ray diffraction using in-situ tensile techniques^{137–140}. However, possible relations between changes in the chain structure and the mechanical behavior of amorphous polymer glasses under external loads still have not been understood at a molecular level as the complexity of their microstructures causes numerous challenges for experimental measurements¹²⁷. Computer simulation methods at different scales have been applied to investigate mechanical deformation processes of amorphous polymer materials. For instance, Chui et al.¹⁴¹ have performed Monte Carlo simulations to investigate stress-strain relations of amorphous polymeric networks constructed by a three-dimensional polybead model. They have

found that the stress-strain behavior of amorphous polymer systems depends on the temperature, pressure and applied strain^{142,143}. Ogura et al.¹⁴⁴ have found in MD simulations of a model amorphous polymer that large deformation processes cover three different steps, namely intrachain bond breaking, void formation and further development of cavities. Additionally, Dupaix et al.¹⁴⁵ have developed a macroscale constitutive model to simulate the mechanical deformation of amorphous polymers. They have concluded that the primary mechanism for strain hardening of amorphous polymers corresponds to molecular orientation and alignment^{146,147}. It should be mentioned that hybrid particle-continuum simulations of polymer nanocomposites are still rarely reported in the literature.

1.3 Description of the tasks set in the present dissertation

Several scientific questions related to the microscopic structure and macroscopic deformation behavior of polymer nanocomposites have still not been addressed properly from a microscopic perspective. How much of the chain reorientation in amorphous polymer glasses can be merely related to an affine transformation¹⁴⁸ of the whole material? Relative to neat polymers, to which extend are the microscopic conformational changes of polymer chains during a tensile deformation influenced by the presence of nanoparticles^{149,150}? How much can the addition of nanoparticles influence the global and interfacial properties of polymer chains as well as macroscopic mechanical properties of polymer nanocomposites¹⁵¹⁻¹⁵⁴? To answer these questions, the aforementioned hybrid MD-FE method has been applied in the present work to simulate uniaxial deformations of polystyrene nanocomposites containing a certain fraction of silica nanoparticles. As shown by the observed results, the hybrid method allows us to capture qualitatively possible correlations between molecular structures and macroscale properties of nanocomposites at an affordable computational cost. In the hybrid MD-FE framework^{7,57}, the continuum domain solved by the FE method serves as an elastically responding surrounding to deform the inner particle domain in which polymer structural properties in nanocomposites are analyzed. The considered polymer nanocomposite systems⁹¹ are generated by mixing a certain amount of silica nanoparticles into a polystyrene matrix. The influence of the nanoparticle properties (i.e. mass fraction, size and grafting state) on the mechanical macroscale behavior of polymer nanocomposites is investigated by both standard periodic MD and hybrid MD-FE



simulations. More details on the deformation simulations of polystyrene–silica nanocomposites are given in the following sections.

The remaining chapters of the present thesis are structured as follows. In the second chapter, the influence of variations of the input parameters on the results of the hybrid MD-FE simulation method is analyzed systematically using an uncertainty quantification method. Subsequently, the role of the interfacial area for the structure and dynamics of polymer nanocomposites is investigated by molecular dynamics simulations of polystyrene with silica nanoparticles of different shapes. In the fourth chapter, hybrid MD-FE simulations are performed to investigate the uniaxial deformation behavior of polystyrene/silica nanocomposites. Finally, the conclusions obtained in the present thesis and an outlook of the hybrid simulations are summarized in the fifth chapter.

References

- ¹ A.A. Azeez, K.Y. Rhee, S.J. Park, and D. Hui, *Compos. Part B Eng.* **45**, 308 (2013).
- ² H. Zou, S. Wu, and J. Shen, *Chem. Rev.* **108**, 3893 (2008).
- ³ A.N. Rider, Q. An, N. Brack, and E.T. Thostenson, *Chem. Eng. J.* **269**, 121 (2015).
- ⁴ H. Eslami and F. Müller-Plathe, *J. Phys. Chem. C* **117**, 5249 (2013).
- ⁵ S. Chandrasekaran, N. Sato, F. Tölle, R. Mülhaupt, B. Fiedler, and K. Schulte, *Compos. Sci. Technol.* **97**, 90 (2014).
- ⁶ M. Bugel, G. Galliéro, and J.-P. Caltagirone, *Microfluid. Nanofluidics* **10**, 637 (2011).
- ⁷ S. Pfaller, M. Rahimi, G. Possart, P. Steinmann, F. Müller-Plathe, and M.C. Böhm, *Comput. Methods Appl. Mech. Eng.* **260**, 109 (2013).
- ⁸ C. Li and A. Strachan, *J. Polym. Sci. Part B Polym. Phys.* **53**, 103 (2015).
- ⁹ S. Takada, *Curr. Opin. Struct. Biol.* **22**, 130 (2012).
- ¹⁰ E. Brini, E. A. Algaer, P. Ganguly, C. Li, F. Rodríguez-Ropero, and N.F. A. Van Der Vegt, *Soft Matter* **9**, 2108 (2013).
- ¹¹ T.E. Karakasidis and C.A. Charitidis, *Mater. Sci. Eng. C* **27**, 1082 (2007).
- ¹² T.H. Yen, C.Y. Soong, and P.Y. Tzeng, *Microfluid. Nanofluidics* **3**, 665 (2007).
- ¹³ B. J. Yang, Y. Y. Hwang, and H. K. Lee, *Compos. Struct.* **99**, 123 (2013).
- ¹⁴ B.J. Yang, H. Shin, H.K. Lee, and H. Kim, *Appl. Phys. Lett.* **103**, 241903 (2013).
- ¹⁵ T. Werder, J.H. Walther, and P. Koumoutsakos, *J. Comput. Phys.* **205**, 373 (2005).
- ¹⁶ Y. Wang and G. He, *Chem. Eng. Sci.* **62**, 3574 (2007).
- ¹⁷ G.J. Wagner and W.K. Liu, *J. Comput. Phys.* **190**, 249 (2003).
- ¹⁸ X.B. Nie, S.Y. Chen, W.N. E, and M.O. Robbins, *J. Fluid Mech.* **500**, 55 (2004).
- ¹⁹ N. Hadjiconstantinou and N.G. Hadjiconstantinou, *J. Comput. Phys.* **154**, 245 (1999).
- ²⁰ K.N. Spanos, S.K. Georgantzinis, and N.K. Anifantis, *Compos. Struct.* **132**, 536 (2015).
- ²¹ K. Binder, J. Horbach, W. Kob, W. Paul, and F. Varnik, *J. Phys. Condens. Matter* **16**, S429 (2004).
- ²² B. Wilfred, V. Gunsteren, and C.

- Berendsen, *Angew. Chemie Int. Ed.* **29**, 992 (1990).
- ²³ M. Karplus and J.A. McCammon, *Nat. Struct. Biol.* **9**, 646 (2002).
- ²⁴ T.V.M. Nodoro, E. Voyiatzis, A. Ghanbari, D.N. Theodorou, M.C. Böhm and F. Müller-Plathe, *Macromolecules* **44**, 2316 (2011).
- ²⁵ O.A. Karim and A.D.J. Haymet, *J. Chem. Phys.* **89**, 6889 (1988).
- ²⁶ A.R. van Buuren, S.J. Marrink, and H.J.C. Berendsen, *J. Phys. Chem.* **97**, 9206 (1993).
- ²⁷ J.B. Maillet, V. Lachet, and P. V Coveney, *Phys. Chem. Chem. Phys.* **1**, 5277 (1999).
- ²⁸ J. Hautman, J.P. Bareman, W. Mar, and M.L. Klein, *J. Chem. Soc. Faraday Trans.* **87**, 2031 (1991).
- ²⁹ M.L. Klein and W. Shinoda, *Science* **321**, 798 (2008).
- ³⁰ G. Srinivas, D.E. Discher, and M.L. Klein, *Nat. Mater.* **3**, 638 (2004).
- ³¹ J. Gsponer and A. Caflisch, *Proc. Natl. Acad. Sci. U. S. A.* **99**, 6719 (2002).
- ³² W.C. Swope, J.W. Pitera, and F. Suits, *J. Phys. Chem. B* **108**, 6571 (2004).
- ³³ Y. Sugita and Y. Okamoto, *Chem. Phys. Lett.* **314**, 141 (1999).
- ³⁴ R. Chang, G.S. Ayton, and G.A. Voth, *J. Chem. Phys.* **122**, 244716 (2005).
- ³⁵ H. Ben Dhia, L. Chamoin, J.T. Oden, and S. Prudhomme, *Comput. Methods Appl. Mech. Eng.* **200**, 2675 (2011).
- ³⁶ H. Lin and D.G. Truhlar, *Theor. Chem. Acc.* **117**, 185 (2007).
- ³⁷ H.M. Senn and W. Thiel, *Top Curr. Chem.* **268**, 173 (2007).
- ³⁸ H.M. Senn and W. Thiel, *Angew. Chemie Int. Ed.* **48**, 1198 (2009).
- ³⁹ G. Odegard, T.S. Gates, K.E. Wise, C. Park, and E.J. Siochi, *Compos. Sci. Technol.* **63**, 1671 (2003).
- ⁴⁰ S.T. O'Connell and P.A. Thompson, *Phys. Rev. E* **52**, 5792 (1995).
- ⁴¹ D. Bakowies and W. Thiel, *J. Phys. Chem.* **100**, 10580 (1996).
- ⁴² N. Bernstein, J.R. Kermode, and G. Csányi, *Reports Prog. Phys.* **72**, 026501 (2009).
- ⁴³ J.L. Bouvard, D.K. Ward, D. Hossain, S. Nouranian, E.B. Marin, and M.F. Horstemeyer, *J. Eng. Mater. Technol.* **131**, 041206 (2009).
- ⁴⁴ C. Carstensen and E.-J. Park, *SIAM J. Numer. Anal.* **53**, 43 (2015).
- ⁴⁵ R.E. Miller and E.B. Tadmor, *Model. Simul. Mater. Sci. Eng.* **17**, 053001 (2009).

- ⁴⁶ W.A. Curtin and R.E. Miller, *Model. Simul. Mater. Sci. Eng.* **11**, R33 (2003).
- ⁴⁷ S.P. Xiao and T. Belytschko, *Comput. Methods Appl. Mech. Eng.* **193**, 1645 (2004).
- ⁴⁸ J. Cui, G. He, and D. Qi, *Acta Mech. Sin.* **22**, 503 (2006).
- ⁴⁹ D.W. Ward, I.M.; Hadley, *Macromolecules* **35**, 9595 (2002).
- ⁵⁰ T.S. Gates, G.M. Odegard, S.J. V Frankland, and T.C. Clancy, *Compos. Sci. Technol.* **65**, 2416 (2005).
- ⁵¹ S. Ahmed and F.R. Jones, *J. Mater. Sci.* **25**, 4933 (1990).
- ⁵² A.P. Awasthi, D.C. Lagoudas, and D.C. Hammerand, *Model. Simul. Mater. Sci. Eng.* **17**, 015002 (2009).
- ⁵³ B. Mortazavi, O. Benzerara, H. Meyer, J. Bardon, and S. Ahzi, *Carbon* **60**, 356 (2013).
- ⁵⁴ R.E. Rudd and J.Q. Broughton, *Phys. Status Solidi* **217**, 251 (2000).
- ⁵⁵ L. Mishnaevsky and E. Levashov, *Comput. Mater. Sci.* **96**, 365 (2015).
- ⁵⁶ J. Rottler, *J. Phys. Condens. Matter* **21**, 463101 (2009).
- ⁵⁷ M. Rahimi, H.A. Karimi-Varzaneh, M.C. Böhm, F. Müller-Plathe, S. Pfaller, G. Possart, and P. Steinmann, *J. Chem. Phys.* **134**, 154108 (2011).
- ⁵⁸ S. Liu, A. Gerisch, M. Rahimi, J. Lang, M.C. Böhm, and F. Müller-Plathe, *J. Chem. Phys.* **142**, 104105 (2015).
- ⁵⁹ J. Blumberger, *Chem. Rev.* **115**, 11191 (2015).
- ⁶⁰ J.A. Greathouse, D.B. Hart, G.M. Bowers, R.J. Kirkpatrick, and R.T. Cygan, *J. Phys. Chem. C* **119**, 17126 (2015).
- ⁶¹ O.A. Vanli, L.-J. Chen, C. Tsai, C. Zhang, and B. Wang, *Int. J. Adv. Manuf. Technol.* **70**, 33 (2014).
- ⁶² R. Wagner, R. Moon, J. Pratt, G. Shaw, and A. Raman, *Nanotechnology* **22**, 455703 (2011).
- ⁶³ J.C. Chang, P.W. Fok, and T. Chou, *Biophys. J.* **109**, 966 (2015).
- ⁶⁴ N. Vu-Bac, R. Rafiee, X. Zhuang, T. Lahmer, and T. Rabczuk, *Compos. Part B Eng.* **68**, 446 (2015).
- ⁶⁵ L.C. Jacobson, R.M. Kirby, and V. Molinero, *J. Phys. Chem. B* **118**, 8190 (2014).
- ⁶⁶ Y. Li, W. Stroberg, T.-R. Lee, H.S. Kim, H. Man, D. Ho, P. Decuzzi, and W.K. Liu, *Comput. Mech.* **53**, 511 (2014).
- ⁶⁷ A. Clément, C. Soize, and J. Yvonnet, *Comput. Methods Appl. Mech. Eng.* **254**, 61 (2013).

- ⁶⁸ M. Rouhi and M. Rais-Rohani, *Compos. Struct.* **95**, 346 (2013).
- ⁶⁹ M. Rouhi, M. Rais-Rohani, and A. Najafi, *Compos. Struct.* **100**, 144 (2013).
- ⁷⁰ N. Chaukura, W. Gwenzi, T. Bunhu, D.T. Ruziwa, and I. Pumure, *Resour. Conserv. Recycl.* **107**, 157 (2016).
- ⁷¹ S. Kumar Sen and S. Raut, *J. Environ. Chem. Eng.* **3**, 462 (2015).
- ⁷² K.M. Zia, H.N. Bhatti, and I. Ahmad Bhatti, *React. Funct. Polym.* **67**, 675 (2007).
- ⁷³ K.M. Liew, Z.X. Lei, and L.W. Zhang, *Compos. Struct.* **120**, 90 (2015).
- ⁷⁴ P. Dittanet and R.A. Pearson, *Polymer* **53**, 1890 (2012).
- ⁷⁵ M. Naffakh, A.M. Díez-Pascual, C. Marco, G.J. Ellis, and M.A. Gómez-Fatou, *Prog. Polym. Sci.* **38**, 1163 (2013).
- ⁷⁶ M.A. Hood, C.S. Gold, F.L. Beyer, J.M. Sands, and C.Y. Li, *Polymer* **54**, 6510 (2013).
- ⁷⁷ M. Salami-Kalajahi, V. Haddadi-Asl, S. Rahimi-Razin, F. Behboodi-Sadabad, M. Najafi, and H. Roghani-Mamaqani, *J. Polym. Res.* **19**, 9793 (2012).
- ⁷⁸ S. Kango, S. Kalia, A. Celli, J. Njuguna, Y. Habibi, and R. Kumar, *Prog. Polym. Sci.* **38**, 1232 (2013).
- ⁷⁹ A.B. Sulong, M.I. Ramli, S.L. Hau, J. Sahari, N. Muhamad, and H. Suherman, *Compos. Part B Eng.* **50**, 54 (2013).
- ⁸⁰ K.S. Khare, F. Khabaz, and R. Khare, *ACS Appl. Mater. Interfaces* **6**, 6098 (2014).
- ⁸¹ M. Martin-Gallego, M.M. Bernal, M. Hernandez, R. Verdejo, and M.A. Lopez-Manchado, *Eur. Polym. J.* **49**, 1347 (2013).
- ⁸² S.U. Khan, J.R. Pothnis, and J.-K. Kim, *Compos. Part A Appl. Sci. Manuf.* **49**, 26 (2013).
- ⁸³ S.C. Tjong, *Mater. Sci. Eng. R Reports* **74**, 281 (2013).
- ⁸⁴ S. Gajjela, V. Ramachandran, and J. Somasekharan, *Compos. Part B Eng.* **88**, 11 (2016).
- ⁸⁵ K. Fukushima, D. Tabuani, M. Arena, M. Gennari, and G. Camino, *React. Funct. Polym.* **73**, 540 (2013).
- ⁸⁶ Y. Zare, *Mech. Mater.* **85**, 1 (2015).
- ⁸⁷ W.K. Chee, H.N. Lim, N.M. Huang, and I. Harrison, *RSC Adv.* **5**, 68014 (2015).
- ⁸⁸ R. Rohini, P. Katti, and S. Bose, *Polymer* **70**, A17 (2015).
- ⁸⁹ T.V.M. Nodoro, M.C. Böhm, and F. Müller-Plathe, *Macromolecules* **45**, 171 (2012).
- ⁹⁰ A. Ghanbari, M.C. Böhm, and F. Müller-

- Plathe, *Macromolecules* **5520** (2011).
- ⁹¹ A. Ghanbari, T.V.M. Nodoro, M. Rahimi, M.C. Böhm, and F. Müller-Plathe, *Macromolecules* **45**, 572 (2012).
- ⁹² A. Ghanbari, M. Rahimi, and J. Dehghany, *J. Phys. Chem. C* **117**, 25069 (2013).
- ⁹³ E. Voyiatzis, M. Rahimi, F. Müller-Plathe, and M.C. Böhm, *Macromolecules* **47**, 7878 (2014).
- ⁹⁴ S.C. Tjong, *Mater. Sci. Eng. R Reports* **53**, 73 (2006).
- ⁹⁵ A. Karatrantosa, N. Clarkea, and M. Kröger, *Polym. Rev.* **56**, 385 (2016).
- ⁹⁶ A.J. Crosby and J.-Y. Lee, *Polym. Rev.* **47**, 217 (2007).
- ⁹⁷ Y. Gao, J. Liu, L. Zhang, and D. Cao, *Macromol. Theory Simulations* **23**, 36 (2014).
- ⁹⁸ J. Liu, Y. Wu, J. Shen, Y. Gao, L. Zhang, and D. Cao, *Phys. Chem. Chem. Phys.* **13**, 13058 (2011).
- ⁹⁹ G.D. Smith, D. Bedrov, L. Li, and O. Bytner, *J. Chem. Phys.* **117**, 9478 (2002).
- ¹⁰⁰ G. Allegra, G. Raos, and M. Vacatello, *Prog. Polym. Sci.* **33**, 683 (2008).
- ¹⁰¹ Q.H. Zeng, A.B. Yu, and G.Q. Lu, *Prog. Polym. Sci.* **33**, 191 (2008).
- ¹⁰² I. Kelnar, J. Kratochvíl, I. Fortelný, L. Kaprálková, A. Zhigunov, M. Nevoralová, M. Kotrisová, and V. Khunová, *RSC Adv.* **6**, 30755 (2016).
- ¹⁰³ E.M. Sullivan, P. Karimineghlani, M. Naraghi, R.A. Gerhardt, and K. Kalaitzidou, *Eur. Polym. J.* **77**, 31 (2016).
- ¹⁰⁴ J.N. Coleman, U. Khan, W.J. Blau, and Y.K. Gun'ko, *Carbon* **44**, 1624 (2006).
- ¹⁰⁵ D. Cai and M. Song, *J. Mater. Chem.* **20**, 7906 (2010).
- ¹⁰⁶ R. Qiao and L. Catherine Brinson, *Compos. Sci. Technol.* **69**, 491 (2009).
- ¹⁰⁷ S. Yu, S. Yang, and M. Cho, *Polymer* **50**, 945 (2009).
- ¹⁰⁸ X. Zhao, Q. Zhang, D. Chen, and P. Lu, *Macromolecules* **43**, 2357 (2010).
- ¹⁰⁹ J. Zhao, H. Li, G. Cheng, and Y. Cai, *Compos. Struct.* **135**, 297 (2016).
- ¹¹⁰ S. Javadi, M. Razzaghi-Kashani, P.N. Reis, and A.A. Balado, *Polym. Compos.* **16**, 1 (2015).
- ¹¹¹ G. Scocchi, P. Posocco, M. Fermeglia, and S. Pricl, *J. Phys. Chem. B* **111**, 2143 (2007).
- ¹¹² P. V. Komarov, I. V. Mikhailov, Y.T. Chiu, S.M. Chen, and P.G. Khalatur, *Macromol. Theory Simulations* **22**, 187 (2013).

- ¹¹³ J. Berriot, H. Montes, F. Lequeux, D. Long, and P. Sotta, *Macromolecules* **35**, 9756 (2002).
- ¹¹⁴ J. Berriot, H. Montes, F. Lequeux, D. Long, and P. Sotta, *Europhys. Lett.* **64**, 50 (2003).
- ¹¹⁵ J.Z. Liang and R.K.Y. Li, *Polym. Compos.* **19**, 698 (1998).
- ¹¹⁶ R. Rafiee, A. Fereidoon, and M. Heidarhaei, *Comput. Mater. Sci.* **56**, 25 (2012).
- ¹¹⁷ R. Krishnamoorti, R.A. Vaia, and E.P. Giannelis, *Chem. Mater.* **8**, 1728 (1996).
- ¹¹⁸ Q. Zhang and L.A. Archer, *Langmuir* **18**, 10435 (2002).
- ¹¹⁹ A.S. Sarvestani and C.R. Picu, *Polymer* **45**, 7779 (2004).
- ¹²⁰ M.A. Guseva, V.A. Gerasin, O.K. Garishin, V.V. Shadrin, O.A. Plekhov, and A. Pawlak, *Polymer* **56**, 416 (2015).
- ¹²¹ J. Shen, J. Liu, H. Li, Y. Gao, X. Li, Y. Wu, and L. Zhang, *Phys. Chem. Chem. Phys.* **17**, 7196 (2015).
- ¹²² S. Jabbari-Farouji, J. Rottler, O. Lame, A. Makke, M. Perez, and J.L. Barrat, *ACS Macro Lett.* **4**, 147 (2015).
- ¹²³ A.D. Printz, A. V. Zaretski, S. Savagatrup, A.S.C. Chiang, and D.J. Lipomi, *ACS Appl. Mater. Interfaces* **7**, 23257 (2015).
- ¹²⁴ L. Malekmotiei, A. Samadi-Dooki, and G.Z. Voyiadjis, *Macromolecules* **48**, 5348 (2015).
- ¹²⁵ A. V. Lyulin, N.K. Balabaev, M.A. Mazo, and M.A.J. Michels, *Macromolecules* **37**, 8785 (2004).
- ¹²⁶ H.E.H. Meijer and L.E. Govaert, *Prog. Polym. Sci.* **30**, 915 (2005).
- ¹²⁷ D. Hossain, M.A. Tschopp, D.K. Ward, J.L. Bouvard, P. Wang, and M.F. Horstemeyer, *Polymer* **51**, 6071 (2010).
- ¹²⁸ J. Li, T. Mulder, B. Vorselaars, A. V. Lyulin, and M.A.J. Michels, *Macromolecules* **39**, 7774 (2006).
- ¹²⁹ Y. Shang, X. Zhang, H. Xu, J. Li, and S. Jiang, *Polymer* **77**, 254 (2015).
- ¹³⁰ F. Zeng, E. Hu, Y. Sun, and J. Qu, *J. Polym. Sci. Part B Polym. Phys.* **53**, 986 (2015).
- ¹³¹ X. Wang, Y. Peng, H. Yuan, C. Liu, L.S. Turng, and C. Shen, *Polym. Test.* **41**, 73 (2015).
- ¹³² B.A.G. Schrauwen, R.P.M. Janssen, L.E. Govaert, and H.E.H. Meijer, *Macromolecules* **37**, 6069 (2004).
- ¹³³ Y. Men, J. Rieger, and G. Strobl, *Phys. Rev. Lett.* **91**, 095502 (2003).

- ¹³⁴ M. Ganß, B.K. Satapathy, M. Thunga, R. Weidisch, P. Pötschke, and D. Jehnichen, *Acta Mater.* **56**, 2247 (2008).
- ¹³⁵ B.A.G. Schrauwen, L.C.A. Von Breemen, A.B. Spoelstra, L.E. Govaert, G.W.M. Peters, and H.E.H. Meijer, *Macromolecules* **37**, 8618 (2004).
- ¹³⁶ Z. Jiang, Y. Wang, L. Fu, B. Whiteside, J. Wyborn, K. Norris, Z. Wu, P. Coates, and Y. Men, *Macromolecules* **46**, 6981 (2013).
- ¹³⁷ G. Machado, E.L.G. Denardin, E.J. Kinast, M.C. Gonçalves, M.A. De Luca, S.R. Teixeira, and D. Samios, *Eur. Polym. J.* **41**, 129 (2005).
- ¹³⁸ G. Machado, E.J. Kinast, J.D. Scholten, A. Thompson, T. De Vargas, S.R. Teixeira, and D. Samios, *Eur. Polym. J.* **45**, 700 (2009).
- ¹³⁹ D. Samios, S. Tokumoto, and E.L.G. Denardin, *Int. J. Plast.* **22**, 1924 (2006).
- ¹⁴⁰ J. Ščudla, M. Raab, K.J. Eichhorn, and A. Strachota, *Polymer* **44**, 4655 (2003).
- ¹⁴¹ C. Chui and M.C. Boyce, *Macromolecules* **32**, 3795 (1999).
- ¹⁴² F.M. Capaldi, M.C. Boyce, and G.C. Rutledge, *Phys. Rev. Lett.* **89**, 175505 (2002).
- ¹⁴³ J. Rottler and M.O. Robbins, *Phys. Rev. E* **64**, 051801 (2001).
- ¹⁴⁴ R. Tarumi, A. Ogura, M. Shimojo, K. Takashima, and Y. Higo, *MRS Proc.* **36**, 1375 (1995).
- ¹⁴⁵ R.B. Dupaix and M.C. Boyce, *Mech. Mater.* **39**, 39 (2007).
- ¹⁴⁶ F.M. Capaldi, M.C. Boyce, and G.C. Rutledge, *Polymer* **45**, 1391 (2004).
- ¹⁴⁷ H.E.H. Meijer and L.E. Govaert, *Macromol. Chem. Phys.* **204**, 274 (2003).
- ¹⁴⁸ T. Oda, S. Nomura, and H. Kawai, *J. Polym. Sci. Part A Polym. Chem.* **3**, 1993 (1965).
- ¹⁴⁹ H. Shin, S. Yang, J. Choi, S. Chang, and M. Cho, *Chem. Phys. Lett.* **635**, 80 (2015).
- ¹⁵⁰ A. Pawlak, A. Galeski, and A. Rozanski, *Prog. Polym. Sci.* **39**, 921 (2014).
- ¹⁵¹ K. Hagita, H. Morita, M. Doi, and H. Takano, *Macromolecules* **49**, 1972 (2016).
- ¹⁵² Y. Fu and J.-H. Song, *Comput. Mater. Sci.* **96**, 485 (2015).
- ¹⁵³ M.A. Rafiee, J. Rafiee, Z. Wang, H. Song, Z.Z. Yu, and N. Koratkar, *ACS Nano* **3**, 3884 (2009).
- ¹⁵⁴ J.C. Huang, C. Bin He, Y. Xiao, K.Y. Mya, J. Dai, and Y.P. Siow, *Polymer* **44**, 4491 (2003).



2. Robustness of Hybrid Molecular Dynamics–Finite Element Method for Amorphous Polystyrene Analyzed by Uncertainty Quantification

2.1 Abstract


Key parameters of a recently developed coarse-grained hybrid molecular dynamics-finite element (MD-FE) approach have been analyzed in the framework of uncertainty quantification (UQ). We have employed a polystyrene sample for the case study. The new hybrid approach contains several parameters which cannot be determined on the basis of simple physical arguments. Among others, this includes so-called anchor points as information transmitters between the particle-based MD domain and the surrounding FE continuum, the force constant between polymer beads and anchor points, the number of anchor points and the relative sizes of the MD core domain and the surrounding dissipative particle dynamics (DPD) domain. Polymer properties such as density, radius of gyration, end-to-end distance and radial distribution functions are calculated as a function of the above model parameters. The influence of these input parameters on the resulting polymer properties is studied by UQ. Our analysis shows that the hybrid method is highly robust. The variation of polymer properties of interest as a function of the input parameters is weak.

2.2 Introduction

Multiscale simulations of soft matter systems have recently received increasing attention. Some multiscale simulation techniques, mainly in the framework of either particle-based models (e.g. molecular dynamics (MD) ¹, Monte Carlo (MC) ² and dissipative particle dynamics (DPD) ³ methods) or continuum models (e.g. finite element (FE) approach ^{4,5}), have been employed to study macroscopic and microscopic (molecular) properties of soft matter systems. Quite generally, particle-based models are of higher resolution than field-based models as they consider explicitly the chemical and physical details of the studied systems. However, it is often impossible to employ particle-based models alone to treat some macroscale problems in soft matter systems due to the unaffordable computational cost. Unfortunately, one of the most often used field-based models, i.e. the finite element method, does not provide a resolution to study microscopic properties of soft matter. These could be local inhomogeneities such as interphases around filler particles in nanocomposites. One essentially unsolved problem in multiscale simulations is how to investigate macroscopic soft matter processes and properties, but under a high resolution. The coupling of a particle-based description of a smaller domain of interest with a much larger surrounding field-based continuum region is a suitable technique to combine the accuracy in the domain of interest with an efficient treatment of the remaining system. To date, some particle-field coupling techniques have been developed for hybrid simulations. Belytschko and Xiao ⁶ proposed an approach to couple a particle and continuum model based on a bridging domain framework, in which the particle and continuum domains overlap; the total energy was derived as a combination from both overlapping domains. The so-called bridging coupling method had been adopted by Khare et al. ⁷, Zhang et al. ⁸, Davydov et al. ⁹ and Xu et al. ¹⁰ to investigate the mechanical behavior of crystalline materials. In addition, an Arlequin method ^{11,12}, similar to the bridging domain framework, was developed by Ben Dhia and co-workers to blend atomistic and continuum energies in hybrid simulations. The Arlequin method has been applied to simulate soft materials such as polymers ^{13,14} because it does not require a lattice structure in the particle domain. Despite these recent advances, applications of particle-continuum hybrid models to simulate polymer nanocomposites are rare.

Recently some of the present authors have developed a hybrid molecular dynamics-finite element (MD-FE) model^{15, 16} to investigate interfacial and mechanical properties of polymer nanocomposites. A fundamental element of the MD-FE model is the coupling of a central particle domain to a surrounding continuum using the Arlequin approach. The particle domain is further divided into a MD core, where molecular properties can be analyzed, and a dissipative particle dynamics (DPD) shell, which provides both the stochastic boundary conditions for the MD core and the hand-shake with the continuum domain. The continuum domain is described by a FE model. The equations of motion in the MD and FE domain are based on Newtonian mechanics and continuum mechanics, respectively. The hand-shake between particle and continuum domain is handled by a number of points, so-called anchor points¹⁷, predefined in the boundary, where the DPD region and the finite element region overlap. Polymer beads in the boundary region are tethered harmonically to these anchor points via a spring with a properly chosen force constant. The transfer of forces and displacements between the MD and FE domain is achieved via a staggered coupling formalism which displaces anchor point positions in the boundary domain under external load. More specifically, the displacement field computed in the FE domain dictates displacements of anchor points within the boundary domain after each FE iteration step. In the intervening MD steps, the anchor points provide a constant external potential for the particle region. In the present MD-FE implementation coarse-grained (CG) MD simulations^{18, 19} are performed in the MD and boundary region until equilibration using stochastic boundary conditions^{17, 20, 21}. During the MD simulation, the forces on the anchor points are accumulated. Their time-averages define surface tractions as additional boundary conditions for the next FE step, which eventually gives rise to displacements of the anchor points which are resubmitted to the MD domain. The developed algorithm defines a staggered MD-FE iteration framework which is executed until convergence standards are satisfied. More details on the iteration procedure in our hybrid MD-FE simulation scheme can be found elsewhere¹⁶.

The applicability of the hybrid MD-FE framework has been demonstrated for simple model systems (pure polystyrene (PS) as well as PS filled with a single silica nanoparticle; both systems were described in CG resolution)^{16, 17, 22}. An upcoming application will be the use of MD-FE coupling models to study polymer composite systems filled with a large number of nanoparticles. To this end, the influence of the many input parameters of the staggered hybrid MD-FE model



on the results of the calculations still has to be quantified. Candidates for parameters, which influence the robustness of the method, include the force constant between polymer beads and anchor points, the number of anchor points in the boundary domain, their distribution and the relative dimensions of the MD and boundary domains. In the present work, the influence of these technical parameters of the coupling model on the simulation results is studied using uncertainty quantification (UQ)^{23, 24}. Some material properties of the studied system (quantities of interest, QoI) are considered as a function of those input parameters. As a powerful analysis tool, UQ has been adopted also recently to study the effect of key parameters on QoI of simulation systems²⁵⁻²⁷. Structural properties (mass density, end-to-end distance, radius of gyration, radial distribution function (RDF)) as well as one dynamic property (diffusion coefficient) of the polymer chains are analyzed in this work. As the input parameters concern primarily the particle domain, the hybrid simulation framework is considered without the FE part here; see one of our recent studies¹⁷. Moreover, a pure PS system without nanoparticles is taken as simulation example in this work.

2.3 Simulation methods and computational details

All MD simulations in the present work are done with our program IBIsCO²⁸, both under non-periodic, stochastic boundary conditions¹⁷ (SBC MD simulations, which do not include the FE part) and under standard periodic boundary conditions (PBC MD simulations). Both methods have been employed to simulate soft matter systems. In this contribution, we mainly discuss the SBC MD simulation model because it is the most important and most time-consuming part of the fully hybrid MD-FE simulations described above^{15,16}. For simplicity, only the basic framework of SBC MD simulations is presented summarily here. The particle domain of the SBC MD simulation model contains three spatial sections, denoted as the MD, DPD and boundary domain. The MD domain is the core of the particle domain. Here, the analysis of molecular properties is done; the movement of the particles is governed by pure Newtonian mechanics; and this part should behave as if it were surrounded by more MD particles, rather than, boundary and continuum domains with their contraptions to facilitate the coupling. The boundary region is the outermost shell of the particle domain. It spatially overlaps with the innermost layer of the continuum domain: in this region, there are both particles and finite elements. Coupling between particles and finite elements is implemented via the anchor points which transmit the forces between both levels of description. The anchor points are located exclusively in the boundary region. A second purpose of the anchor points is to prevent polymer molecules from leaving the particle region. While the MD simulation is running in the particle domain, it is surrounded by vacuum; were it not for the anchor points, the molecules would start to evaporate. Thirdly, by acting as a confining external potential, the anchor points provide an effective “wall” on the particle domain and define the internal pressure. Because of their different actions, the anchor points play a very important role in SBC MD as well as in hybrid MD-FE simulations. This is the reason why modifications in the QoI as a function of anchor-point density and distribution should be understood quantitatively. Their number is a direct input parameter. Their distribution depends besides its functional form (we use both uniform and exponential profiles) chiefly on the thickness of the boundary region. We have, however, established previously¹⁷ that it has a large enough safe range. Therefore, the thickness of the boundary region in this work is always chosen as 1.5 nm. Equally, the force constant k between selected polymer beads and their anchor points

should be neither too large nor too small. A strong spring may constitute an unphysical perturbation of the particle domain into the MD core region. On the other hand, if the force constant is too small, too many polymer beads might leave the particle domain. Then the shape of the particle domain might change in an uncontrollable way. Thus both the pressure and the density in the particle domain might be wrong. This force constant is, therefore, another parameter whose influence on the QoI must be known. The third particle region in the present MD-FE approach is the so-called DPD region. It includes the boundary region, but can reach further into the particle domain if necessary. The particle motion follows the stochastic DPD³ equation of motion, rather than the Newtonian equation of motion in the core. It serves as a thermal bath which keeps the temperature of the particle region at the desired value. Moreover, it pretends to the MD core that there are more particles outside the particle domain by mimicking random collisions with outside particles. The extension of the DPD region also has the potential to influence the QoI. If too thin, it fails to provide adequate randomness at the boundary. If too thick, it interferes with the dynamics in the MD core. Therefore, the width of the DPD region (the boundary domain and the DPD extension), is an important input parameter, too, and its influence is investigated here.

In this technical study, a coarse-grained model of atactic polystyrene (PS) was used as example. The tabulated coarse-grained potential is taken from our previous work²⁹⁻³². The potential has been determined by Iterative Boltzmann Inversion^{33,34} at a temperature of 590 K and a pressure of 1 bar. The repeating units in atactic PS chains have two conformations, R and S. In our coarse-grained model they are represented by two different beads. Results from standard PBC MD simulations were employed as reference to allow a comparison with the results from the SBC MD. The PBC box contains 3000 chains of 20 monomers. The simulation box is equilibrated at 590 K and 1 bar in the isothermal-isobaric (NPT) ensemble for 10 ns using the Nosé-Hoover method to control temperature and pressure with coupling times of 1.0 ps and 5.0 ps, respectively. The non-bonded cut-off radius was set to 1.5 nm. The velocity-Verlet integration approach was employed with a time step of 0.01 ps. After this stage, the system was cooled from 590 K to 300 K at a rate of 10 K/ns. After this procedure the system had a size of $21.39 \times 21.39 \times 21.39 \text{ nm}^3$ and a density of $1063 \pm 3.26 \text{ kg/m}^3$ at 1 bar. With the cooled structures

we performed PBC MD simulations of 4 ns from which the properties of the polymer were estimated for comparison with SBC MD simulations.

The initial structure for the SBC MD simulations is the final structure of a PBC MD calculation. In removing the periodic boundary conditions, all polymer chains which extend out of the simulation box are cut and the outside polymer fragments are shifted back into the simulation cell (the particle region in the language of MD-FE hybrid methods) using periodic boundary conditions. Most of the shortened fragments are located in the boundary domain (thickness $L_{boundary} = 1.5$ nm) of the simulation box. About 80 percent of all polymer chains keep their original length of 20 monomers (Figure 2.1); and nearly all (98.12 %) polymer chains in the core

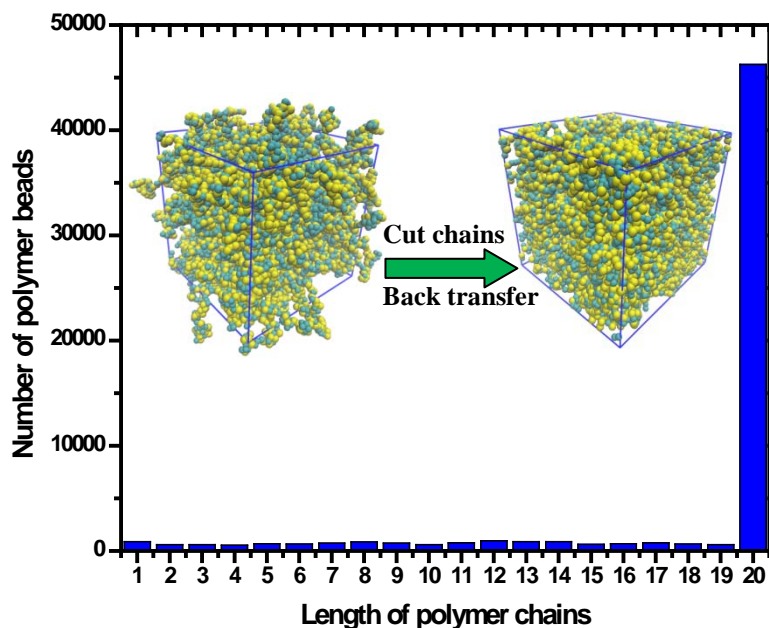



Figure 2.1 The distribution of PS chain lengths in the simulation box after shifting all beads outside the box back to the simulation box. The original PS chains are 20 beads long.

MD domain ($17.39 \times 17.39 \times 17.39$ nm³) are uncut; here the thickness of DPD domain is 2.0 nm. The SBC MD calculations are carried out with the same general settings as the PBC MD calculations, except for the following differences: The temperature is maintained at 300 ± 2.7 K



by the thermostat in the DPD domain (thickness 1.0 nm) with a friction constant of 2.32 N/m. The anchor atoms are distributed randomly in the boundary region. There are between 2625 and 11078 of them (see below). In all cases, there are at least 1.27 anchor points per polymer fragment in the boundary region, to reduce the escape of chains and to maintain the pressure in the MD region at 1 ± 0.054 bar.

2.4 Uncertainty quantification analysis methodology

Uncertain input parameters are those, whose value cannot be determined precisely a priori, yet the simulation outcome, in particular the quantities of interest (QoI), of a model may depend on their actual values. Examples of uncertain input parameters arise from physical limitations of the studied model (e.g. fluctuations of temperature around a target temperature) or also from algorithmic requirements (e.g. the choice of the MD timestep). The quantitative statistical analysis of the impact of uncertainty in input parameters on QoI of a given model, a methodology termed Uncertainty Quantification (UQ), is of high significance for the application of simulation techniques. In this work, we employ UQ to compute in particular estimates of the mean and the variance of different QoI when uncertain input parameters exhaust their stochastic space, i.e. vary over their parameter range according to a suitable distribution. In fact the selection of this distribution corresponds to model the uncertainty in the parameter under investigation. In the present study all uncertain input parameters are scalars and represented by a random variable with a uniform distribution over a particular interval. Furthermore, while having different uncertain input parameters, we consider only a single one of these as uncertain at a time and keep all others at fixed basic values. Table 2.1 summarizes the uncertain parameters with their ranges as well as model parameters that have been fixed to their basic values. These basic values were set to the safe values for the model according to the recent work ¹⁷. As described earlier, the QoI considered in this work include mass density, end-to-end distance, and radius of gyration of the PS chains for both the entire simulation box and the inner MD box. Note that the more general investigation of the combined effect of all uncertain input parameters at once on QoI of the model is subject of ongoing work.

Uncertain input parameter	Force constant k (N/m)	Number of anchor points N	DPD domain size L_{DPD} (nm)
Parameter range	$3.0 < k < 150.0$	$2625 < N < 11078$	$1.5 < L_{DPD} < 10.0$
Predefined fixed parameters	$N = 8775, L_{DPD} = 5.0$	$k = 2.32, L_{DPD} = 5.0$	$k = 2.32, N = 8775$

Table 2.1 Uncertain input parameters and parameter ranges in the uncertainty quantification analysis (second row). Other input parameters (bottom row) are fixed when one was chosen as the uncertain input parameter. The number of anchor points is controlled by a comparison between a random number r ($0 \leq r < 1$) and the anchor point distribution density.

The goal of the UQ analysis applied to our hybrid simulation model is to provide quantitative information of the effect of uncertain algorithmic parameters on model robustness and thus contributes to understand the hybrid simulation model more systematically. We remark here that the diffusion coefficient and the radial distribution function of PS are QoI of the model but calculated and analyzed without using the UQ methodology. For simplicity they will be analyzed directly in terms of the natural fluctuations of the QoI.

In the remainder of this section we give a brief account of the main ingredients of our UQ approach, for more details we refer the reader to the literature^{23, 24}. Figure 2.2 illustrates briefly the basic workflow of UQ analysis for the hybrid MD-FE model.

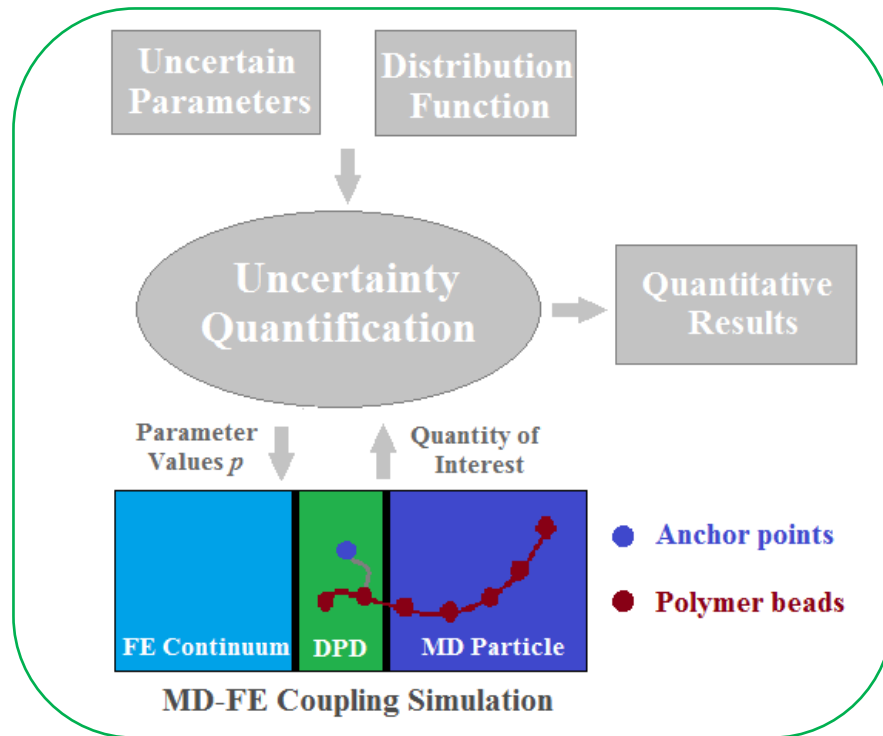


Figure 2.2 The figure illustrates the workflow of uncertainty quantification analysis for hybrid MD-FE approach. Note that the FE continuum is the outermost region of hybrid MD-FE model but it is not included in the SBC MD simulations of the present study.

The main advantage of our scheme over an ad-hoc exploration of the stochastic space associated with parameter uncertainty is that we proceed in a systematic and cost-efficient manner and provide results which are accurate up to a user-specified tolerance. We proceed in two phases. In Phase I we construct a global polynomial $q(p)$ which maps parameter values p from the uncertain parameter range to approximate values of the QoI of the model, i.e. $q(p) \approx \text{QoI}(p)$. The polynomial q is constructed using a collocation technique, that is: (i) a number of collocation points p_j in the uncertain parameter range are chosen and each of which corresponds to a particular choice of the uncertain parameters, (ii) for each collocation point p_j , the model is simulated with uncertain parameters set to p_j and the corresponding $\text{QoI}(p_j)$ is derived, and (iii) the unique polynomial q of suitable degree is determined such that $q(p_j) = \text{QoI}(p_j)$ holds for all collocation points p_j . Clearly the appropriate number and position of the collocation points in (i) determines the accuracy with which $q(p)$ approximates $\text{QoI}(p)$ at non-collocation points. In our UQ scheme we select appropriate collocation points to ensure that for all possible uncertain parameter values p we have:

$$|q(p) - \text{QoI}(p)| \leq \text{TOL}. \quad (2.1)$$

We set the user-specified tolerance to $\text{TOL} = 10^{-7}$ in all UQ computations of this study. However, also observe that the number of collocation points determines the computational effort required in (ii), that is how many expensive simulations of our hybrid simulation model need to be performed, and thus should be chosen as small as possible. How both of these aims, i.e. approximation accuracy and computational efficiency, can be reached simultaneously by iterative improvement will be discussed below. The constructed polynomial $q(p)$ is evaluated cheaply for any particular parameter value p . It is now used as a surrogate of our hybrid simulation model in Phase II, where we compute approximations of statistical quantities of the QoI as the uncertain input parameters vary according to their distribution. Thus we avoid the expensive simulation of the model in this phase. In particular in this work we compute

approximations μ and σ^2 to the expected value $E[QoI]$ and the variance $V[QoI]$ of the QoI, respectively, that is

$$E[QoI] \approx \int_a^b q(p) f(p) dp, \quad (2.2)$$


$$V[QoI] \approx \sigma^2 := \int_a^b f(p) (q(p) - \mu)^2 dp. \quad (2.3)$$

Here the integral boundaries are the finite values (a and b) according to the interval of the uniform distribution of the uncertain input parameter under investigation and f denotes the density function of that distribution. Observe that by ensuring tolerance TOL in the construction of polynomial q implies that, for instance, also μ is an approximation of $E[QoI]$ with the same accuracy, i.e.

$$|\mu - E[QoI]| = \left| \int_a^b (q(p) - QoI(p)) f(p) dp \right| \leq \int_a^b |q(p) - QoI(p)| f(p) dp \leq TOL, \quad (2.4)$$

where we have used that the integral over the non-negative density function equals one. Note that the intervals for uncertain input parameters, for example $[3.0, 150.0]$ (N/m) for force constant, were set to make sure that the SBC MD simulations can be performed safely.

We now finally address, on a more technical basis, the choice of the collocation points p_j and the construction of the polynomial $q(p)$ in Phase I and relate this to the objectives of our computational UQ scheme. We iteratively add new p_j to the set of collocation points until the corresponding polynomial q satisfies the accuracy requirement. That means that we construct a sequence of increasingly finer, nested grids, each covering the uncertain parameter space and for each grid a corresponding polynomial q . Thanks to the nested nature of the grids, we reuse the expensive QoI computation of earlier collocation points. Furthermore, the p_j are taken from a sparse grid if there is more than one uncertain parameter in order to avoid dimensionality problems associated with full, multi-dimensional grids. The result is typically a small number of



required runs of the hybrid simulation model in Phase I. In addition, for improved approximation accuracy and consequently an efficient scheme, the p_j are the zeros of special polynomials and distributed not equally spaced but denser towards the boundary of the parameter space. The sequence of nested grids allows that the sequence of corresponding polynomials q can be written with a hierarchical basis representation. The latter has advantages when computing the new polynomial q after adding new collocation points and provides the error indicator employed to stop the iteration. Complete details can be found in ref. 23.

2.5 Results and discussions

2.5.1 Force constant for the interaction between anchor points and polymer beads

The migration of polymer beads from the inner MD domain to the boundary region and beyond will increase when the harmonic interaction between polymer beads and anchor points is weak. This can be monitored by the mass density in the MD core region. When the force constant is very small (0.001 N/m) the mass density of PS in the core MD domain drops from $1060 \pm 6.17 \text{ kg/m}^3$ to $1000 \pm 4.62 \text{ kg/m}^3$ in a simulation of 4 ns (Figure 2.3 (a)). This demonstrates that the mass density of PS in the MD domain is not stable when the force constant is too small. However, the mass density of PS in the central MD region remains constant when a force constant of at least 2.32 N/m and an exponential profile of the anchor points are adopted (Figure 2.3 (b)). In our recent hybrid simulation this value has been adopted as standard^{15, 16}. It is quite important to understand how a variation of the force constant influences properties of PS chains. The range of force constants listed in Table 2.1 was analyzed by UQ. Note that the computational procedure starts at 3.00 N/m, i.e. above the safe value of 2.32 N/m. Fifteen force constant values were chosen at regular intervals. For each value the properties of PS in the MD core region were determined:

Neither the mass density (Figure 2.4 (a)), nor the squared end-to-end distance (Figure 2.4 (b)) and the squared radius of gyration (Figure 2.4 (c)) of the PS chains depend sizably on the value of the force constant (SBC simulation). The values for the entire simulation box differ from the MD core (lower mass density due to a small amount of escaping polymer; lower squared radius of gyration and squared end-to-end distance due to the presence of cut chains, see Section 2.3). However, they are more or less independent from the value of the force constant. The standard deviations of these three QoI obtained from UQ analysis (Table 2.2, below) are 0.761 kg/m^3 for the mass density, 0.0409 nm^2 for the squared end-to-end distance and 0.0034 nm^2 for the squared radius of gyration, respectively. These standard deviations are quite small compared with the corresponding average values. Our UQ results demonstrate quantitatively that the effect of changing the anchor point - polymer bead force constant on QoI can be ignored, once it is above the threshold of 2.32 N/m.

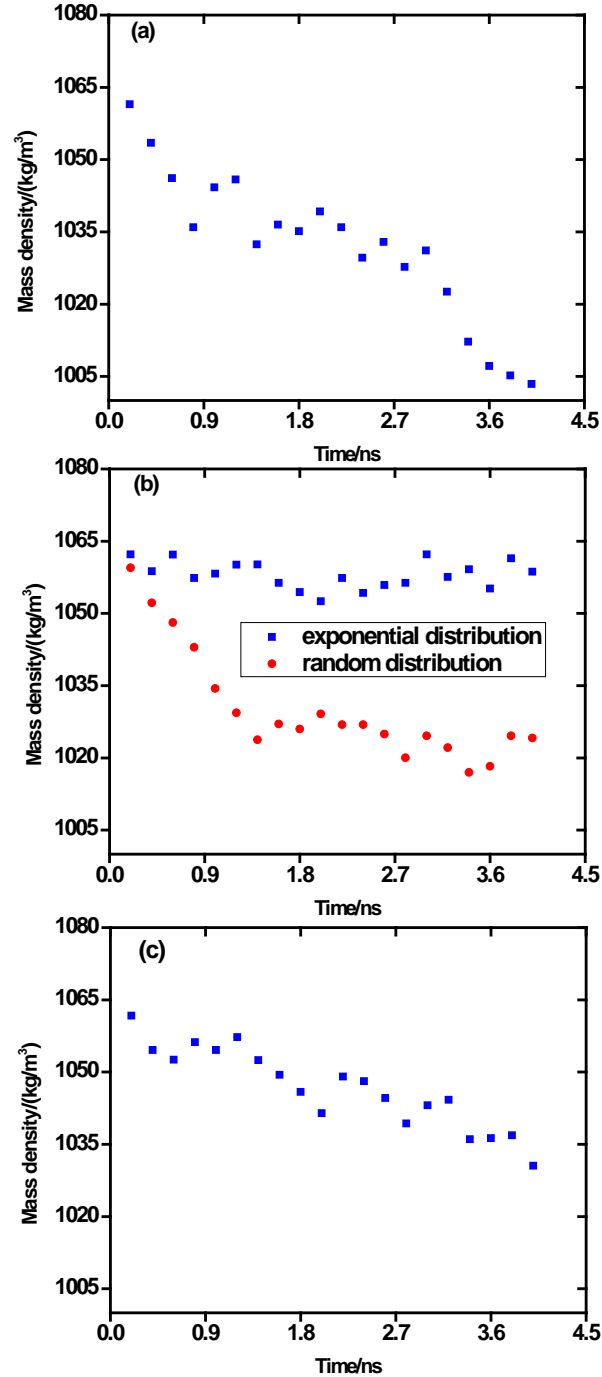


Figure 2.3 Mass density of PS in the inner MD domain as a function of the simulation time under different conditions of (a) force constant $k = 0.001$ N/m, number of anchor points $N = 8775$ and DPD domain size $L_{DPD} = 5.0$ nm; (b) force constant $k = 2.32$ N/m, number of anchor points $N = 3126$ and DPD domain size $L_{DPD} = 5.0$ nm for an exponential and random distribution of the anchor points; (c) force constant $k = 2.32$ N/m, number of anchor points $N = 2243$ and DPD domain size $L_{DPD} = 5.0$ nm.

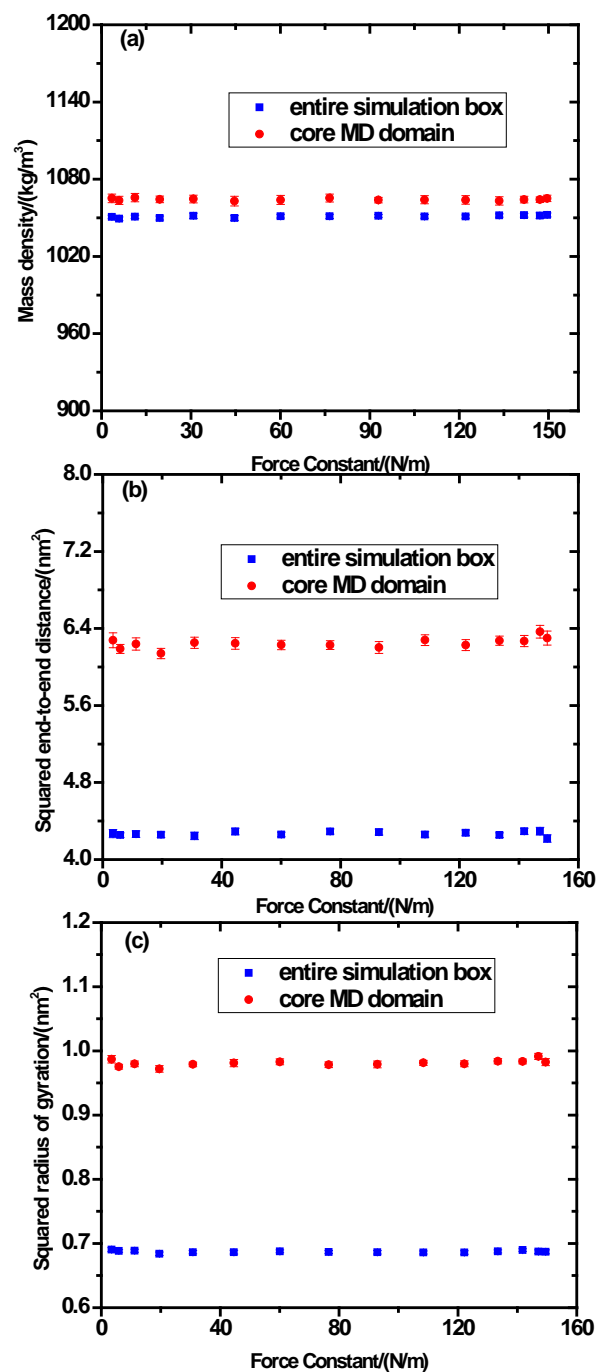


Figure 2.4 Mass density (a), squared end-to-end distance (b) and squared radius of gyration (c) of PS chains in the entire simulation box (blue) and in the core MD domain (red) as a function of force constant between polymer beads and anchor points. Note that the error bars are in most cases smaller than the symbols.

		Force Constant			Number of anchor points			DPD domain size		
		Mass density (kg/m ³)	Squared end-to-end distance (nm ²)	Squared radius of gyration (nm ²)	Mass density (kg/m ³)	Squared end-to-end distance (nm ²)	Squared radius of gyration (nm ²)	Mass density (kg/m ³)	Squared end-to-end distance (nm ²)	Squared radius of gyration (nm ²)
MD box	Mean value	1064.248	6.248	0.981	1065.508	6.321	0.984	1063.753	6.296	0.983
	Standard deviation	0.761	0.0409	0.0034	0.5837	0.0668	0.0059	8.9369	0.2667	0.0219
Entire box	Mean value	1051.033	4.268	0.687	1045.757	4.363	0.699	1044.916	4.281	0.688
	Standard deviation	1.291	0.0171	0.0013	2.0886	0.0401	0.0066	0.3639	0.0167	0.0012

Table 2.2 Mean values and standard deviations for different quantities of interest in simulations under a change of the force constant, the number of anchor points and the DPD domain size. The values of standard deviation are calculated using uncertainty quantification method. The mean values of different quantities of interest are listed for comparison with the standard deviations.

The radial distribution functions of PS chains for the entire box for two different force constants ($k = 2.32$ and 9.31 N/m) were also calculated (Figure 2.5 (a)). These two radial distribution function curves are nearly identical. The relative deviations of the radial distribution functions from the reference curves for different values of the force constant are quite small (Figure 2.6 (a)). This shows again that a variation of the force constant does not have a prominent influence on the structure of PS in SBC MD simulations. The values of the mean square displacement of the PS chains were fitted linearly to obtain their diffusion coefficients. Note that the diffusion coefficient of the PS chains in the MD domain fluctuates slightly (Figure 2.7 (a)) when running simulations with different force constants. In analogy to static structural properties, changes in the force constant do not have a big influence on the diffusion coefficient of the PS chains both in the MD domain and the entire box (SBC MD simulations).

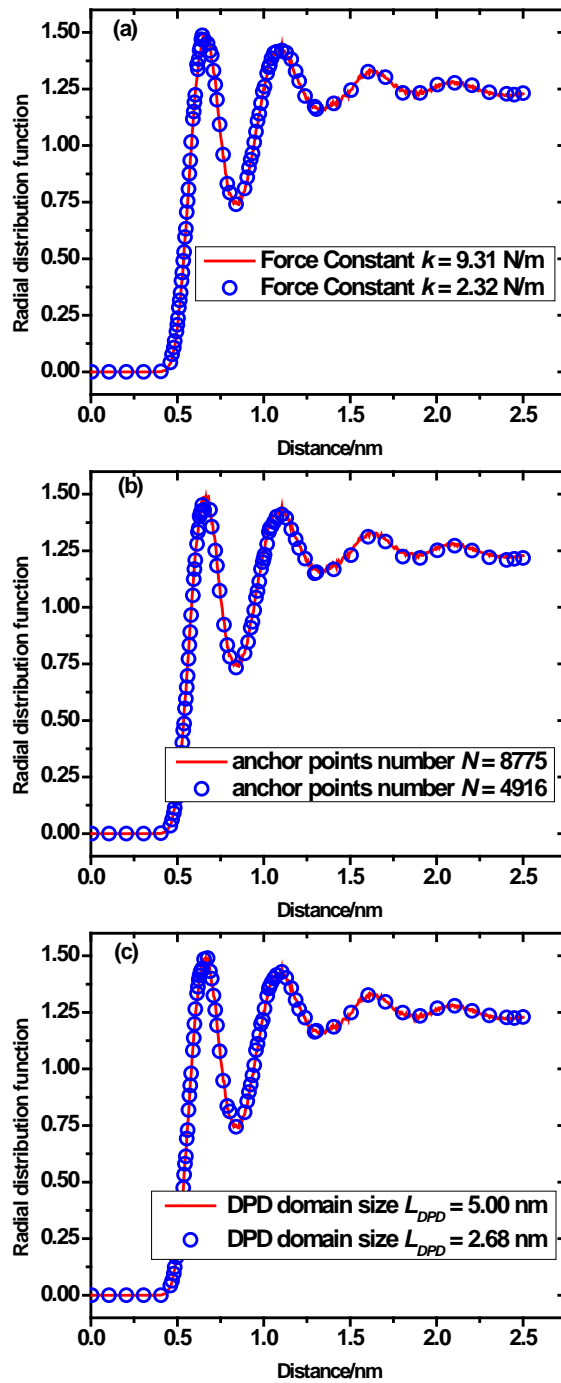


Figure 2.5 Comparison of non-bonded radial distribution functions for polystyrene chains as a function of different input parameters (a) force constant, (b) number of anchor points and (c) DPD domain size.

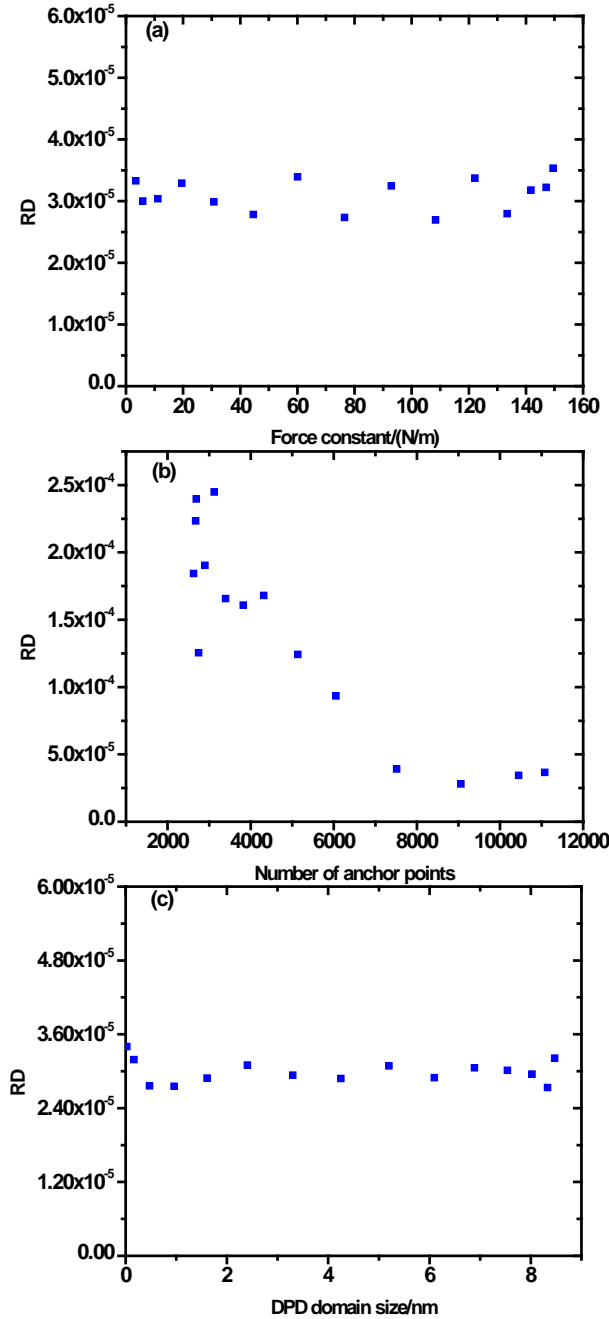


Figure 2.6 Relative deviation of the radial distribution function as a function of (a) force constant, (b) the number of anchor points and (c) the DPD domain size. Relative deviations (RD) were calculated with the formula $RD = \frac{1}{M} \sum_{i=1}^M \left(\frac{RDF_i(x) - RDF_i(0)}{RDF_i(0)} \right)^2$. Here, M is the number of discrete points in the RDF curves, $RDF(x)$ is calculated via changing input parameters x ($x = k$, N or L_{DPD}) and $RDF(0)$ is the standard value of the RDF when k , N and L_{DPD} are 2.32 N/m, 8775 and 2.0 nm, respectively .

2.5.2 Anchor point distribution in the dissipative-particle-dynamics domain

Two different distributions of anchor points (a random profile with an exponential decay towards the inner MD domain and a uniform random distribution without preferential direction) have been employed in our simulations. For a detailed description of our strategy to generate a profile with an exponential decay we refer to our previous article¹⁷. As polymer beads are tethered to the space fixed anchor points in the boundary region, their escape into the surrounding “vacuum” is increasingly hindered with increasing anchor point density. For an identical number of anchor points in both distributions, the exponential shape is superior to the random profile. This is evident when analyzing the PS mass density for both distributions as a function of the simulation time (Figure 2.3 (b)). In addition to the spatial distribution of the anchor points, their total number also exerts an influence on the migration of polymer beads from the boundary domain into the surrounding vacuum. With an increasing number of anchor points, more polymer beads are fixed, and the polymer is better confined in the particle domain. For a too small number of anchor points (2243), the mass density of the PS in the MD domain decreases from 1060 ± 4.37 kg/m³ to 1030 ± 5.89 kg/m³ (Figure 2.3 (c)). In contrast, the density in the MD domain remains constant, when the number of anchor points is at least 2800. From that number of anchor points onward, the QoI, including mass density, squared end-to-end distance and squared radius of gyration, remain more or less constant (Figure 2.8) up to the upper end of the investigated range of 11500 anchor points. The standard deviations for these three QoI are very small (Table 2.2) in comparison to their average values. To sum up, as long as the number of anchor points does not fall below the limit of 2800, any value can be used without affecting the structural properties of the PS chains. In addition, the splitting between the radial distribution functions of the PS chains in the entire simulation box for two numbers of anchor points ($N = 4916$ and 8775) is quite small (Figure 2.5 (b)). The same is of course observed for the relative deviation of the radial distribution functions for different numbers of anchor points (Figure 2.6 (b)). Similar to the structural properties of the polymer, a variation in the number of anchor points does not have a big influence on the studied dynamic property, the diffusion coefficient, of the PS chains in the MD domain. This is shown in Figure 2.7 (b). However, note that the diffusion coefficient of the PS chains in the entire simulation box decreases as the number of anchor points increases. The reason has been touched already above, i.e. anchor points confine the movement of polymer

beads in the boundary domain. In contrast, they do not influence the movement of PS chains in the MD domain.

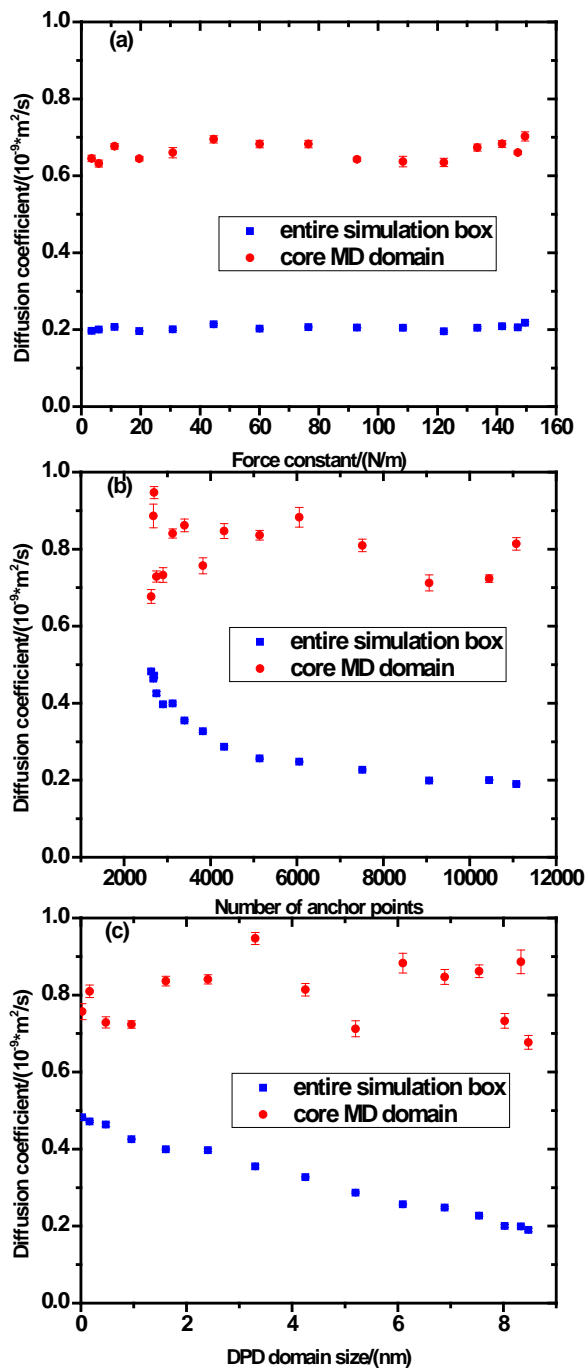


Figure 2.7 Diffusion coefficient of PS as a function of (a) the force constant, (b) the number of anchor points and (c) the DPD domain size.

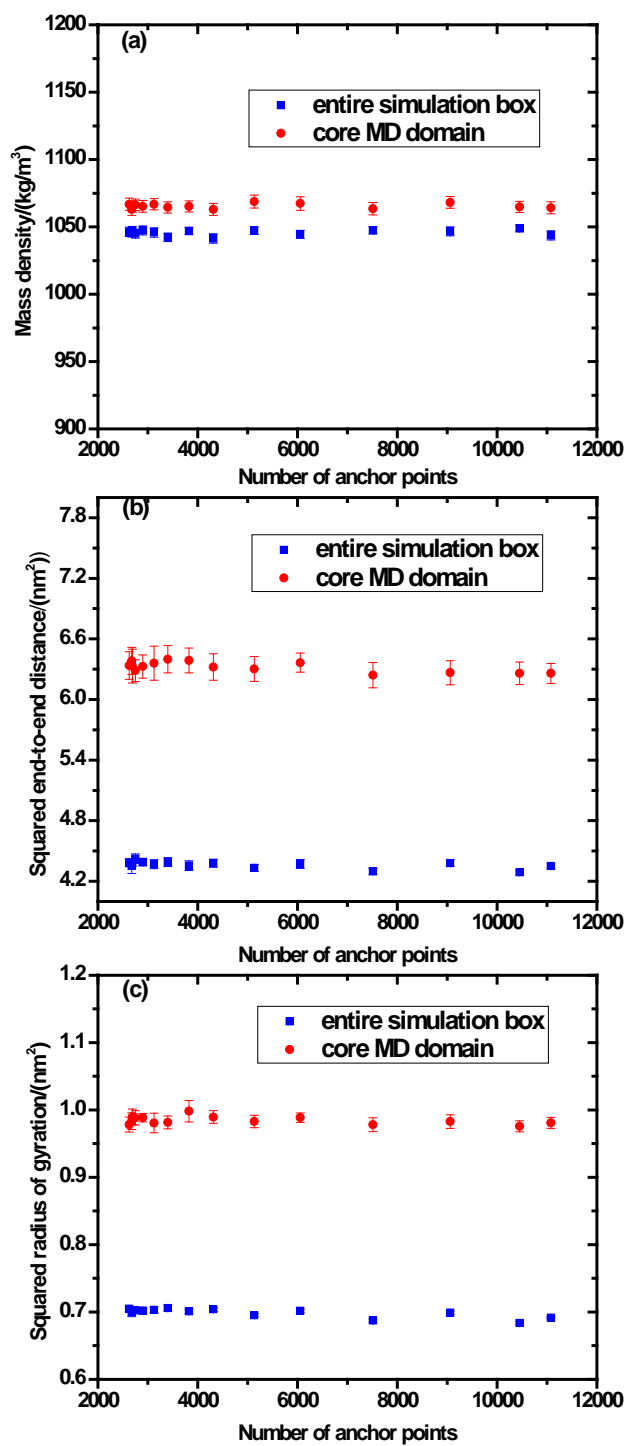


Figure 2.8 Mass density (a), squared end-to-end distance (b) and squared radius of gyration (c) of PS chains in the entire simulation box (blue) and the core MD domain (red) as a function of the number of anchor points.

2.5.3 Size of dissipative-particle-dynamics domain

The size of the entire cubic particle simulation region has been fixed at $(21.39 \text{ nm})^3$ during all computations. The length of each dimension of the core MD domain size is therefore $L_{MD} = 21.39 \text{ nm} - 2L_{DPD}$. Also this parameter has a range of practical usefulness: If L_{MD} is smaller than a critical limit, i.e. when the end-to-end distance of PS chains becomes larger than the core domain size, it cannot map the PS structure under SBCs correctly. On the other hand, the core MD domain also should not cover too much of the entire box size, as otherwise the DPD domain will be too small to mimic the randomness brought about by collisions with particles, which in reality would exist outside the particle domain. It has been observed that for surrounding DPD domain thicknesses between 2.0 ~ 8.0 nm, and corresponding MD core dimensions between 17.39 nm and 5.39 nm, the mass density (Figure 2.9 (a)), the squared end-to-end distance (Figure 2.9 (b)) and the squared radius of gyration (Figure 2.9 (c)) of PS are constant and have small error bars. The standard deviations from UQ analysis reflect that the variation of mass density, squared end-to-end distance, squared radius of gyration, diffusion coefficient and radial distribution function of PS were calculated under both SBC and PBC.

2.5.4 Comparison with molecular dynamics simulation under periodic boundary condition

The recent work in our group has demonstrated that the SBC MD simulation under a standard force constant 2.32 N/m can reproduce the structural properties of polymer chains in the PBC MD simulations very well¹⁷, i.e. end-to-end distance and radius of gyration. To verify further the validity of our non-periodic, stochastic boundary conditions in different ranges of input parameters, we performed the SBC MD simulations with a stronger force constant (9.309 N/m), a denser anchor point profile (8775 anchor points distributed in the DPD domain of 2.0 nm thickness) in this work. Mass density, squared end-to-end distance, squared radius of gyration, diffusion coefficient and radial distribution function of PS were calculated under both SBC and PBC. Table 2.3 and Figure 2.10 demonstrate that the SBC MD simulation reproduces the polymer properties of PBC MD simulation very well. It was also observed that both the static and the kinetic properties (i.e. diffusion coefficient) of PS chains evaluated from SBC MD

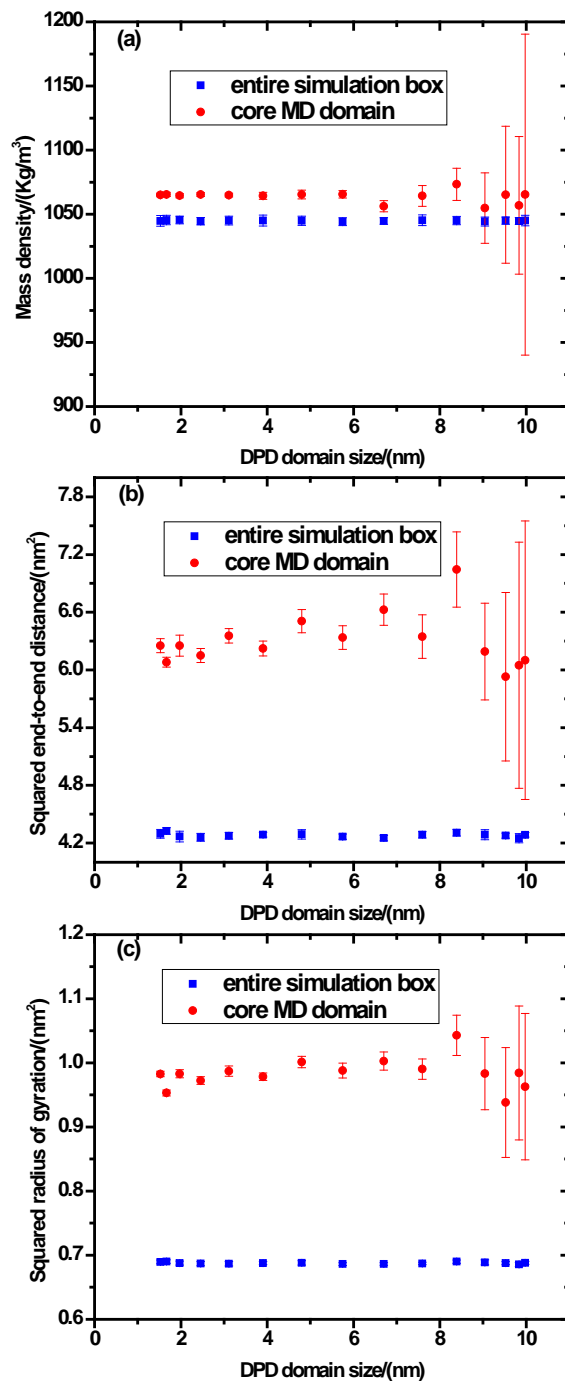


Figure 2.9 Mass density (a), squared end-to-end distance (b) and squared radius of gyration (c) of PS chains in the entire simulation box (blue) and the core MD domain (red) as a function of the DPD domain size. Note that the squared end-to-end distance for DPD size parameters larger than 6.5 nm are no longer of sufficient accuracy.

Condition	Mass density (kg/m ³)	Squared end-to-end distance (nm ²)	Squared radius of gyration (nm ²)	Diffusion coefficient (m ² /s)
PBC	1047.401±0.271	6.145±0.189	0.981±0.016	(9.112±0.166)×10 ⁻¹⁰
SBC	1064.538±3.321	6.223±0.195	0.979±0.015	(8.923±0.402)×10 ⁻¹⁰

Table 2.3 Comparison of properties of PS chains at 300 K estimated by PBC and SBC molecular dynamics simulations. The original PS chains contain 20 beads in case of the PBC simulations. The PBC and the SBC simulations are performed under identical conditions except the chosen boundary condition. The SBC values are obtained only from the core region. For all quantities we have given the standard deviation. For the static quantities (mass density, squared end-to-end distance, squared radius of gyration), the standard deviations were based on the statistical fluctuation at different simulation times for three different parallel simulations. For the dynamics quantity (diffusion coefficient), the standard deviation was based on the standard errors of linear fitting for three different parallel simulations.

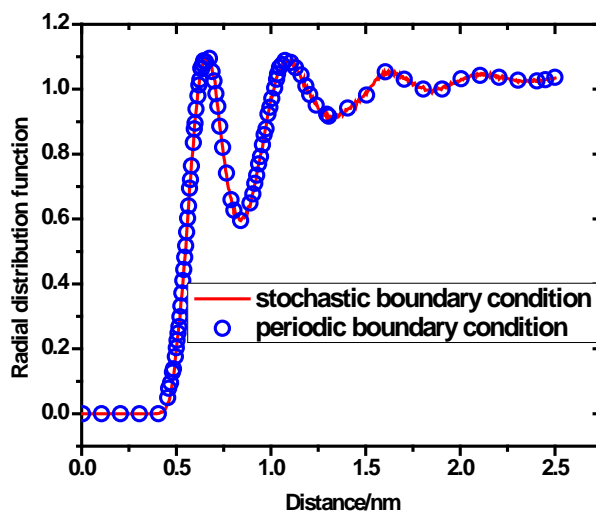



Figure 2.10 Non-bonded radial distribution function for polystyrene chains estimated in the periodic boundary condition (PBC) and stochastic boundary condition (SBC) model.



simulations present a good agreement with PBC MD simulations. Thus the SBC MD approach can be classified as a simulation tool robust with respect to the choice of its input parameters used to control the nonperiodic, stochastic boundary conditions. This makes it a robust component of the recently developed hybrid MD-FE framework^{15, 16}.

2.6 Summary and conclusions

Molecular dynamics simulations using nonperiodic, stochastic boundary conditions (SBC) are essential ingredients in hybrid particle-continuum coupling schemes for the structural mechanics of materials. Our implementation has several crucial input parameters which define these boundary conditions and which cannot be determined simply by physical considerations. They cover the number and distribution of anchor points, which affect the coupling to the finite-element part of the hybrid calculations, the thickness of the surrounding DPD region, where they are located, and the force constant between them and selected polymer beads. We have used the technique of uncertainty quantification to establish their influence on selected simulation results or quantities of interest (QoI) and thus to define safe ranges for these parameters, to be used in future work. As QoI, we choose mass density, squared end-to-end distance and squared radius of gyration, the center-of-mass tracer diffusion coefficient of the polymer chains, and the radial distribution function between nonbonded monomers. The validation has been done using an established coarse-grained model of polystyrene (one bead per chemical repeat unit) at 300 K.

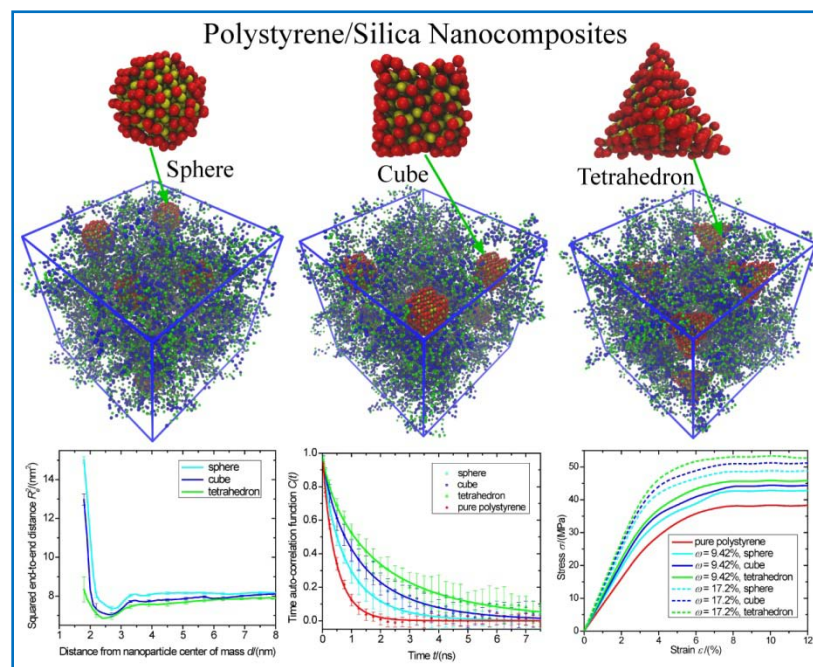
It turns out that, provided the thickness of the surrounding DPD domain and the inner core of the MD domain are both large enough, the SBC method is surprisingly robust with respect to its parameters. All parameter ranges have a limit, below which their choices are unsafe. Above this limit there is usually quite a wide range of values which are safe to use. Here, the calculated QoI are independent of the precise value of the SBC input parameters. Moreover, SBC simulations with their parameters set in the safe range also reproduce the results of reference MD calculations for the same system using traditional periodic boundary conditions. In summary, we can conclude the molecular dynamics under SBC is a method which is robust in a technical sense and accurate when compared to established simulation protocols. This method is safe to use the particle domain in horizontal hybrid schemes, which couple detailed molecular dynamics of the region of interest to a finite element description of the surroundings.

References

- [1] D.C. Rapaport, The art of molecular dynamics simulation, Cambridge University Press 2004.
- [2] D. P. Landau, K. Binder, A Guide to Monte-Carlo Simulations in Statistical Physics (Third Edition), Cambridge University Press 2009.
- [3] P. J. Hoogerbrugge, J. M. V. A. Koelman, Europhys. Lett. 19, 155 (1992).
- [4] O.C. Zienkiewicz, The Finite Element Method in Engineering Science, London: McGraw Hill 1971.
- [5] P. Wriggers, Nonlinear Finite Element Methods, Springer, Berlin 2008.
- [6] T. Belytschko, S. P. Xiao, J. Mult. Comput. Engrg.. 1, 115 (2003).
- [7] L.R. Khare, S.L. Mielke, J.T. Paci, S. Zhang, R. Ballarini, G.C. Schatz and T. Belytschko, Phys. Rev. B. 75, 075412 (2007).
- [8] S.L. Zhang, R. Khare and Q. Lu and T. Belytschko, Int. J. Numer. Methods Engrg. 70, 913 (2007).
- [9] D. Davydov, J.P. Pelteret, and P. Steinmann, Comput. Methods Appl. Mech. Eng.. 277, 260 (2014).
- [10] M. Xu, R. Gracie and T. Belytschko, Int. J. Numer. Methods Engrg.. 81, 1635 (2010).
- [11] H. Ben Dhia, G. Rateau, Int. J. Numer. Methods Engrg.. 62, 1442 (2005).
- [12] P.T. Bauman, H. Ben Dhia, H. Elkhodja, J.T. Oden, S. Prudhomme, Comput. Mech. 42, 511 (2008).
- [13] L. Chamoin, J.T. Oden, S. Prudhomme, Comput. Methods Appl. Mech. Engrg.. 197, 3530 (2008).
- [14] P.T. Bauman, J.T. Oden, S. Prudhomme, Comput. Methods Appl. Mech. Engrg.. 198, 799 (2009).
- [15] S. Pfaller, G. Possart, P. Steinmann, M. Rahimi, F. Müller-Plathe, and M.C. Böhm, Comput. Mech. 49, 565 (2012).
- [16] S. Pfaller, M. Rahimi, G. Possart, P. Steinmann, F. Müller-Plathe, and M.C. Böhm, Comput. Methods Appl. Mech. Eng. 260, 109 (2013).
- [17] M. Rahimi, H.A. Karimi-Varzaneh, M.C. Böhm, F. Müller-Plathe, S. Pfaller, G. Possart, and P. Steinmann, J. Chem. Phys.. 134, 154108 (2011).
- [18] H. A. Karimi-Varzaneh and F. Müller-Plathe, in *Multiscale Molecular Methods in Applied Chemistry* (Topics in Current

- Chemistry), Vol 307 (Eds: B. Kirchner and J. Vrabec), Springer Verlag, Heidelberg, Germany 2012, Ch. 9.
- [19] H. A. Karimi-Varzaneh, N. F. A. van der Vegt, F. Müller-Plathe, and P. Carbone, *ChemPhysChem*, 13, 3428 (2012).
- [20] M. Berkowitz and J.A. McCammon, *Chem. Phys. Lett.*, 90, 215 (1982).
- [21] A. Brünger, C.L. Brooks III and M. Karplus, *Chem. Phys. Lett.*, 105, 495 (1984).
- [22] D. Davydov, E. Voyiatzis, G. Chatzigeorgiou, S.Y. Liu, P. Steinmann, M. C. Böhm, F. Müller-Plathe, *Soft Materials*, 12, S142 (2014).
- [23] B. Schieche. Unsteady adaptive stochastic collocation methods in Uncertainty Quantification. PhD thesis, TU Darmstadt, 2012.
- [24] R. C. Smith, *Uncertainty Quantification: Theory, Implementation, and Applications*, SIAM, 2014.
- [25] R. Wagner, R. Moon, J. Pratt, G. Shaw and A. Raman, *Nanotechnology*, 22, 455703 (2011).
- [26] B. Kouchmeshky, N. Zabaras, *Computational Material Science*, 48, 213 (2010).
- [27] S. Sriramula, M.K. Chryssanthopoulos, *Composites Part A: Applied Science and Manufacturing*, 40, 1673 (2009).
- [28] H.A. Karimi-Varzaneh, H. Qian, X. Chen, P. Carbone, and F. Müller-Plathe, *J. Comput. Chem.*, 32, 1475 (2011).
- [29] H. Qian, P. Carbone, X. Chen, H.A. Karimi-Varzaneh, C.C. Liew, and F. Müller-Plathe, *Macromolecules*, 41, 9919 (2008).
- [30] T.V.M. Nodoro, E. Voyiatzis, A. Ghanbari, D.N. Theodorou, M.C. Böhm and F. Müller-Plathe, *Macromolecules*, 44, 2316 (2011).
- [31] A. Ghanbari, T.V.M. Nodoro, F. Leroy, M. Rahimi, M.C. Böhm and F. Müller-Plathe, *Macromolecules*, 45, 572 (2011).
- [32] A. Ghanbari, M. Rahimi, and J. Dehghany, *J. Phys. Chem. C*, 117, 25069 (2013).
- [33] D. Reith, M. Pütz and F. Müller-Plathe, *J. Comput. Chem.*, 24, 1624 (2003).
- [34] G. Milano and F. Müller-Plathe, *J. Phys. Chem. B*, 109, 18069 (2005).

3. Role of Interfacial Area for Structure and Dynamics in Polymer Nanocomposites: Molecular Dynamics Simulations of Polystyrene with Silica Nanoparticles of Different Geometries



3.1 Abstract

Polystyrene nanocomposites containing a fraction of silica nanoparticles of different geometries (sphere, cube and regular tetrahedron) have been simulated using a molecular dynamics method at a coarse-grained scale. Structural and dynamic properties of the polymer chains in the presence of the nanoparticles have been analyzed in terms of the nanoparticle mass fraction and geometrical shape. It has been found that the dimension of the polymer chains in the interphase expands due to the polymer-nanoparticle interaction. Their global dimension (averaged over the whole sample), however, shrinks as a function of the total surface area of the nanoparticles. The conformational changes of polymer chains in the interphase are monitored by a chain orientation parameter. The profiles of the chain dimension and orientation as a function of their distance from the nanoparticle center of mass show that the interphase thickness is roughly equal to the radius of gyration of the polymer chains. Moreover, the dynamic behavior of the polymer chains in nanocomposites is analyzed by the center of mass diffusion coefficient, the relaxation time of the chain end-to-end vector and the characteristic escape time of the polymer chains from the interphase. Compared with neat polymers, both the global and local chain dynamics in nanocomposites is hindered with an increasing nanoparticle mass fraction and with an increasing surface area. The local chain dynamics in the interphase is stronger affected by the surface area of the nanoparticles than the global one. Specifically, the global diffusion coefficient of polymer chains is almost linearly reduced with the total surface area of the nanoparticles, whereas the global relaxation time of the chain end-to-end vector is almost linearly increased with it. Their interphase relaxation time increases superlinearly with the surface area of an individual nanoparticle. Additionally, the characteristic escape time of polymer chains from the interphase is largely influenced by the geometrical shape of the nanoparticle. Due to their larger surface area, tetrahedral nanoparticles impede the global and local chain dynamics more efficiently than cubic nanoparticles, followed by spherical nanoparticles. Uniaxial tensile tests show that both the Young's modulus and yield strength of polymer nanocomposites increase monotonically with their total interphase area. Our simulations demonstrate that polymer structural and dynamic properties are both largely influenced by a common parameter, i.e. the interphase area which has a fundamental influence on the mechanical properties of polymer nanocomposites.

3.2 Introduction

Polymer nanocomposites¹⁻³ are typical heterogeneous materials that contain a polymer matrix and a fraction of nanofillers, e.g. spherical silica^{4,5}, fibrous carbon^{6,7} and layered clay^{8,9}. Polymer nanocomposites surpass the properties of neat polymers and show good thermal¹⁰⁻¹² and electrical conductivities^{13,14} as well as high mechanical strength^{2,5,7}. Their mechanical properties are attributed to their interfacial region in which the chain behavior differ from the bulk¹. An increase in the interphase area between the matrix and the nanofiller is coupled to a strengthened modification of the mechanical properties of polymer nanocomposites¹⁵. As we know, the macroscopic properties of polymer nanocomposites are largely influenced by the molecular structure and conformation of the matrix chains. The properties of polymer chains, in turn, are affected by the presence of nanoparticles¹⁶⁻¹⁸. Both the nanoparticle mass fraction and their geometrical shape (and hence their surface area) are the factors commonly considered to improve the properties of polymer nanocomposites in industrial applications^{1-4,9,18}. It is thus of theoretical and practical relevance to understand the possible correlations between both the local as well as global behavior of polymer chains and the observed nanoparticle characteristics.

Experimental techniques have been employed to investigate the changes of structural and dynamic properties of polymer chains in nanocomposites. For instance, the global dimension of polymer chains in nanocomposites (i.e. chain radius of gyration) has been analyzed by scattering experiments¹⁹⁻²⁵. The nanofiller-induced perturbations of global chain dimensions in nanocomposites depend on the relative ratio of the chain radius of gyration and the nanoparticle size. In general, polymer chains expand if they are much larger than the nanoparticles^{21,22}. In contrast, they are reduced if the chain dimension is roughly equal to or smaller than the nanoparticle size. From small angle neutron scattering of poly(dimethyl siloxane)/polysilicate nanocomposites, Nakatani et al.²⁵ have found that the chain dimension reduces in the presence of nanoparticles for short chains which have approximately the same size as the nanofiller and increases for longer chains. Similar conclusions have been also reported by other researchers in polystyrene/polysilicate²² and polystyrene/carbon nanotube^{19,24} nanocomposites. Additionally, simulation studies have been performed to investigate the impact of nanoparticles on the global chain dimension in different nanocomposites systems. By applying a self-consistent polymer

reference interaction side model²⁶ to simulate a polymer melt containing nanoparticles, Frischknecht et al.²⁷ have found that the matrix chains swell with the nanoparticle concentration if the nanoparticle radii are smaller than the chain radii of gyration. Erguney et al.^{28,29} have employed a Monte Carlo (MC) method to simulate a nanocomposite defined by polyethylene chains and nanoparticles formed from the self cross-linking of the same chains. They have found that the chain dimension increases relative to the chain in the pure melt when the matrix chains are larger than the nanoparticles and reduces when the matrix chains are smaller. It is worth mentioning that some investigations^{30–32} have shown that the overall chain configuration is only weakly influenced by the nanoparticle concentration and size.

Due to the polymer-nanoparticle interaction the motion of the matrix chains in nanocomposites is impeded in comparison to the underlying neat polymer^{33–35}. The global suppression of the dynamics^{36–42} has been investigated experimentally and theoretically by tracer diffusion and structural relaxation of the polymer chains in nanocomposites. As an example, a reduction of the diffusion coefficients of the matrix chains in nanocomposites relative to the neat polymers have been reported by Hu et al.³⁷ in dynamic secondary ion mass spectrometry (DSIMS) experiments of poly(methyl methacrylate)/organosilicate nanocomposites. By performing molecular dynamics (MD) simulations with the Kremer-Grest nanocomposite model^{43,44}, Desai et al.³⁸ have found that the center of mass diffusion coefficient of the matrix chains in nanocomposites decreases with increasing nanoparticle concentration when the polymer-nanoparticle interaction is attractive, whereas it increases when the interaction is repulsive. Similar phenomena have been also observed by Gao et al.³⁴ and Liu et al.³⁵ in MD simulations of a model polymer-nanoplate and a polymer-nanosphere nanocomposite. Moreover, Oh and Green³⁹ have concluded from broadband dielectric spectroscopy experiments that the overall relaxation dynamics of the matrix chains in athermal mixtures of polystyrene and polystyrene-grafted golden nanoparticles is influenced by the nanoparticle concentration. Similar conclusions have been also obtained by Chanmal et al.³⁶ and Mijović et al.⁴⁰ in poly(vinylidene fluoride)/BaTiO₃ and polyisoprene/silicate nanocomposites. Smith et al.⁴¹ and Starr et al.⁴⁵ have found from MD simulations that the overall relaxation dynamics of the matrix chains is largely affected by the polymer-nanoparticle interaction. In general, the overall polymer relaxation in nanocomposites for attractive interactions is slower than for repulsive ones. The global chain dynamics in

nanocomposites has been also investigated in terms of macroscopic properties such as the melt viscosity⁴⁶ or the glass transition temperature⁴⁷.

The global changes of the chain structure and dynamics in nanocomposites are mainly attributed to the local perturbations of the chain properties in the vicinity of nanoparticles¹⁸. The polymer chains in this region exhibit a local expansion or contraction as well as a preferred orientation relative to unperturbed chains^{17,48}. The interfacial adsorption at attractive nanoparticles implies that the chains in the interphase move slower than the bulk ones^{2,49}. Experimental methods have intrinsic difficulties to investigate quantitatively the local chain behavior, as local perturbations of chains take place at a molecular scale. MD and MC simulation techniques have been used successfully to study such local changes of polymer properties. Using atomistic MD simulations, Nodoro et al.^{50,51}, Eslami et al.⁵², Barbier et al.⁵³ and Capaldi et al.⁵⁴ have investigated the interphase chain structure and dynamics in polystyrene/silica, polyamide-66/carbon nanotube, poly(ethylene oxide) oligomer/silica and polyethylene/polysilsesquioxane nanocomposites. Local layer structures and a reduction of the chain dynamics in the interphase have been observed in these nanocomposite systems. It can be summarized from the observed results that the local chain properties in the interphase are affected by nanoparticle properties such as the polymer-surface interaction, curvature and grafting state. Similar results have been reported by Ghanbari et al.^{55,56}, Chao et al.^{57,58}, Starr et al.^{42,45} and Vogiatzis et al.⁵⁹⁻⁶¹ using either MC or coarse-grained MD simulations. It should be mentioned that the aforementioned simulations mainly concentrate on the influence of the nanoparticles on the local structure and dynamics of the polymer chains in the interphase versus bulk.

The size of nanoparticles is often of the order of magnitude of the matrix chain. The high surface-to-volume ratio of nanoparticles leads to a considerable increase of the surface area of nanocomposites. The amount of the surface area is thought to have a crucial role in the mechanical enhancement of nanocomposites^{2,48,49}. An increasing nanoparticle mass fraction or an increasing surface area per nanoparticle produces a larger interphase area. Note that the interphase area depends on the geometrical shape of the nanoparticle and thus is changed when having a transition from a nanosphere to a nanoplate^{1,4,18}. Xia et al.⁶² and Luo et al.⁶³ have observed an increase of the elastic modulus with the exfoliation degree of the clay nanofillers in

polyurethane/clay and epoxy/clay nanocomposites, respectively. Mortazavi et al.⁶⁴ and Saber-Samandari et al.⁶⁵ have demonstrated by finite element simulations that mechanical reinforcement effects of cylindrical nanoparticles with low aspect ratios are stronger than that of spherical ones. To our best knowledge, possible correlations between polymer properties and the interphase area of nanocomposites are still far from a systematic understanding. In this contribution, polystyrene nanocomposites containing a fraction of silica nanoparticles of different shapes (sphere, cube and regular tetrahedron) are simulated by using a coarse-grained MD method. It is worth mentioning that (i) the studied particle shapes are intentionally taken to be extremes, in order to highlight the limiting behavior that can be expected as one plays with particle geometry; (ii) the present study allows to compare the influence of different particle geometries and to analyze quantitatively the influence of the interphase area without concomitant change of the nanoparticle concentration (more particles of the same type) or size (more particles of smaller size, but same geometry). Specifically, both structural (i.e. chain dimension and orientation) and dynamic properties (i.e. center of mass diffusion coefficient, decorrelation of the chain end-to-end vector and chain escape behavior from the interphase) of the polymer chains are calculated as a function of the nanoparticle mass fraction and geometrical shape. We aim to understand at a molecular scale the influence of the nanoparticles on both global and local properties of the polymer chains in nanocomposites. Furthermore, we analyze the correlation between the interphase area and mechanical improvements of nanocomposites.

3.3 Simulation systems and computational details

3.3.1 Polystyrene blended with silica nanoparticles of different geometrical shapes

Polymer nanocomposites are generated by blending a fraction of silica nanoparticles of different geometrical shapes (sphere, cube and regular tetrahedron) into a polystyrene matrix. For simplicity the term “regular tetrahedron” is shortened as “tetrahedron” in the following sections. All considered nanocomposite systems are described by a coarse-grained model. It has been developed by Qian et al.⁶⁶ for simulations of atactic polystyrene using the Iterative Boltzmann Inversion (IBI)⁶⁷ method. The model has been also applied to investigate other polystyrene-containing systems^{33,55,56,68,69}. In the adopted mapping scheme, each polystyrene monomer is treated as one bead that is placed at the center of mass of the respective atomistic monomer. To describe reasonably the chirality of the atactic polystyrene chains, two different beads (Figure 3.1) are used to represent R and S repeat units. Both types of beads are identical except for their chirality. The structure of the coarse-grained silica nanoparticles is constructed according to the workflow of Ghanbari et al.^{55,56,70}. Each SiO₂ formula unit in an atomistic silica crystal is grouped into a silica bead located at the position of the silicon atom. The total mass of the atomistic silica crystal is uniformly distributed to the silica beads. After removing all oxygen atoms from the atomistic silica crystal (Figure 3.1a), the coordinates of the remaining silicon atoms are taken as centers of the silica beads in the coarse-grained structures (Figure 3.1b).

Subsequently, the configuration of silica nanoparticles in the chosen geometrical shape is constructed by cutting the coarse-grained silica structure according to the associated geometrical rules. The center of mass of the silica crystal is taken to be the origin of the Cartesian system, and the coordinates of the i -th silica bead are labelled as x_i, y_i and z_i , respectively. All silica beads whose coordinates satisfy the geometrical condition (i), i.e. $x_i^2 + y_i^2 + z_i^2 \leq r^2$, constitute a spherical nanoparticle with a radius of r . The geometrical conditions to obtain a cubic and tetrahedral nanoparticle are expressed by the inequality conditions (ii) and (iii). Here, L_c and L_t refer to the side length of the cubic and tetrahedral nanoparticles.

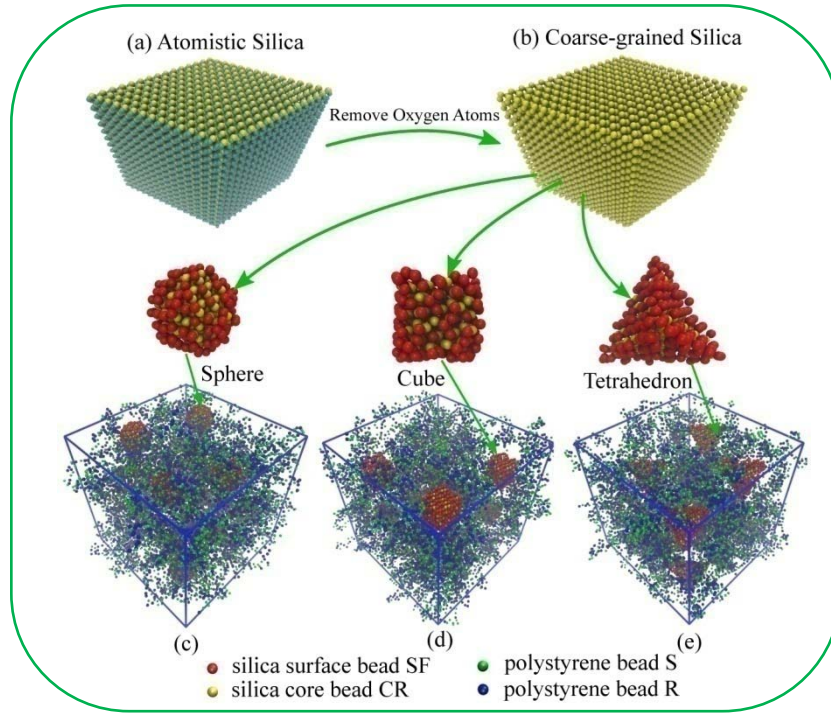


Fig. 3.1 Schematic graph of polystyrene nanocomposites blended with silica nanoparticles in different geometrical shapes. The structural details of three different kinds of nanoparticles are listed in Table 3.1. Note that the size of the nanoparticles outside the simulation box is scaled by a factor of 2.5 relative to the associated one inside the box.

$$\begin{cases} -\frac{L_c}{2} \leq x_i \leq \frac{L_c}{2} \\ -\frac{L_c}{2} \leq y_i \leq \frac{L_c}{2} \\ -\frac{L_c}{2} \leq z_i \leq \frac{L_c}{2} \end{cases} \quad (\text{ii})$$

$$\begin{cases} \frac{\sqrt{2}}{4} x_i L_t - \frac{\sqrt{2}}{4} y_i L_t - \frac{\sqrt{2}}{4} z_i L_t + \frac{1}{8} L_t^2 \geq 0 \\ -\frac{\sqrt{2}}{4} x_i L_t + \frac{\sqrt{2}}{4} y_i L_t - \frac{\sqrt{2}}{4} z_i L_t + \frac{1}{8} L_t^2 \geq 0 \\ \frac{\sqrt{2}}{4} x_i L_t + \frac{\sqrt{2}}{4} y_i L_t + \frac{\sqrt{2}}{4} z_i L_t + \frac{1}{8} L_t^2 \geq 0 \\ -\frac{\sqrt{2}}{4} x_i L_t - \frac{\sqrt{2}}{4} y_i L_t + \frac{\sqrt{2}}{4} z_i L_t + \frac{1}{8} L_t^2 \geq 0 \end{cases} \quad (\text{iii})$$

The structural information of the nanoparticles in spherical, cubic and tetrahedral shapes is given in Table 3.1. To treat the interaction between the polymer and the nanoparticle physically reliable, silica beads are divided into two different sets, namely core and surface beads (Figure 3.1). The inner beads are chemically bonded to four nearest neighboring beads. The outer ones have less than four chemical bonds. Each individual nanoparticle in the three different shapes contains the same number of beads, whereas the ratio of the surface to core beads differs (Table

3.1). It should be mentioned that the surface beads have the same molar mass as the core beads, but have a stronger interaction with the polymer compared to the core beads⁵⁶.

Table 3.1 Structural information of coarse-grained silica nanoparticles in different geometrical shapes used in the MD simulations. For an explanation of surface and core silica beads see Section 3.3.1. Here, R_c and R_i are the radii of a circumscribed and inscribed sphere of nanoparticles. L is the cubic or tetrahedral side length. The surface area A of an individual nanoparticle is calculated by an ideal sphere, cube and tetrahedron, i.e. using r , L_c and L_t of the conditions (i)-(iii), see text. The labels S , C and T refer to sphere, cube and regular tetrahedron.

Type of nanoparticle	Geometric shape of nanoparticle	Number of surface beads	Number of core beads	Radius of circumscribed sphere R_c (nm)	Radius of inscribed sphere R_i (nm)	Side length L (nm)	Surface area A (nm ²)
1	S	141	222	1.50	1.50	-	28.2
2	C	170	193	2.20	1.27	2.52	38.1
3	T	192	171	3.18	1.06	5.18	46.7

The initial configurations of the nanocomposite systems are generated by the following procedure. In the first step, the centers of mass of the silica nanoparticles are distributed randomly in the simulation box. Subsequently, the polystyrene chains grow gradually bead-by-bead in the remaining space of the simulation box. The chiral type of each polystyrene bead is randomly chosen. During the generation of a new polystyrene chain, possible overlaps with the existing polystyrene and silica beads are prevented by using a self-avoiding random walk procedure⁷¹.

3.3.2 Computational details of molecular dynamics simulations

The composition details of the nanocomposite systems are listed in Table 3.2. Note that their initial mass densities prepared by the procedures in Section 3.3.1 are roughly 30% smaller than the respective equilibrium values to reduce possible overlaps between different molecules. The initial structures differ strongly from the equilibrium one. Prior to the production runs they are

equilibrated by the following procedure. At first, the initial configurations of all nanocomposite systems are simulated in the NVT ensemble for 10 ns at 590 K. The simulation ensemble is then switched to NPT for a further relaxation of 50 ns at the same temperature and standard atmospheric pressure (1 bar). After the relaxation in the NPT ensemble, all nanocomposite systems reach a stable density (Table 3.2).

Table 3.2 Composition of the nanocomposite systems containing nanoparticles of different shapes used in MD simulations. The silica beads comprise the surface and core beads, cf. Table 3.1. We have employed one monomer of the polystyrene chains, i.e. one bead, to define the length unit of the polymer. The mass of each polystyrene and silica bead in the coarse-grained system is 0.104 kg/mol and 0.0639 kg/mol, respectively.

System	Number of polymer chains N_{ps}	Length of polymer chains /(bead)	Number of nanoparticles N_{np}	Number of silica beads	Geometry of nanoparticles	Mass fraction of nanoparticles/(%)	Mass density after equilibrium/(g/cm ³)
1	600	25	7	363	S	9.42	0.99
2	600	25	14	363	S	17.2	1.06
3	600	25	7	363	C	9.42	1.01
4	600	25	14	363	C	17.2	1.09
5	600	25	7	363	T	9.42	1.02
6	600	25	14	363	T	17.2	1.11
7	600	25	0	0	-	0	0.93

The MD production runs are performed at a temperature of 590 K and at standard atmospheric pressure under NPT conditions. Periodic boundary conditions are employed in all Cartesian directions. The Berendsen algorithm is applied in all directions to control the system pressure (coupling time 5 ps) and temperature (coupling time 0.2 ps). All calculated structural and dynamic properties of the polymer chains in all nanocomposite systems are averaged over 15 different initial configurations. Every production run requires 7.5 ns; properties are calculated every 10 ps.

After the melt simulations, all considered systems are cooled down from 590 K to 100 K at a rate of 5 K ns^{-1} . Note that the glass transition temperature of pure polystyrene in our coarse-grained model is roughly 170 K^{67} . Subsequently, uniaxial tensile deformations are applied to all considered systems by MD simulations under $NLP_{\perp}T$ conditions at the same temperature. Specifically, the length of the simulation box is elongated with a constant rate in the y direction, while the box lengths in the two perpendicular directions are coupled to a pressure bath by the Berendsen algorithm during the uniaxial elongation. The relation between the strain ε and the simulation time t is expressed as $\varepsilon(t) = \frac{vt}{l_0} \times 100\%$, where l_0 and v refer to the initial box length in the tensile direction and the deformation rate (i.e. 15 nm ns^{-1}). Young's moduli of all systems are determined in the elastic region ($\varepsilon \leq 3\%$) of the obtained stress-strain curves.

3.4 Results and discussion

3.4.1 Structural properties of polymer chains in nanocomposites

Chain dimensions in the presence of nanoparticles. The squared end-to-end distances R_e^2 (Figures 3.2 (a) and (b)) and squared radii of gyration R_g^2 (Figures 3.2 (c) and (d)) of polymer chains are calculated as a function of the distance d of their center of mass from the nearest nanoparticles' center of mass at nanoparticle mass fractions $\omega = 9.42\%$ or 17.2% . The R_e^2 and R_g^2 are both obtained by averaging over all nanoparticles and time frames. The polymer chains are sorted into 80 spherical bins of the same thickness of 0.1 nm concentrically arranged around the centers of mass of the nanoparticles. It should be mentioned that the centers of mass of all polymer chains lie outside the inscribed spheres of the nanoparticles.

At larger distances, i.e. $d > 3.2 \text{ nm}$, the R_e^2 of the polymer chains in all considered nanocomposites start to approach a plateau. The R_e^2 for the nanocomposites containing the cubic or tetrahedral nanoparticles approach a common plateau value more slowly than samples with spherical nanoparticles. This indicates that the influence of cubic and tetrahedral nanoparticles on the dimension of the polymer chains is longer ranged than that of spherical nanoparticles. The reason is that the radius of the circumscribed sphere of a cubic or tetrahedral nanoparticle is

larger than the radius of a spherical nanoparticle (Table 3.1). Below a distance of 2.5 nm, the R_e^2 increase as the polymer chains move closer to the nanoparticle surface. This demonstrates that polymer chains at close distances are forced to stretch by the interaction with nanoparticle surfaces. In Figures 3.2 (a) and (b) we can see that the stretching of polymer chains in the interphase of the nanocomposites blended with tetrahedral nanoparticles is weaker than in the ones blended with cubic or spherical nanoparticles. At an intermediate distance of 2.5 to 3.2 nm all curves have a minimum. This distance range corresponds to roughly the radius of the (spherical) nanoparticle (1.5 nm) plus one R_g of the unperturbed polymer chains (1.16 nm). The compression at a distance to the surface of about one or two R_g is a known effect^{51,56}, as is the expansion at very short distances mentioned above: As the first few beads of the polymer coil feel the presence of the nanoparticle surface, the coil is compressed in the directions of the surface normal. Those chains which approach even closer, have to expand tangential to the surface. This expansion overcompensates the compression in the normal direction. As a result, R_e first decreases and then increases as the chains approach the nanoparticle.

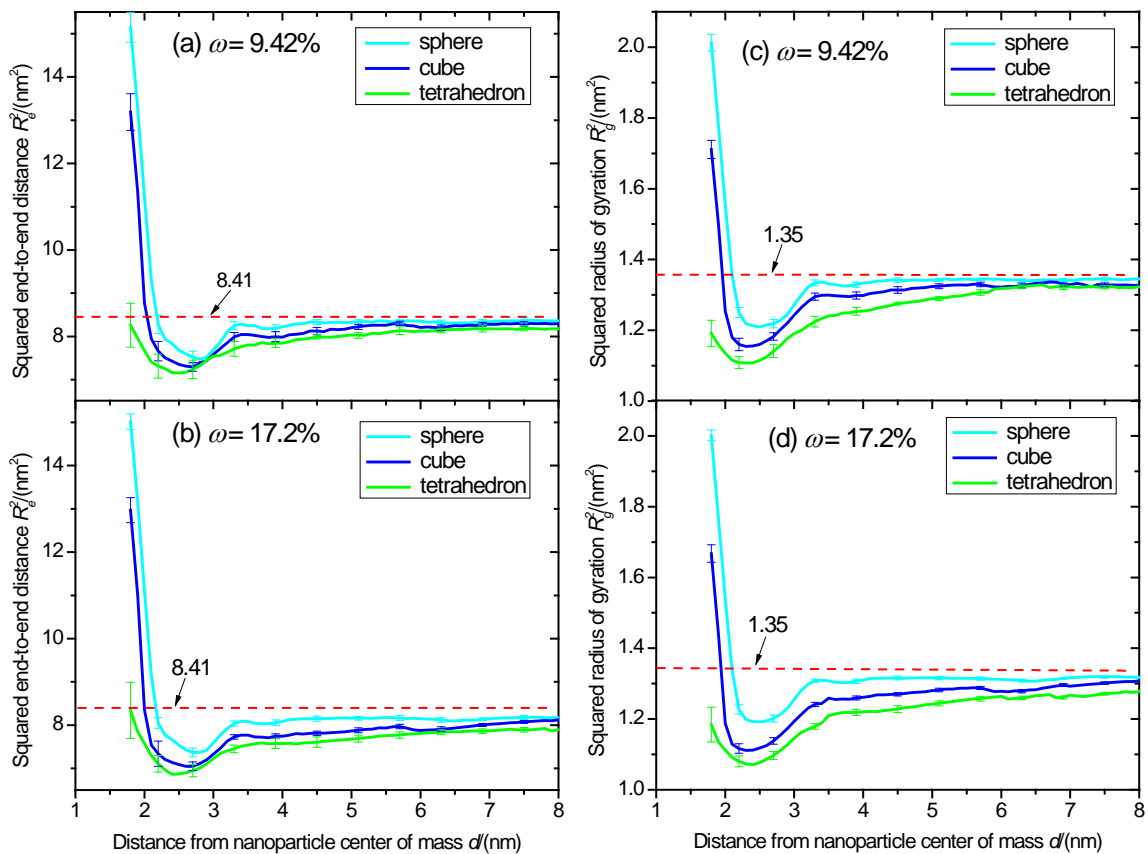


Fig. 3.2 Squared end-to-end distance R_e^2 (a and b) and squared radius of gyration R_g^2 (c and d) of polymer chains in nanocomposite systems blended with nanoparticles of different geometrical shapes and different mass fraction ω as a function of the distance d from the nanoparticle center of mass. The horizontal lines refer to R_e^2 or R_g^2 of polymer chains in neat polystyrene. The vertical lines at selected data points represent the error bars. In all other figures they have the same meaning.

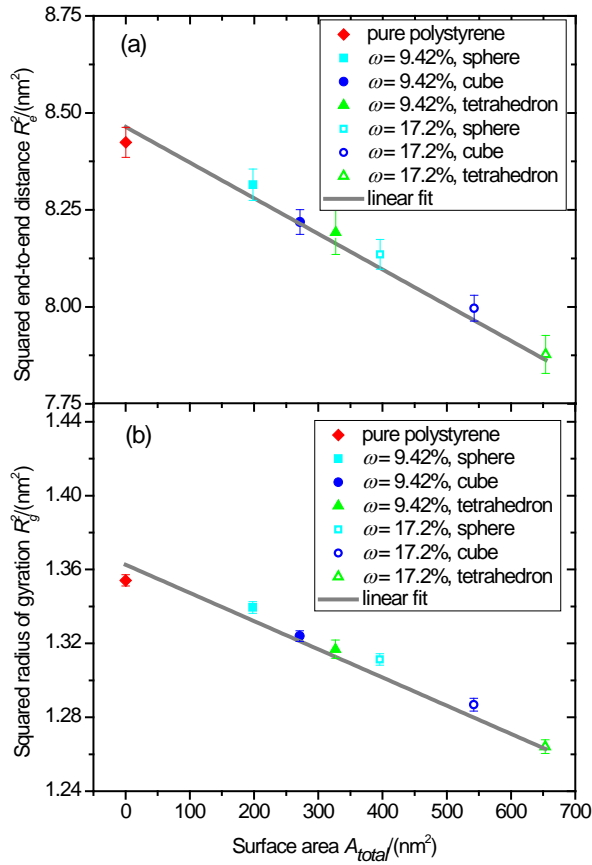


Fig. 3.3 Squared end-to-end distance R_e^2 and squared radius of gyration R_g^2 averaged over all chains in nanocomposites containing nanoparticles of different geometrical shapes and mass ratios ω as a function of total nanoparticle surface area A_{total} . The solid lines represent linear fits: (a) $R_e^2 = -9.19 \times 10^{-4} A_{total} + 8.42$ (in nm²); (b) $R_g^2 = -1.51 \times 10^{-4} A_{total} + 1.37$ (in nm²).

According to Figures 3.2 (a) and (b), a significant influence of the nanoparticle mass fraction on the profiles of the R_e^2 with the distance d cannot be observed, indicating that the phenomenon is local. The profiles of the R_g^2 and R_e^2 (Figures 3.2 (c) and (d)) as a function of the distance d are

similar. The overall averages of R_e^2 and R_g^2 as a function of the total surface area A_{total} of the nanoparticles are presented in Figures 3.3 (a) and (b). Both are almost linearly reduced with the total surface area A_{total} of the nanoparticles. The fits can be extrapolated to zero interphase estimates of R_e^2 (8.42 nm^2) and R_g^2 (1.37 nm^2). They are close to the calculated values for neat polystyrene of 8.41 and 1.35 nm^2 . Our simulations show that the addition of nanoparticles leads

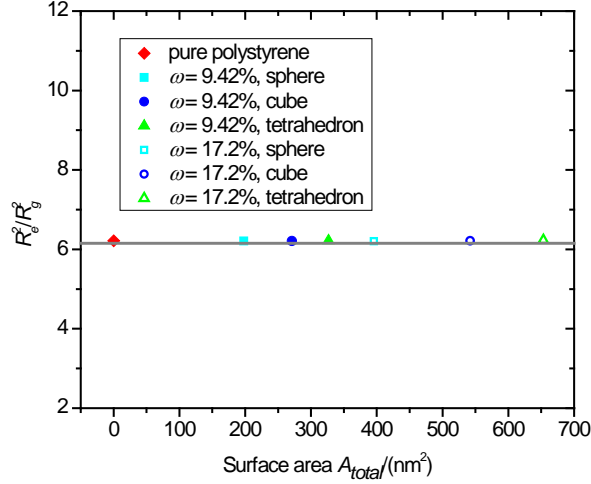


Fig. 3.4 Ratio $\frac{R_e^2}{R_g^2}$ of the squared end-to-end distance and squared radius of gyration of polymer chains as a function of the total surface area A_{total} of nanoparticles. The solid line refers to a model with $\frac{R_e^2}{R_g^2} \approx 6.2$ deviating slightly from an ideal polymer chain.

to an overall shrinking of the polymer chains. At moderate distances it overcompensates the expansion of the chains which are in immediate contact with the nanoparticles. Our findings are consistent with experimental and theoretical investigations^{17,25,27-29} also reporting a reduction of the global polymer dimension in nanocomposites. This is caused by the strong excluded volume effect of the nanoparticles when the dimension of the polymer coils is comparable to or smaller than the nanoparticles size. As shown in Figure 3.4, the ratio $\frac{R_e^2}{R_g^2}$ for all nanocomposite systems is approximately equal to the one (≈ 6.2) of pure polystyrene. This reflects that the polymer coils in the presence of nanoparticles still keep their slight deviation from an ideal chain behavior as observed for the neat polymer.

Chain orientation in the interphase. The orientation parameter of the chain end-to-end vector relative to the radial direction of the nanoparticles is defined by the second-order Legendre polynomial,

$$\langle P_2 \rangle = \frac{3}{2} \langle \cos^2 \beta \rangle - \frac{1}{2} \quad (3.1)$$

where β refers to the angle between the chain end-to-end vector \vec{R}_e and the vector \vec{X} pointing from the nanoparticle center of mass to the midpoint of the vector \vec{R}_e . The bracket $\langle \dots \rangle$ denotes averaging over polymer chains, nanoparticles and frames. Note that $\langle P_2 \rangle$ is nearly zero if the polymer chains are randomly orientated; $\langle P_2 \rangle$ is -0.5 if all \vec{R}_e are perpendicular to their associated \vec{X} . Figure 3.5 presents the profiles of $\langle P_2 \rangle$ of the polymer chains as a function of their distance d from the nanoparticle's center of mass. Specifically, $\langle P_2 \rangle$ is roughly zero at

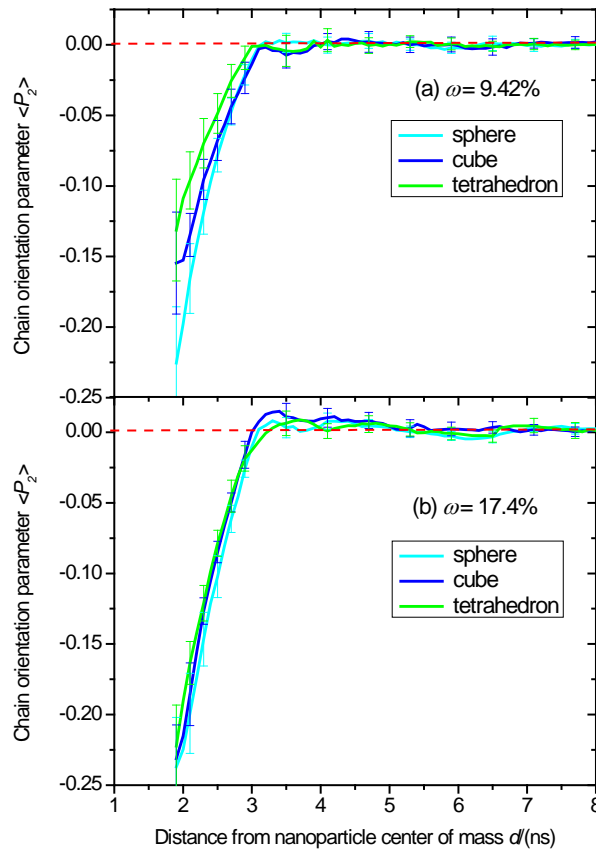


Fig. 3.5 Orientation parameter $\langle P_2 \rangle$ of polymer chains in nanocomposite systems blended with nanoparticles of different geometrical shapes as a function of the distance d from the nanoparticle center of mass and the nanoparticle mass fraction.

larger distances (i.e. $d > 4$ nm). This means that the polymer chains have a random orientation, when they are far from the nanoparticles. In their vicinity ($2 \text{ nm} < d < 3.2 \text{ nm}$), $\langle P_2 \rangle$ is less than zero. It is gradually reduced with decreasing distance d . This demonstrates that under the influence of polymer-nanoparticle interactions, the chain end-to-end vectors prefer to align perpendicularly to the radial directions of the nanoparticles. The reason has been given in Section 3.4.1. According to the profiles of chain dimensions (Figure 3.2) and orientations (Figure 3.5) as a function of their distance from the nanoparticle, the interphase thickness is roughly equal to one R_g . This phenomenon has been also reported in other experimental and simulation investigations^{17,45,51,56,72}. As shown in Figure 3.5 (a), the reduction of $\langle P_2 \rangle$ is stronger in nanocomposites with spherical nanoparticles than in the cubic case, followed by tetrahedral nanoparticles. The differences between the $\langle P_2 \rangle$ profiles of different nanocomposites are smaller when the nanoparticle mass fraction ω is 17.2%. Additionally, a small region with parallel chain orientation occurs at distances $3 \text{ nm} < d < 4 \text{ nm}$. This has been also observed in atomistic MD simulations of polyethylene/polyhedral oligomeric silsesquioxane nanocomposites⁵⁴. It is not yet clear whether this behavior reflects only a statistic artifact.

3.4.2 Dynamic properties of polymer chains and nanoparticles

Center of mass mean square displacement and diffusion coefficient of polymer chains and nanoparticles. Figure 3.6 (a) shows the center of mass mean square displacement (MSD) of the polymer chains in pure polystyrene and nanocomposites with nanoparticles of different geometrical shapes and mass fractions ($\omega = 9.42\%$ and 17.2%). The center of mass MSD of the polymer chains in pure polystyrene is expectedly larger than in the presence of nanoparticles. For each type of nanoparticles, the center of mass MSD of polymer chains in nanocomposites is reduced with increasing nanoparticle mass fraction when the nanoparticles are in the same shape. Any enhancement of the interfacial adsorption hinders the motion of polymer chains. Concomitant with the polymer MSD, also the MSD of the nanoparticles themselves is reduced in the same ordering (Figure 3.6 (b)).

To quantify the global dynamical behavior of the studied composites, we determine the center of mass diffusion coefficients of polymer chains (D_{ps}) and nanoparticles (D_{np}) on the basis of center of mass MSDs. Figure 3.7 (a) presents D_{ps} as a function of the total surface area A_{total} of the nanoparticles with different geometrical structures. $A_{total} = 0$ refers to the pure polystyrene system (red symbol, Figure 3.7 (a)). The reduction of the center of mass D_{ps} with A_{total} approximately follows a linear relation: $D_{ps}(A_{total}) = -5.91 \times 10^5 A_{total} + 9.06 \times 10^{-10}$ (in $\text{m}^2 \text{s}^{-1}$). Similar linear relations for the polymer dynamics as a function of the nanoparticle surface area have been also observed in other experimental and simulation investigations. As an example, the atomistic MD simulations of Capaldi et al.⁵⁴ have demonstrated that the diffusion coefficient of the polyethylene chains at 500 K is almost linearly reduced with the total surface area of polyhedral oligomeric silsesquioxane nanoparticles. Additionally, the viscosity experiments of Hyun et al.⁷³ have shown that the zero shear viscosity of a poly(ethylene oxide) melt at 393 K is almost linearly increased with the total surface area of organoclay nanoparticles. In additional

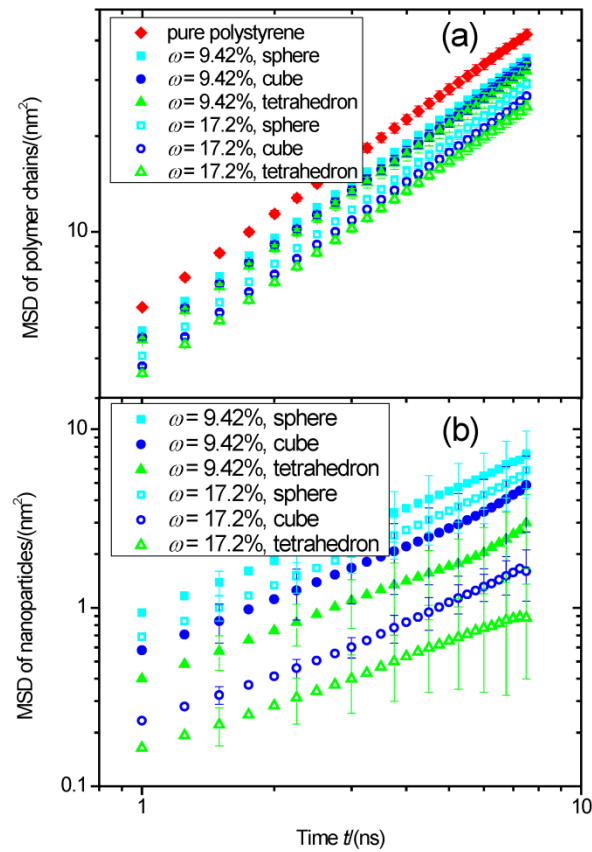


Fig. 3.6 Center of mass mean square displacement (MSD) of polymer chains (a) and nanoparticles of different geometrical shapes (b) as a function of time t . For selected data points error bars have been given.

simulations, we have found that D_{ps} have almost the same value for identical nanoparticle surface areas independent of their geometrical shape. For instance, the center-of-mass D_{ps} in a system containing 7 spherical nanoparticles ($D_{ps} = 7.78 \times 10^{-10} \text{ m}^2 \text{ s}^{-1}$, $A_{total} = 197 \text{ nm}^2$) is roughly equal to the one in a system with 5 cubic nanoparticles ($D_{ps} = 7.79 \times 10^{-10} \text{ m}^2 \text{ s}^{-1}$, $A_{total} = 193 \text{ nm}^2$) and the one in a system with 4 tetrahedral nanoparticles ($D_{ps} = 7.81 \times 10^{-10} \text{ m}^2 \text{ s}^{-1}$, $A_{total} = 187 \text{ nm}^2$). These findings indicate at a molecular scale that the global polymer dynamics is not influenced by geometrical details of the nanoparticles but only by their total surface area.

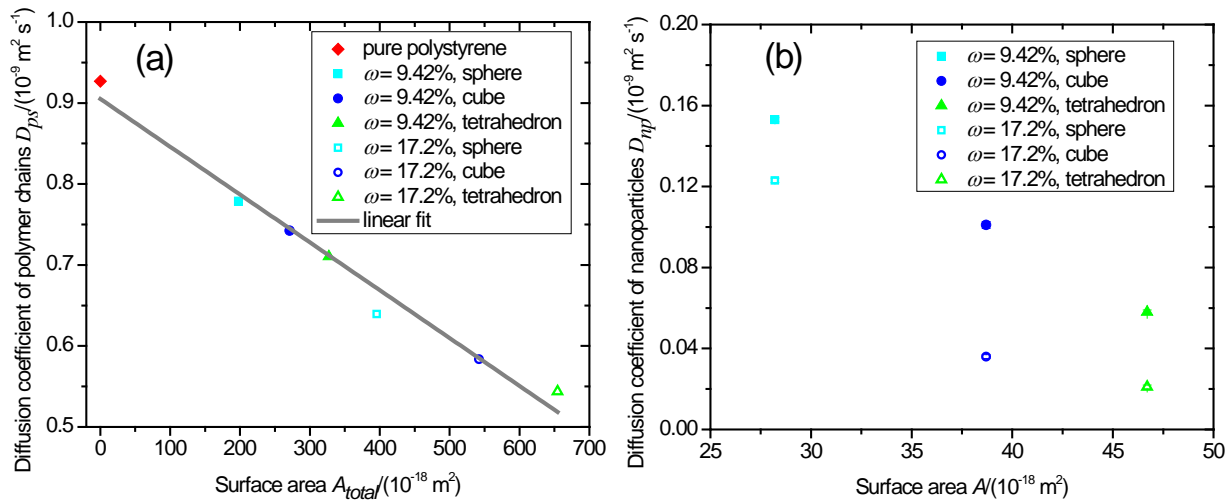


Fig. 3.7 (a) Diffusion coefficient D_{ps} of polymer chains as a function of the total surface area A_{total} and (b) diffusion coefficient D_{np} of nanoparticles as a function of surface area A of an individual nanoparticle. Note that the zero surface area (red symbol) represents the pure polystyrene system. The solid line refers to the linear fit: $D_{ps}(A_{total}) = -5.91 \times 10^5 A_{total} + 9.06 \times 10^{-10}$ (in $\text{m}^2 \text{ s}^{-1}$). Error bars are not visible due to their small values.

For systems with identical mass fractions (i.e. $\omega = 9.42\%$ or 17.2%), the D_{ps} value in samples with tetrahedral nanoparticles is smaller than in systems of cubic nanoparticles, followed by

spherical nanoparticles. Specifically, the center of mass D_{ps} in systems with tetrahedral, cubic and spherical nanoparticles is reduced by 24.1% ($1.67 \times 10^{-10} \text{ m}^2 \text{ s}^{-1}$), 21.3% ($1.56 \times 10^{-10} \text{ m}^2 \text{ s}^{-1}$) and 17.8% ($1.37 \times 10^{-10} \text{ m}^2 \text{ s}^{-1}$), when the nanoparticle mass fraction ω increases from 9.42% to 17.2%. These results indicate that tetrahedral nanoparticles slow down the global chain dynamics more strongly than cubic nanoparticles, followed by spherical nanoparticles, when the nanoparticle mass fraction is constant. In general, both the interfacial adsorption and excluded volume effects suppress the motion of polymer chains more efficiently for a nanoparticle with a larger surface area than for a nanoparticle with a smaller surface area, when the nanoparticle masses are identical ($6.39 \times 10^4 \text{ amu}$). The surface area of the tetrahedral nanoparticle ($A_T = 46.7 \text{ nm}^2$, Table 3.1) is 1.21 and 1.66 times as large as the surface area of the cubic ($A_C = 38.1 \text{ nm}^2$) and spherical ($A_S = 28.2 \text{ nm}^2$) nanoparticle. This explains in a simple way that tetrahedral nanoparticles reduce the global diffusion of polymer chains more efficiently than those with smaller specific surface areas (i.e. cubic and spherical).

Similar to the D_{ps} , the diffusion coefficients of the nanoparticles D_{np} in Figure 3.7 (b) also become smaller with increasing nanoparticle mass fraction for the nanoparticles of the same shape. Additionally, the D_{np} in the systems with nanoparticles of different shape, but the same mass fraction, rank as: sphere > cube > tetrahedron. This is attributed to differences in both the excluded volume and the frictional resistance. Both factors are mainly controlled by the surface area of the nanoparticles and the diffusion of the polymer chains (Figure 3.7 (a)). It is worth mentioning that D_{np} of spherical nanoparticles at mass fraction $\omega = 17.2\%$ ($1.23 \times 10^{-10} \text{ m}^2 \text{ s}^{-1}$) is even larger than that ($1.01 \times 10^{-10} \text{ m}^2 \text{ s}^{-1}$) of cubic nanoparticles at $\omega = 9.42\%$. This shows that D_{np} is influenced not only by internal features (i.e. geometrical shape) but also by global properties (i.e. nanoparticle mass fraction). The comparison of Figures 3.7 (a) and (b) verifies that in a given system polymer chains diffuse by about a factor of 5 to 25 faster than the nanoparticles. This is due to the fact that the mass of the nanoparticles is almost 9 times the mass of the polymer coils, even though the dimension of the polymer coils (i.e. radii of gyration) is similar to the nanoparticle size.

Chain end-to-end vector relaxation times. The decorrelation of the end-to-end vector of polymer chains⁷⁴ with time is another descriptor of the overall chain dynamics. The time auto-correlation function $C(t)$ of the chain end-to-end vector is given by,

$$C(t) = \frac{\langle \overrightarrow{R_e}(t) \overrightarrow{R_e}(0) \rangle}{\langle \overrightarrow{R_e}(0) \overrightarrow{R_e}(0) \rangle} \quad (2)$$

where $\overrightarrow{R_e}(t)$ denotes the chain end-to-end vectors at time t and the bracket $\langle \dots \rangle$ symbolizes the average over all polymer chains as well as over all time origins. Figure 3.8 (a) presents the decay of $C(t)$ as a function of time t in pure polystyrene and in different nanocomposite systems at a nanoparticle mass fraction $\omega = 9.42\%$. The decay of $C(t)$ in pure polystyrene is faster than in the nanocomposite systems. The same tendency is also observed at a higher nanoparticle mass fraction $\omega = 17.2\%$ in Figure 3.8 (b). This shows that the addition of nanoparticles slows down the decorrelation of the chain end-to-end vector with time.

To analyze quantitatively the decorrelation of the chain end-to-end vector with time, the $C(t)$ curves in Figures 3.8 (a) and (b) are fitted to a modified stretched exponential (Kohlrausch-Williams-Watts) function,

$$C(t) = \exp\left(-\left(\frac{t}{a}\right)^b\right) \quad (3)$$

where the fitting parameters a and b are derived from a nonlinear least squares optimization⁷⁵. The relaxation time τ_{ee} of the chain end-to-end vector is calculated as the analytic time integral of the modified stretched exponential function,

$$\tau_{ee} = \int_0^{\infty} \exp\left(-\left(\frac{t}{a}\right)^b\right) dt = \frac{a}{b} \Gamma\left(\frac{1}{b}\right) \quad (4)$$

where $\Gamma\left(\frac{1}{b}\right)$ is Euler's Gamma function⁷⁶. The parameters a , b and the corresponding τ_{ee} for all systems are listed in Table 3.3. As shown in Figure 3.9 (a), the global τ_{ee} (averaged over all chains, regardless of their positions) increases almost linearly with the total surface area A_{total} of the nanoparticles (i.e. $\tau_{ee}(A_{total}) = 6.23 \times 10^5 A_{total} + 4.43 \times 10^{-10}$ (in s)). Kutvonen et al.⁷⁷ have demonstrated by MD simulations that the relaxation time of the polymer end-to-end vector increases almost linearly with the total interphase area in a nanocomposite. As another example, Kalfus et al.⁷⁸ have also found by dynamic-mechanical thermal measurements that the relaxation

time of storage moduli of poly(vinyl acetate) nanocomposites exhibits a linear increase with the surface area of hydroxyapatite nanoparticles. In additional simulations, we have also found that the global τ_{ee} have almost the same value when the total surface area A_{total} of the nanoparticles coincides. For instance, the global τ_{ee} in a system with 14 spherical nanoparticles (0.67 ns, $A_{total} = 394 \text{ nm}^2$) is identical to the one in a system with 10 cubic nanoparticles ($A_{total} = 387 \text{ nm}^2$) and to the one with 8 tetrahedral nanoparticles ($A_{total} = 374 \text{ nm}^2$). When the nanoparticle mass fraction is identical (i.e. $\omega = 9.42\%$ or 17.2%), the global τ_{ee} in the system blended with tetrahedral nanoparticles is larger than the one with cubic nanoparticles, followed by spherical nanoparticles. For the systems containing tetrahedral, cubic and spherical nanoparticles, the global τ_{ee} increases by 37.3% (0.24 ns), 31.4% (0.19 ns) and 20.2% (0.11 ns), when the nanoparticle mass fraction ω increases from 9.42% to 17.2%. These findings emphasize again that the influence of the nanoparticle geometry and mass fraction on the global chain relaxation can be mapped to a single parameter, namely the surface area.

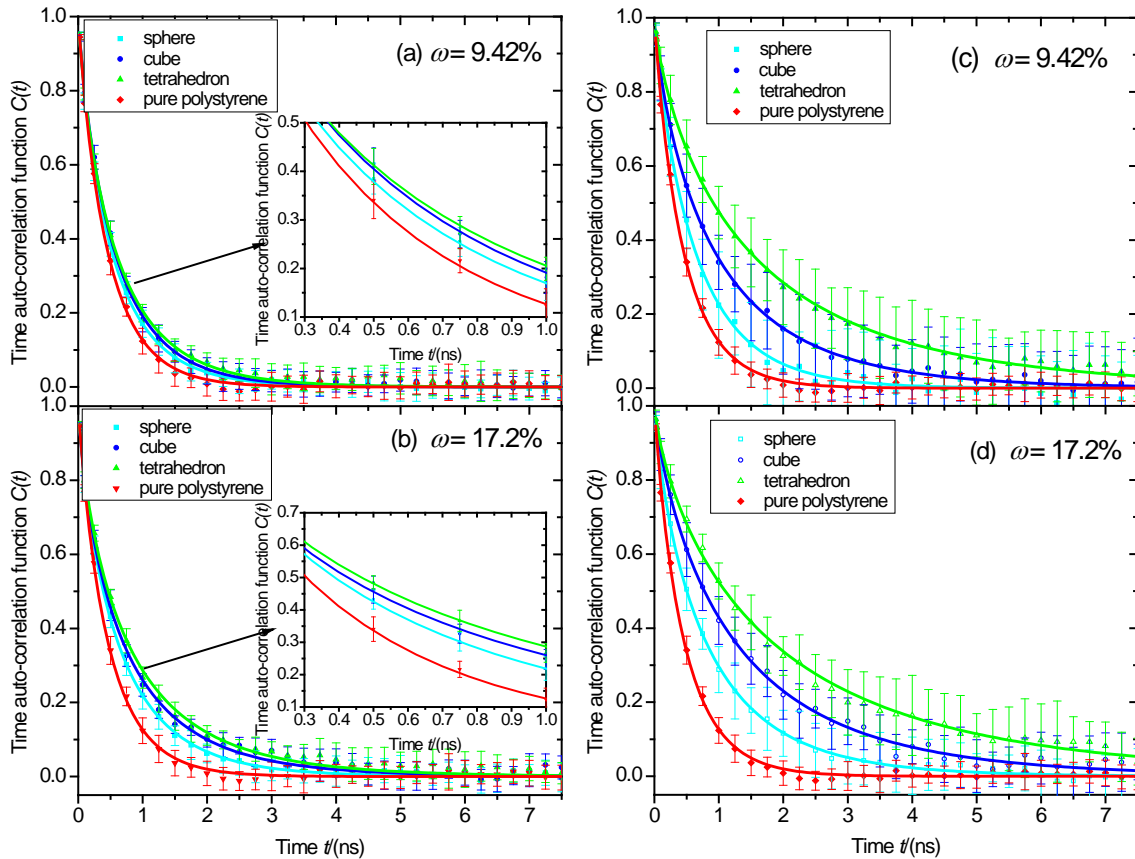


Fig. 3.8 Time auto-correlation function $C(t)$ of the end-to-end vector of all polymer chains (a and b) and of polymer chains in the interphase (c and d) as a function of time t . The red symbols representing the pure polystyrene system are used as a reference. Both insets in Figures 3.8 (a) and (b) are used to show clearly the deviation of $C(t)$ between different systems. The data of the time auto-correlation function $C(t)$ are fitted with a stretched exponential function: $C(t) = \exp(-(\frac{t}{a})^b)$. The fitting parameters a and b are listed in Table 3.3.

Table 3.3 Parameters a and b are obtained from a stretched exponential fitting of the time auto-correlation function $C(t)$. The relaxation time τ_{ee} is defined as the analytic time integral of the fitting function. All simulated systems are defined in Table 3.2. The terms “global” and “local” represent the relaxation of all chains and those in the interphase, respectively.

System	a (ns)		b		τ_{ee} (ns)	
	global	local	global	local	global	local
sphere, $\omega = 9.42\%$	0.52	0.64	0.87	0.88	0.56	0.68
sphere, $\omega = 17.2\%$	0.56	0.94	0.87	0.79	0.60	1.07
cube, $\omega = 9.42\%$	0.58	1.48	0.84	0.76	0.64	1.75
cube, $\omega = 17.2\%$	0.60	0.79	0.83	0.82	0.67	0.87
tetrahedron, $\omega = 9.42\%$	0.68	1.23	0.77	0.79	0.79	1.41
tetrahedron, $\omega = 17.2\%$	0.75	1.79	0.77	0.75	0.87	2.13
pure polymer, $\omega = 0$	0.45		0.92		0.47	

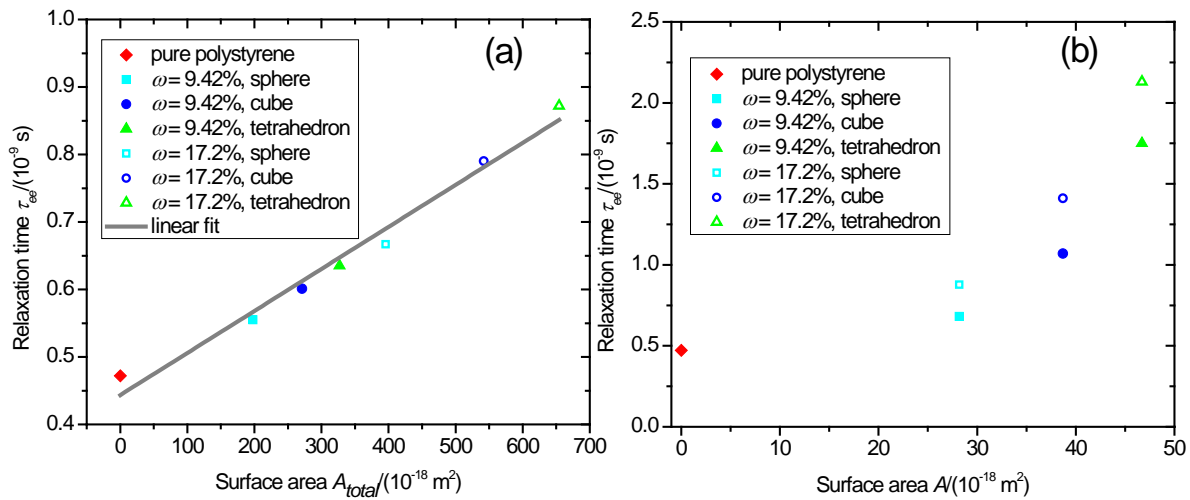


Fig. 3.9 (a) Global relaxation time τ_{ee} of the end-to-end vector of polymer chains as a function of the total surface area A_{total} of nanoparticles and (b) local relaxation time τ_{ee} of the end-to-end vector of polymer chains in the interphase as a function of the surface area A of an individual nanoparticle. “Global” and “local” have the same meaning as in Table 3.3. The red symbol representing the pure polystyrene system is used as a reference. The solid line denotes a linear fit: $\tau_{ee}(A_{total}) = 6.23 \times 10^5 A_{total} + 4.43 \times 10^{-10}$ (in s).

The suppression of the overall dynamics of polymer chains is fundamentally related to the reduction of the local mobility in the interphase. Probing the local decorrelation of the chain end-to-end vector in the vicinity of nanoparticles enables us to understand the details of the reduction of the global chain mobility. For this purpose, we calculated the local $C(t)$ of the end-to-end vector of polymer chains whose centers of mass stay for 4 ns within a distance of 3.18 nm (i.e. radius of the circumscribed sphere of the tetrahedral nanoparticle) from the nanoparticle center of mass. We are aware that using this geometrical criterion to locate the interphase includes, for the different nanoparticles, different distributions of “interphase” chains, due to the different shapes of the nanoparticles. We use it anyway for lack of a better suitable definition. For the calculation of the local $C(t)$, the average is taken over all nanoparticles, all polymer chains in their vicinity as well as over all time origins. Note that polymer chains are excluded from the remaining average once their centers of mass cross the spherical boundary. This means that the local $C(t)$ for each polymer chain is only calculated up to the time its center of mass spends in the interphase thus defined. The local $C(t)$ (Figures 3.8 (c) and (d)) decay by a stretched exponential relation with time t , as for the global relaxation. The deviations of the $C(t)$ curves between nanocomposites and pure polystyrene are much larger than for the overall dynamics (Figures 3.8 (a) and (b)). This is because the analysis is now focused on the chains in the immediate vicinity to the nanoparticles, which experience the largest hindrance to their movements. The $C(t)$ curves for the interphase chains in Figures 3.8 (c) and (d) are also fitted with the stretched exponential function. As shown in Table 3.3, the local τ_{ee} of polymer chains in the nanocomposite interphase is about 2~4 times the τ_{ee} in the pure polystyrene. Similar phenomena have been also observed by Nodoro et al.⁵⁰ in atomistic MD simulations of polystyrene/silica nanocomposites. In their simulations, the interphase τ_{ee} in the studied nanocomposites is roughly 2 or 3.5 times greater than the τ_{ee} in the neat polymer, when the

nanoparticle surface area A is 28.2 nm^2 (radius $R = 1.5 \text{ nm}$) and 49.6 nm^2 ($R = 2 \text{ nm}$). When comparing the global and local τ_{ee} in Table 3.3, one realizes that all local τ_{ee} are larger than the associated global ones. Specifically, the local τ_{ee} in the systems blended with tetrahedral, cubic and spherical nanoparticles at the same mass fraction ($\omega = 9.42$ or 17.2%) exceeds the global value by a factor of about 2.5, 1.8 and 1.3. This confirms that local relaxations of chain end-to-end vectors are affected more significantly by the presence of the nanoparticles than the global ones. The local τ_{ee} of the chain end-to-end vectors increases with the nanoparticle mass fraction when the nanoparticle shape is identical. As for the overall relaxation, also the local chain relaxation slows down with the total surface area. We note that (i) the slowing down is stronger than the overall relaxation. (ii) it increases monotonically (Figure 3.9 (b)) but not linearly, and (iii) increasing the nanoparticle mass fraction leads to a small but visible slowing down for the nanoparticles of a given shape. The latter happens in spite of our analyses concentrating on the environment around individual particles. We have, at present, no explanation. We can only surmise that at a higher nanoparticle concentration more polymer chains come under the direct or indirect influence of two neighboring nanoparticles at the same time.

Escape of polymer chains from the interphase and characteristic escape time. Polymer chains in the interphase (i.e. center of mass within 3.18 nm of the nearest nanoparticle center) can exchange positions with chains further away from the nanoparticles due to their diffusion denoted here as escape. The polymer chains in the interphase would exhibit different escape behavior if the specific surface areas of the nanoparticles differ. To monitor the escape behavior of the polymer chains from the interphase, we define a normalized escape function $\Omega(t)$,

$$\Omega(t) = \left\langle \frac{N_{ps}^b(t)}{N_{ps}^b(0)} \right\rangle \quad (5)$$

where $N_{ps}^b(t)$ is the total number of polymer chains whose centers of mass still stay inside the spherical boundary defined in Section 3.4.2 at time t . If a certain number of chains are found in the interphase at time $t = 0$, then $\Omega(t)$ is the fraction of these chains, which have remained in the interphase uninterruptedly until a time t later. Note that the bracket $\langle \dots \rangle$ denotes the average over all nanoparticles. Figure 3.10 shows the decay of the normalized escape function $\Omega(t)$ with time t . It decays very fast by at least 30% within the first nanosecond. This means that a fraction

of the labeled chains leaves the interphase in a short time. The reason is that the polymer chains at the boundary of the interphase region are still capable of diffusing effectively. From time $t = 3$ ns onwards, the decay of $\Omega(t)$ becomes gradually slower, as the remaining labeled chains not only have to diffuse a longer distance but also diffuse slower than the ones at the boundary due to stronger interfacial adsorptions. Similar to the time auto-correlation function $C(t)$ of the

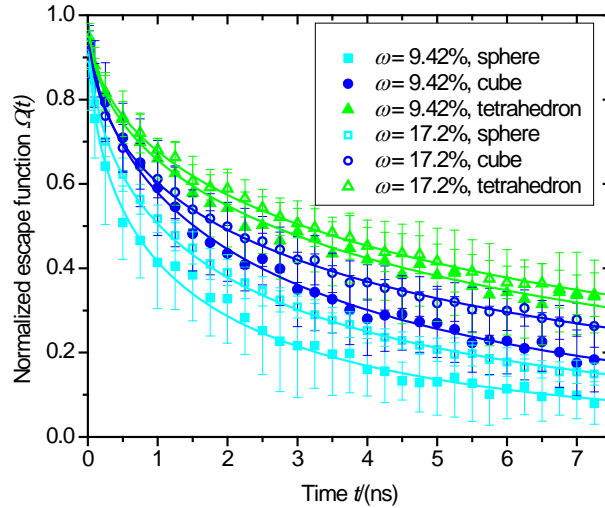


Fig. 3.10 Normalized escape function $\Omega(t)$ of polymer chains in the interphase versus time t . The decay of $\Omega(t)$ is fitted by a stretched exponential function (see Table 3.4): $C(t) = \exp(-(\frac{t}{a})^b)$.

Table 3.4 Parameters a and b are obtained from a stretched exponential fitting of the normalized escape function $\Omega(t)$. Characteristic escape time τ_{esc} of polymer chains in the interphase is defined as the analytic time integral of the modified stretched exponential function.

System	a (ns)	b	τ_{esc} (ns)
sphere, $\omega = 9.42\%$	1.29	0.51	2.51
sphere, $\omega = 17.2\%$	2.90	0.57	4.72
cube, $\omega = 9.42\%$	5.39	0.51	10.3
cube, $\omega = 17.2\%$	2.11	0.51	4.03
tetrahedron, $\omega = 9.42\%$	4.02	0.49	8.38
tetrahedron, $\omega = 17.2\%$	6.32	0.51	12.2

chain end-to-end vector, the normalized escape function also can be expressed by a stretched exponential decay function. All fitting parameters we have derived are listed in Table 3.4. To quantify the escape behavior of polymer chains in the interphase, a characteristic escaping time τ_{esc} is defined as the analytic time integral of the associated fitting function. The characteristic escape time τ_{esc} in Table 3.4 is about 4 ~ 6 times larger than the associated local relaxation time τ_{ee} in Table 3.3. Note that τ_{esc} depends on the definition of the boundary of the interphase. Moreover, the characteristic escape times τ_{esc} show that polymer systems with spherical nanoparticles have the largest mobility followed by cubic and tetrahedral nanoparticles. This holds at both nanoparticle mass fractions.

3.4.3 Relation between mechanical properties of nanocomposites and the interphase area

Figure 3.11 (a) presents the stress-strain curves for all considered systems at 100 K, in which the stress first increases almost linearly with the strain (up to $\varepsilon = 3\%$) and then yield takes place at about 5~6% strain before reaching a plateau. It can be observed that (i) an increase of the nanoparticle mass fraction for a given geometry or (ii) an increase of the nanoparticle surface area for a given mass fraction enhances the yield strength of the nanocomposites. Similar phenomena have been found by other experimental and simulation investigations^{16,18,48,49}. Young's moduli E of all systems are calculated from the slope of the stress-strain curves in the linear region (up to $\varepsilon = 3\%$). It should be mentioned that the glass transition temperature of the nanocomposites identified from our simulations and other experiments⁷⁹ is roughly 170 K and 373 K, respectively. The Young's modulus of the nanocomposites obtained by our simulations is about 4~5 smaller than the associated experimental value^{80,81} (3000~3500 MPa). The smaller Young's modulus relative to the experiment value is due to the application of a coarse-grained potential which is softer than an atomistic potential. Nevertheless, the investigations of Rahimi et al.⁶⁷ have demonstrated that the adopted coarse-grained potential can capture qualitatively the interfacial properties and the mechanical behavior of polystyrene/silica nanocomposites.

As shown in Figure 3.11 (b), the Young's modulus E of all nanocomposites is higher than in the neat polymer. It increases monotonically with increasing overall surface area A_{total} of the

nanoparticles. When the nanoparticle mass fraction is constant, the nanocomposites containing tetrahedral nanoparticles have a larger Young's modulus than the ones containing nanoparticles of a smaller surface area (i.e. cubic or tetrahedral). This indicates that the total surface area of the nanoparticles has a significant impact on the modification of mechanical properties of nanocomposites, as clarified by other investigations^{80,82–84}. Specifically, in our simulations an about 20% improvement of Young's modulus is found at an interphase area/volume ratio of about $0.08 \text{ nm}^2/\text{nm}^3$. This finding is comparable to the experimental result of Dorigato et al.⁸⁵ that the Young's modulus of polyethylene/silica nanocomposites is enhanced by about 25% when the interphase area/volume ratio is about $0.05 \text{ nm}^2/\text{nm}^3$. Kaur et al.⁸⁶ and Kalfus et al.⁸⁷ have also observed from thermomechanical measurements a 20%~30% increase of elastic moduli of poly(ϵ -capro-lactone)/hydroxylapatite and poly(vinyl-acetate)/hydroxyapatite nanocomposites, when the interphase area/volume ratio is about $0.06 \text{ nm}^2/\text{nm}^3$. Additionally, based on a continuum model, Odegard et al.⁸⁸ and Boutaleb et al.⁸⁹ have found that the elastic moduli of polyimide/silica and polyethylene/silica nanocomposites are enhanced by about 30% at an interphase area/volume ratio of about $0.03 \text{ nm}^2/\text{nm}^3$. It has been shown in Sections 3.4.1 and 3.4.2 that a higher fraction of interphase chains is strongly adsorbed by the nanoparticle surface if the nanoparticle mass fraction or the specific surface area is enlarged. Recall that in our model the polymer-nanoparticle interaction is attractive. This explains at a microscopic level that the mechanical enhancement in polymer nanocomposites is determined both by the nanoparticle mass fraction and their geometrical shape. They are fundamentally related to a common factor, i.e. the interphase area.

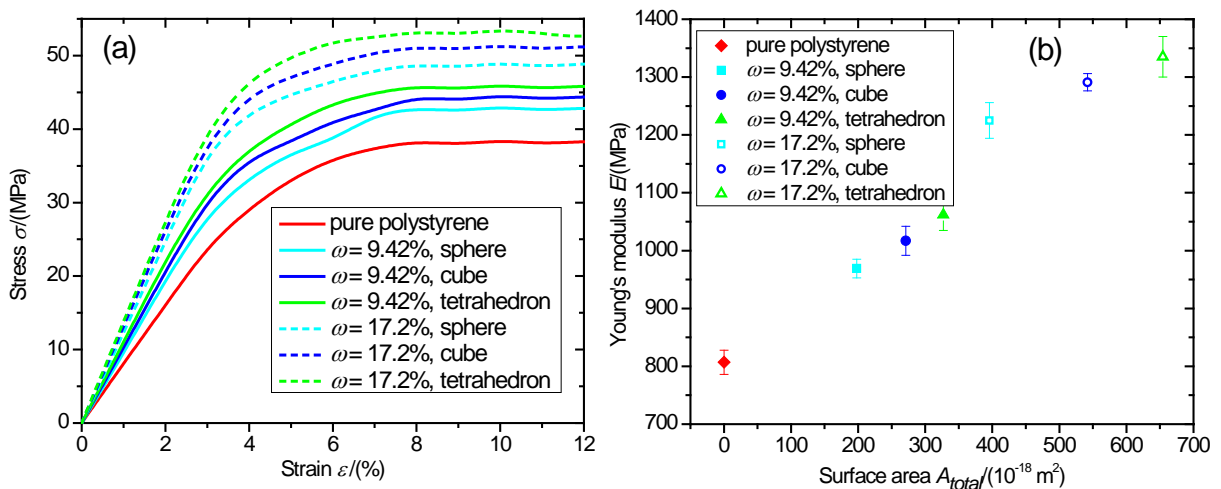


Fig. 3.11 (a) Stress-strain curves of pure polystyrene and different nanocomposite systems; (b) Young's modulus E of pure polystyrene and different nanocomposite systems as a function of the total surface area A_{total} of the nanoparticles.

3.5 Summary and conclusions

Coarse-grained molecular dynamics simulations have been performed to investigate structural and dynamic properties of polymer chains in polystyrene nanocomposites containing a fraction of silica nanoparticles of different geometries (sphere, cube and regular tetrahedron). Polymer structural properties that are calculated as a function of their distance from the nanoparticle center of mass are the end-to-end distance and radius of gyration of the polymer chains. It has been found that both increase locally in the intermediate vicinity of the nanoparticles, contract at distances corresponding to few chain radii of gyration (R_g), and almost converge to the averaged overall value at larger separations from the nanoparticle. Averaged over the whole sample, the global chain dimension is reduced with increasing total surface area of the nanoparticles. Moreover, the nanoparticle geometry has a significant impact on the local dimension of the polymer chains in the interphase. The matrix chains are aligned parallel to the surface tangent, when they are at close distances ($\leq R_g$). Further away, they prefer random orientations. According to the profiles of the chain dimension and orientation as a function of their distance from the nanoparticle, the interphase thickness approximately equals one R_g .


The global and interphase chain dynamics is monitored by the center of mass diffusion coefficient, the relaxation time of the chain end-to-end-vector, and the time a chain uses to escape from the interphase. For all mobility parameters we find that both the nanoparticle mass fraction and geometrical shape influence largely the dynamic properties of the polymer chains. Specifically, the global chain center-of-mass diffusion coefficient decreases almost linearly with the total surface area of the nanoparticles, whereas the global relaxation time of the chain end-to-end vectors increases almost linearly with it. Both trends indicate that a larger surface area of nanoparticles leads to a stronger reduction of the polymer mobility. Due to their larger surface area, tetrahedral nanoparticles hinder the global chain dynamics stronger than cubic

nanoparticles, followed by spherical nanoparticles, when the nanoparticle mass fraction is constant.

Excluded volume effects and interfacial adsorption make the relaxation of the polymer chains in the interphase much slower than for the whole sample. In contrast to the global relaxation time, the relaxation time of the interphase chains increases superlinearly with the surface area of the individual nanoparticles. We find the same ordering of the interphase mobility as for the other chain dynamical parameters, namely tetrahedral < cubic < spherical. The same is also found for the characteristic time a polymer chain needs to escape from an interphase around a nanoparticle into the bulk. In the present work the boundary between the interphase and the bulk is arbitrarily but consistently drawn.

To probe the relation between overall mechanical properties of nanocomposites and nanoparticle characteristics, uniaxial tensile deformations are applied for all systems below the glass transition temperature. Yield strengths of the nanocomposites are enhanced with increasing nanoparticle mass fraction for a given geometrical shape or increasing surface area of an individual nanoparticle for a given mass fraction by changing their shapes. The Young's modulus of the nanocomposites increases monotonically with the total interphase area. The universal parameter "interphase area", which is a function of nanoparticle mass fraction and geometry, plays a critical role in the mechanical enhancement of polymer nanocomposites. Specifically, modifications of mechanical properties due to the addition of tetrahedral nanoparticles are stronger than for the ones with a smaller surface area (i.e. cubic and spherical structure) when the nanoparticle mass fraction is constant.

Finally, we want to point out that as a common factor, the interphase area influences almost linearly the global chain geometry (R_e^2 and R_g^2), dynamics (D_{ps} , τ_{ee} and τ_{esc}) as well as the bulk elastic properties. Nevertheless, the local chain geometry and dynamics is different in the interphase region ($\leq R_g$ from the nanoparticle surface), and their dependence on the interphase area can be nonlinear. There are probably local effects playing a role, which are different for the different nanoparticle shapes and concentrations. Contaminant with other experimental



investigations (i.e. Kaur et al.⁸⁶ and Kalfus et al.⁸⁷), our simulations reflect faithfully at molecular scales the correlation between the interphase area and mechanical enhancements of nanocomposites. It should be emphasized that the conclusions about the interphase area being the dominating factor apply to the particular nanoparticle shape, size and concentration range studied here. They should be reevaluated if the system compositions differ sizeably from the one studied in the present work.

References

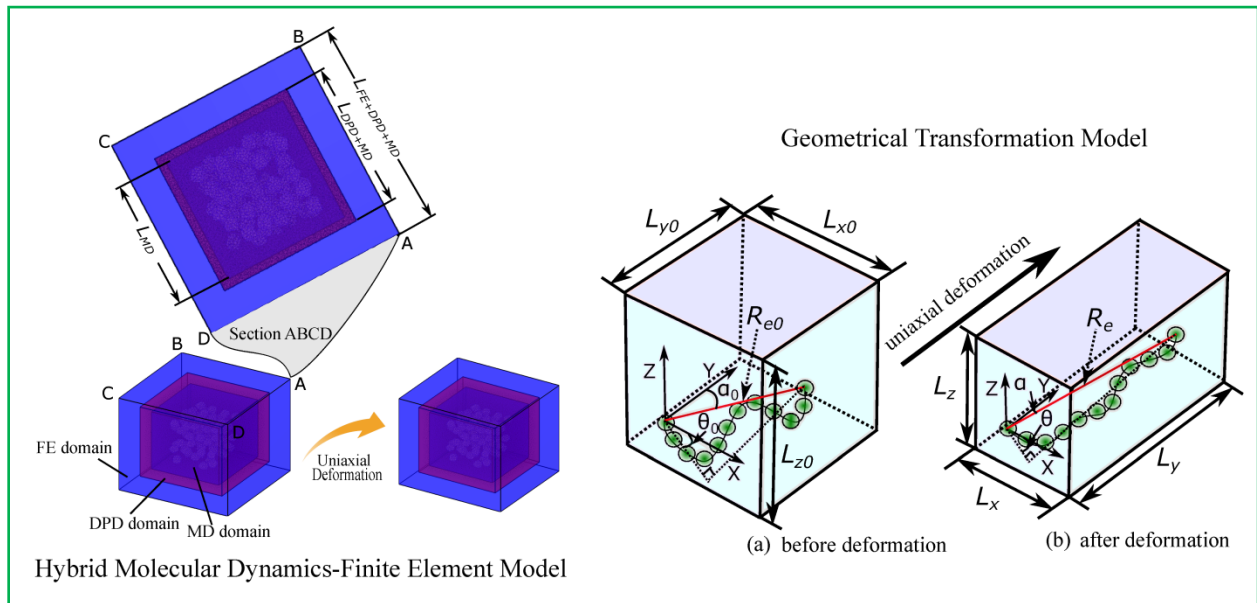
- [1] Crosby, A. J.; Lee, J.-Y. *Polym. Rev.* 47, 217–229 (2007).
- [2] Tjong, S. C. *Mater. Sci. Eng. R Reports* 53, 73–197 (2006).
- [3] Paul, D. R.; Robeson, L. M. *Polymer* 49, 3187–3204 (2008).
- [4] Jordan, J.; Jacob, K. I.; Tannenbaum, R.; Sharaf, M. A.; Jasiuk, I. *Mater. Sci. Eng. A* 393, 1–11 (2005).
- [5] Ray, S.S.; Okamoto, M. *Prog. Polym. Sci.* 28, 1539–1641 (2003).
- [6] Andrews, R.; Weisenberger, M. C. *Curr. Opin. Solid State Mater. Sci.* 8, 31–37 (2004).
- [7] Sahoo, N. G.; Rana, S.; Cho, J. W.; Li, L.; Chan, S. H. *Prog. Polym. Sci.* 35, 837–867 (2010).
- [8] Choudalakis, G.; Gotsis, A. D. *Eur. Polym. J.* 45, 967–984 (2009).
- [9] Kiliaris, P.; Papaspyrides, C. D. *Prog. Polym. Sci.* 35, 902–958 (2010).
- [10] Han, Z.; Fina, A. *Prog. Polym. Sci.* 36, 914–944 (2011).
- [11] Spitalsky, Z.; Tasis, D.; Papagelis, K.; Galiotis, C. *Prog. Polym. Sci.* 35, 357–401 (2010).
- [12] Pradhan, D. K.; Choudhary, R. N. P.; Samantaray, B. K. *Express Polym. Lett.* 2, 630–638 (2008).
- [13] Bauhofer, W.; Kovacs, J. Z. *Compos. Sci. Technol.* 69, 1486–1498 (2009).
- [14] Li, J.; Seok, S. Il; Chu, B.; Dogan, F.; Zhang, Q.; Wang, Q. *Adv. Mater.* 21, 217–221 (2009).
- [15] Lee, J. Y.; Zhang, Q.; Emrick, T.; Crosby, A. J. *Macromolecules* 39, 7392–7396 (2006).
- [16] Buryachenko, V. A.; Roy, A.; Lafdi, K.; Anderson, K. L.; Chellapilla, S. *Compos. Sci. Technol.* 65, 2435–2465 (2005).
- [17] Karatrantosa, A.; Clarke, N.; Kröger, M. *Polym. Rev.* 56, 385–428 (2016).
- [18] Jancar, J.; Douglas, J. F.; Starr, F. W.; Kumar, S. K.; Cassagnau, P.; Lesser, A. J.; Sternstein, S. S.; Buehler, M. J. *Polymer* 51, 3321–3343 (2010).
- [19] Tung, W.-S.; Composto, R. J.; Clarke, N.; Winey, K. I. *ACS Macro Lett.* 4, 916–920 (2015).
- [20] Nusser, K.; Neueder, S.; Schneider, G. J.; Meyer, M.; Pyckhout-Hintzen, W.; Willner, L.; Radulescu, A.; Richter, D. *Macromolecules* 43, 9837–9847 (2010).
- [21] Banc, A.; Genix, A. C.; Dupas, C.; Sztucki, M.; Schweins, R.; Appavou, M. S.; Oberdisse, J. *Macromolecules* 48, 6596–6605 (2015).

- [22] Tuteja, A.; Duxbury, P. M.; MacKay, M. E. *Phys. Rev. Lett.* 100, 077801 (2008).
- [23] Crawford, M. K.; Smalley, R. J.; Cohen, G.; Hogan, B.; Wood, B.; Kumar, S. K.; Melnichenko, Y. B.; He, L.; Guise, W.; Hammouda, B. *Phys. Rev. Lett.* 110, 196001 (2013).
- [24] Tung, W.; Bird, V.; Composto, R. J.; Clarke, N.; Winey, K. I. *Macromolecules* 46, 5345–5354 (2013).
- [25] Nakatani, A. I.; Chen, W.; Schmidt, R. G.; Gordon, G. V.; Han, C. C. *Polymer* 42, 3713–3722 (2001).
- [26] Schweizer, K. S. and Curro, J. G. *Phys. Rev. Lett.* 58, 246–249 (1987).
- [27] Frischknecht, A. L.; McGarrity, E. S.; MacKay, M. E. *J. Chem. Phys.* 132, 204901 (2010).
- [28] Erguney, F. M.; Lin, H.; Mattice, W. L. *Polymer* 47, 3689–3695 (2006).
- [29] Erguney, F. M.; Mattice, W. L. *Polymer* 49, 2621–2623 (2008).
- [30] Dattani, R.; Michels, R.; Nedoma, A. J.; Schweins, R.; Westacott, P.; Huber, K.; Cabral, J. T. *Macromolecules* 47, 6113–6120 (2014).
- [31] Genix, A. C.; Tatou, M.; Imaz, A.; Forcada, J.; Schweins, R.; Grillo, I.; Oberdisse, J. *Macromolecules* 45, 1663–1675 (2012).
- [32] Karatrantos, A.; Composto, R. J.; Winey, K. I.; Clarke, N. *Macromolecules* 44, 9830–9838 (2011).
- [33] Chen, T.; Qian, H. J.; Zhu, Y. L.; Lu, Z. Y. *Macromolecules* 48, 2751–2760 (2015).
- [34] Gao, Y.; Liu, J.; Zhang, L.; Cao, D. *Macromol. Theory Simulations* 23, 36–48 (2014).
- [35] Liu, J.; Wu, Y.; Shen, J.; Gao, Y.; Zhang, L.; Cao, D. *Phys. Chem. Chem. Phys.* 13, 13058–13069 (2011).
- [36] Chanmal, C. V.; Jog, J. P. *Express Polym. Lett.* 2, 294–301 (2008).
- [37] Hu, X.; Zhang, W.; Si, M.; Gelfer, M.; Hsiao, B.; Rafailovich, M.; Sokolov, J.; Zaitsev, V.; Schwarz, S. *Macromolecules* 36, 823–829 (2003).
- [38] Desai, T.; Keblinski, P.; Kumar, S. K. *J. Chem. Phys.* 122, 134910 (2005).
- [39] Oh, H.; Green, P. F. *Nat. Mater.* 8, 139–143 (2009).
- [40] Mijović, J.; Lee, H.; Kenny, J.; Mays, J. *Macromolecules* 39, 2172–2182 (2006).
- [41] Smith, G. D.; Bedrov, D.; Li, L.; Bytner, O. J. *J. Chem. Phys.* 117, 9478–9490 (2002).
- [42] Starr, F. W.; Schröder, T. B.; Glotzer, S. C. *Macromolecules* 35, 4481–4492 (2002).

- [43] Kremer, K.; Grest, G. S. *J. Chem. Phys.* 92, 5057 (1990).
- [44] Grest, G. S.; Kremer, K. *Phys. Rev. A* 33, 3628–3631 (1986).
- [45] Starr, F. W.; Schröder, T. B.; Glotzer, S. C. *Phys. Rev. E* 64, 021802 (2001).
- [46] Hyun, Y. H.; Lim, S. T.; Choi, H. J.; Jhon, M. S. *Macromolecules* 34, 8084–8093 (2001).
- [47] Chen, K. H.; Yang, S. M. *J. Appl. Polym. Sci.* 86, 414–421 (2002).
- [48] Zeng, Q. H.; Yu, A. B.; Lu, G. Q. *Prog. Polym. Sci.* 33, 191–269 (2008).
- [49] Allegra, G.; Raos, G.; Vacatello, M. *Prog. Polym. Sci.* 33, 683–731 (2008).
- [50] Nodoro, T. V. M.; Böhm, M. C.; Müller-Plathe, F. *Macromolecules* 45, 171–179 (2012).
- [51] Nodoro, T. V. M.; Voyiatzis, E.; Ghanbari, A.; Theodorou, D. N.; Böhm, M. C.; Müller-Plathe, F. *Macromolecules* 44, 2316–2327 (2011).
- [52] Eslami, H.; Behrouz, M. *J. Phys. Chem. C* 118, 9841–9851 (2014).
- [53] Barbier, D.; Brown, D.; Grillet, A. C.; Neyertz, S. *Macromolecules* 37, 4695–4710 (2004).
- [54] Capaldi, F. M.; Rutledge, G. C.; Boyce, M. C. *Macromolecules* 38, 6700–6709 (2005).
- [55] Ghanbari, A.; Rahimi, M.; Dehghany, J. *J. Phys. Chem. C* 117, 25069–25076 (2013).
- [56] Ghanbari, A.; Nodoro, T. V. M.; Rahimi, M.; Böhm, M. C.; Müller-Plathe, F. *Macromolecules* 45, 572–584 (2012).
- [57] Chao, H.; Riggleman, R. A. *Polymer* 54, 5222–5229 (2013).
- [58] Chao, H.; Hagberg, B. A.; Riggleman, R. A. *Soft Matter* 10, 8083–8094 (2014).
- [59] Vogiatzis, G. G.; Theodorou, D. N. *Macromolecules* 47, 387–404 (2014).
- [60] Vogiatzis, G. G.; Theodorou, D. N. *Macromolecules* 46, 4670–4683 (2013).
- [61] Vogiatzis, G. G.; Voyiatzis, E.; Theodorou, D. N. *Eur. Polym. J.* 47, 699–712 (2011).
- [62] Xia, H.; Shaw, S. J.; Song, M. *Polym. Int.* 54, 1392–1400 (2005).
- [63] Luo, J.; Daniel, I. M. *Compos. Sci. Technol.* 63, 1607–1616 (2003).
- [64] Mortazavi, B.; Baniassadi, M.; Bardon, J.; Ahzi, S. *Compos. Part B Eng.* 45, 1117–1125 (2013).
- [65] Saber-Samandari, S.; Afaghi-Khatibi, A. *Polym. Compos.* 28, 405–411 (2007).
- [66] Qian, H.; Carbone, P.; Chen, X.; Karimi-varzaneh, H. A.; Liew, C. C.; Müller-Plathe, F. *Macromolecules* 41, 9919–9929 (2008).

- [67] Reith, D.; Pütz, M.; Müller-Plathe, F. *J. Comput. Chem.* 24, 1624–1636 (2003).
- [68] Liu, S.; Gerisch, A.; Rahimi, M.; Lang, J.; Böhm, M. C.; Müller-Plathe, F. *J. Chem. Phys.* 142, 104105 (2015).
- [69] Rahimi, M.; Iriarte-Carretero, I.; Ghanbari, A.; Böhm, M. C.; Müller-Plathe, F. *Nanotechnology* 23, 305702 (2012).
- [70] Ghanbari, A.; Böhm, M. C.; Müller-Plathe, F. *Macromolecules* 44, 5520–5526 (2011).
- [71] Fisher, M. E. *J. Chem. Phys.* 44, 616 (1966).
- [72] Voyiatzis, E.; Rahimi, M.; Müller-Plathe, F.; Böhm, M. C. *Macromolecules* 47, 7878–7889 (2014).
- [73] Hyun, Y. H.; Lim, S. T.; Choi, H. J.; Jhon, M. S. *Macromolecules* 34, 8084–8093 (2001).
- [74] Genix, A.-C.; Oberdisse, J. *Curr. Opin. Colloid Interface Sci.* 20, 293–303 (2015).
- [75] Marquardt, D. J. *Soc. Ind. Appl. Math.* 11, 431–441 (1963).
- [76] Lanczos, C. *J. Soc. Ind. Appl. Math.* 1, 86–96 (1964).
- [77] Kutvonen, A.; Rossi, G.; Ala-Nissila, T. *Phys. Rev. E* 85, 2–7 (2012).
- [78] Kalfus J.; Jancar, J. *Polym. Compos.* 28, 743–747 (2007).
- [79] Mark, J. E. *Polymer Data Handbook*; Oxford University Press, 1999.
- [80] Ji, X. L.; Jing, J. K.; Jiang, W.; Jiang, B. *Z. Polym. Eng. Sci.* 42, 983–993 (2002).
- [81] Vaziri, S.H.; Abadyan, M.; Nouri, M.; Omaraei, I. A.; Sadredini, Z.; Ebrahimnia, M. *J. Mater. Sci.* 46, 5628–5638 (2011).
- [82] Tannenbaum, R.; Zubris, M.; David, K.; Ciprari, D.; Jacob, K.; Jasiuk, I.; Dan, N. *J. Phys. Chem. B* 110, 2227–2232 (2006).
- [83] Ash, B. J.; Rogers, D. F.; Wiegand, C. J.; Schadler, L. S.; Siegel, R. W.; Benicewicz, B. C.; Apple, T. *Polym. Compos.* 23, 1014–1025 (2002).
- [84] Ciprai, D.; Jacob, K.; Tannenbaum, R. *Macromolecules* 39, 6565–6573 (2006).
- [85] Dorigato, A.; Dzenis, Y.; Pegoretti, A. *Mech. Mater.* 61, 79–90 (2013).
- [86] Kaur, J.; Shofner, M. L. *Macromol. Chem. Phys.* 210, 677–688 (2009).
- [87] Kalfus J.; Jancar, J. *Polym. Compos.* 28, 365–371 (2007).
- [88] Odegard, G. M.; Clancy, T. C.; Gates, T. S. *Polymer* 46, 553–562 (2005).
- [89] Boutaleb, S.; Zaïri, F.; Mesbah, A.; Naït-Abdelaziz, M.; Gloaguen, J. M.; Boukharouba, T.; Lefebvre, J. M. *Int. J. Solids Struct.* 46, 1716–1726 (2009).

4. Uniaxial Deformation of Polystyrene–Silica Nanocomposites Studied by Hybrid Molecular Dynamics–Finite Element Simulations



4.1 Abstract

This contribution investigates, based on molecular dynamics (MD), the mechanical deformation behavior of polystyrene-silica nanocomposites and focuses on the influence of micromechanical properties as e.g. filler particle size and filler mass fraction. With regard to simulations of macroscopic problems with system sizes not capable by pure MD approaches, our investigations are complemented by hybrid molecular dynamics – finite element (MD-FE) simulations. Our simulations show that an increasing total interfacial area between the nanoparticles and the polymer matrix stiffens the nanocomposite. As expected, small nanoparticles have more significant impact on the macroscopic mechanical properties of nanocomposites than large ones. We show that, for the same mass fraction of nanoparticles, the Young's modulus increases by about 4 to 5% when the nanoparticle diameter is decreased from 5 to 2 nm. Furthermore, we find that: (i) the end-to-end distances of free polymer chains in the vicinity of nanoparticles are larger than in the bulk; (ii) the addition of nanoparticles slows down the global dynamics of free polymer chains; and (iii) the interphase thickness of nanocomposites is about 1 to 1.5 nm. Beyond that, we study structural properties at the microscale under uniaxial tension and find that the presence of nanoparticles hinders the orientation of free polymer chains under deformation. This hindrance is more pronounced for small nanoparticles and high mass fractions. Polymer structural descriptors as the chain end-to-end vector and a molecular anisotropy parameter largely change in line with the geometrical transformation of the whole sample.

4.2 Introduction

Polymer nanocomposites¹⁻³ are produced by blending a matrix polymer with nanoparticles (e.g. spherical silica⁴⁻⁶, carbon nanotubes⁷⁻⁹ and delaminated clay¹⁰⁻¹³). In the past decades they have been applied extensively in different industries. However, it is still a challenge to understand the improvement of mechanical and other properties by nanoparticle inclusion at a molecular level. Due to their large surface, nanoparticles contact efficiently with polymer chains in nanocomposites. The interphase between the polymer matrix and the nanoparticles has a significant influence on the mechanical properties of nanocomposite materials. For instance, an interphase can hinder effectively the formation and propagation of fatigue cracks in nanocomposite materials⁴. This has been attributed to the fact that a strong interphase reduces the internal stress of polymer nanocomposites during a deformation process.

Experimental investigations¹⁴⁻¹⁶ have demonstrated that an increase of the nanoparticle concentration leads to an increase of elastic moduli. However, above a certain threshold nanoparticle aggregation leads to a reduction of the contact area between the polymer matrix and the nanoparticles¹⁵. A good dispersion of the nanoparticles^{17,18} in the polymer matrix attenuates effectively local stress concentrations. In addition, the influence of the nanoparticle size on the mechanical properties has been investigated by experimental methods. For polypropylene–CaCO₃ nanocomposites, Mishra et al.¹⁹ have observed that the Young's modulus of composites with smaller nanoparticles is greater than the one of composites with larger nanoparticles. In other contributions²⁰⁻²², similar results have been obtained for polyamide-6–silica thermoplastics, polysiloxane–silica coatings and epoxy–silica resins. A reduction of the nanoparticle size at a constant concentration causes an increase of the interphase area, which consequently enhances the overall surface energy between polymer chains and nanoparticles²¹. The grafting of nanoparticle surfaces by polymer chains is another way to modify the interaction between the polymer and the nanoparticles. Rong et al.^{21,22} applied either ungrafted or polymer-grafted (i.e. polymethylmethacrylate or polystyrene) silica nanoparticles. They have found that grafted nanoparticles disperse better in the composites. In accordance with Rong et al., Bikiaris et al.²³ have also observed that isotactic polypropylene nanocomposites containing surface modified silica nanoparticles have improved mechanical properties such as the Young's modulus.

Simulation studies have been applied widely to investigate the mechanical and other properties of polymer nanocomposites. Papakonstantopoulos et al.^{24,25} have employed a Monte Carlo (MC) approach to study the influence of the polymer-nanoparticle interactions on the mechanical properties of nanocomposites. They found that the average shear and Young's moduli of nanocomposites filled with inert or attractive nanoparticles were larger than those of the pure polymer. Raos et al.²⁶ have performed dissipative particle dynamics (DPD) simulations to examine polymer networks mixed with spherical particles at a volume fraction of 20%. Their results indicated that the polymer-particle interaction is a significant factor influencing the dynamic shear modulus of filler-cross-linked polymer networks²⁷⁻²⁹. Ndoro et al.^{30,31} have demonstrated by atomistic molecular dynamics (MD) simulations that the size and the grafting density of silica nanoparticles have an influence on the interphase structure of nanocomposites. Due to the polymer-nanoparticle interaction, the properties of polymer chains in the interphase differ from those of the bulk. Ghanbari et al.^{32,33} and Rahimi et al.³⁴ also formulated similar conclusions by coarse-grained MD simulations of polymer–silica nanocomposites.

In contrast to particle-based methods, continuum-based approaches (i.e. micromechanics³⁵ and the finite element (FE) method³⁶) tackle macroscopic problems by applying continuous meshing units. Fornes et al.³⁷ have adopted a micromechanically based model to simulate a nylon-6–layered-clay system. They concluded that the exfoliated clay contributed to a mechanical reinforcement of nylon-6. The reinforcement, however, decreased when the number of clay platelets per stack grew. By using a three-dimensional FE approach, Mortazavi and coworkers³⁸ have evaluated the influence of the interphase on the elastic modulus of nanocomposites containing either unidirectionally or randomly oriented particles. They demonstrated that the interphase effects for spherical nanofillers were stronger than for the anisometric nanofillers.

While particle-based methods address appropriately molecular and mesoscopic structures of soft materials, their computational cost is prohibitive when facing macroscopic problems. Continuum-based methods allow a macroscopic modeling of soft materials, frequently relying on finite element meshes for numerical solution. Thereby, microstructural resolution like in terms of

particles and their interactions is not longer captured. Hybrid particle-continuum methods have been developed to overcome their intrinsic drawbacks: a small particle domain with a high resolution for analyzing quantities of interest is coupled to an extended surrounding continuum that makes macroscale simulations computationally affordable. They may be categorized into sequential and concurrent couplings³⁹⁻⁴². Sequential coupling⁴³ provides a bridging solution in which hierarchical methods are coupled by passing material parameters (e.g. elastic moduli) derived from one scale in an off-line way to another scale. Yang et al.⁴⁴ developed such a combined framework based on MD, FE and micromechanics. In their approach, the bulk modulus of nanocomposites calculated by an atomistic MD simulation was used to parameterize the FE model. The results reflected qualitatively the influence of the nanoparticle size on the mechanical properties of nanocomposites. Concurrent coupling combines simulation methods at different scales in an on-line way⁴⁵. A bridging domain method has been developed by Xiao and Belytschko⁴⁶ to couple the continuum with molecular models. Their investigations have indicated that such a bridging domain approach can reduce the spurious wave reflections at the interphase region. Zhang et al.⁴⁷, Khare et al.⁴⁸ and Davydov et al.⁴⁹ have demonstrated that the bridging domain method addresses appropriately deformation problems of crystalline materials. Ben Dhia et al.^{50,51} have proposed the Arlequin method in which the energies of the particle and continuum domains are coupled. Both the bridging domain and the Arlequin method do not require a lattice description in the particle domain. Therefore, they have been applied by some researchers (i.e. Bauman et al.⁵² and Chamoin et al.⁵³) to simulate soft materials such as polymers.

Different to the aforementioned methods, some of us^{54,55} have developed a hybrid MD-FE framework based on the Arlequin approach. A large number of so-called anchor points are introduced in this scheme to communicate information (i.e. forces and displacements) between the MD and FE computations when performing the staggered iteration cycles. Details of the present MD-FE coupling⁵⁴⁻⁵⁶ are explained in Section 4.2. Recently the hybrid method has been employed to simulate pure polystyrene and polystyrene nanocomposites containing a single ungrafted silica nanoparticle [55]. In the present contribution, this method is applied to investigate the influence of the mass fraction, size and grafting density of nanoparticles on the mechanical properties of polystyrene–silica nanocomposites in a coarse-grained resolution. At

first, standard periodic MD simulations without coupling to the FE domain are performed to identify the effective mechanical parameters (i.e. Young's modulus and Poisson's ratio) of polystyrene–silica nanocomposites. In addition, the influence of nanoparticle inclusion on structural and dynamic properties of polymer chains is also investigated. Subsequently, the considered nanocomposite systems are elongated at a constant deformation step size by the hybrid MD-FE method. The changes of the mean normal stress with the strain are monitored, too. Furthermore, a geometrical transformation model is proposed to analyze the changes of structural polymer properties at a glassy state during a uniaxial elongation. These results allow us to understand from a molecular perspective the improvements in the mechanical properties by nanofiller inclusion as well as the changes of polymer properties as a function of the applied deformation.

4.3 Simulation method and computational details

4.3.1 Hybrid molecular dynamics-finite element method

The hybrid simulation space consists of three regions, i.e. the outer FE, the inner MD and the intermediate dissipative particle dynamics (DPD) region (Figure 4.1). The FE region allows an application of an external load to deform the entire box during the hybrid simulation. The particles in the MD region move under classical Newtonian mechanics. The interactions between the beads in the MD region are described by a coarse-grained force field⁵⁷ developed by Ghanbari et al.³³. In our recent simulations^{34,54,55,58}, the applicability of the adopted force field has been investigated either with the help of qualitative scaling relations (Young's modulus) or quantitative property predictions (e.g. Poisson ratio and the interphase thickness). It should be mentioned that the Young's modulus derived from the present MD simulations is somewhat lower than the experimental number. This is reasonable, as the coarse-grained potential is softer than the atomistic one. More details will be given later. The MD computations in the hybrid framework are non-periodic and employ stochastic boundary conditions. Particles in the DPD region share the coarse-grained force field with the MD region. This means that the interactions between particles in the DPD region also contain the conservative forces as between

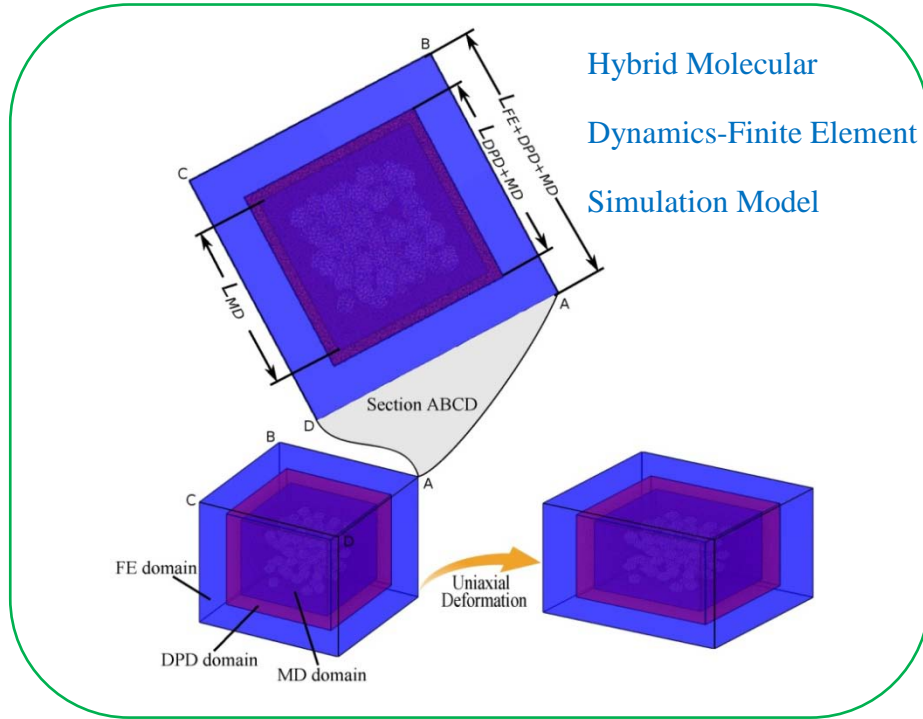


Fig. 4.1 Spatial decomposition in the employed hybrid MD-FE simulation model. The outer, middle and kernel region refer to the FE, DPD and MD domain of the hybrid simulation space. The sizes of the FE, DPD and MD domain are denoted as L_{FE} , L_{DPD} and L_{MD} .

Table 4.1 Structural details of coarse-grained polystyrene chains and silica nanoparticles. Note that the grafting density of silica nanoparticles is defined as the ratio between the number of the grafted polymer chains on the nanoparticle surface and the entire surface area of the nanoparticle. For an explanation of the bead types see Figure 4.2. Here l_{PS} , Φ , and ρ are the polymer chain length, nanoparticle diameter and nanoparticle grafting density.

Bead type	Bead mass/(kg/mol)	Polystyrene chain	Ungrafted silica nanoparticle		Grafted silica nanoparticle		
		$l_{PS} = 20$ (beads)	$\Phi = 5$ (nm)	$\Phi = 2$ (nm)	$\Phi = 5$ (nm), $\rho = 0.25$ (chains/nm ²)	$\Phi = 5$ (nm), $\rho = 0.60$ (chains/nm ²)	$\Phi = 5$ (nm), $\rho = 0.95$ (chains/nm ²)
S	0.104	20	0	0	30	30	30
R	0.104	0	447	57	447	447	447
SF	0.0639	0	1273	44	1273	1273	1273
CR	0.0639	0	0	0	2	2	2
L1	0.0541	0	0	0	2	2	2
L2	0.0582	0	0	0	2	2	2

particles in the MD region, augmented by the pairwise interactions from DPD. Additionally, there are a number of virtual particles, called anchor points, in the DPD region. They attenuate the escape probability of polymer beads from the DPD region to the FE “vacuum”. To this end, a large number of polymer beads in the DPD region are tethered to the anchor points by a harmonic interaction. The anchor points pass the changes of their positions and the average forces acting on them between the particle and continuum region during the hybrid simulation. The selection criteria for the number of virtual anchor points as well as their distribution in the overlapping domain have been quantified in detail in our recent publications^{54,56}. For a first analysis of the stability of our coupling scheme, see ref. 55. Nevertheless, we have to point out that the spatial anchor point distribution is a compromise between the MD domain (exponential increase of the anchor point density towards the outer MD boundary) and the FE domain (uniform distribution in the overlapping region). First investigations to overcome this issue, e.g. by choosing the weighting factor for the mixing of the MD and FE contribution to this region in a more sophisticated way, are carried out in the two groups. To sum up, the observed results indicate that the system properties in the inner MD domain are almost not influenced by variations in the number and distribution of the anchor points when their number is chosen in a reasonable range.

The hybrid MD-FE method couples the continuum-based FE region to the particle-based MD region based on the Arlequin method^{50,52}. The iterative MD-FE computation in the hybrid simulations is performed in a staggered way^{55,58}. The external shape of the MD region is designed to be static when carrying out the FE step and vice versa. The macroscale continuum and the microscale particle region feel each other only by the forces and the displacements of anchor points. Both the MD and the DPD region (including anchor points) are defined prior to each hybrid run. After the MD step, the time-averaged forces on the anchor points exerted by polymer beads are transmitted to the FE run as required computational input^{59,60}. After the completion of an FE step, the updated anchor point positions from the previous FE computation are passed to the next MD run where they play the role of a static external potential. The staggered MD-FE loops end when the predefined number of load steps has been performed. Our uncertainty quantification (UQ) analysis⁵⁶ has demonstrated that non-periodic MD simulations with parameters in a safe range reproduce the results of a standard periodic MD simulation of the

same system. Guided by the UQ results, we have chosen the material parameters for ten different systems (i.e. pure polystyrene, ungrafted and grafted polystyrene–silica mixtures) as summarized in Tables 4.1, 4.2 and 4.3.

Table 4.2 Components of the considered systems in the hybrid MD-FE simulations. The structural details of the coarse-grained polystyrene chains and silica nanoparticles used in the hybrid MD-FE simulations are given in Table 4.1. The number of the polystyrene chains in all systems is 3000.

System	Silica nanoparticle number N_{silica}	Silica nanoparticle diameter \emptyset /(nm)	Grafting density ρ /(chains/nm ²)	Nanoparticle mass fraction ω (%)
1	2	5	0	3.403
2	5	5	0	8.094
3	8	5	0	12.350
4	34	2	0	3.400
5	85	2	0	8.081
6	136	2	0	12.340
7	1	5	0.25	1.731
8	1	5	0.60	1.731
9	1	5	0.95	1.730
10	0	0	0	0

Table 4.3 Material parameters of polymer nanocomposite systems that are studied by hybrid MD-FE simulations. Two mechanical parameters (Young’s modulus and Poisson’s ratio) for the different polymer nanocomposite systems have been identified from standard periodic MD computations. Here, the step size $\Delta\epsilon$ is the increase of the strain (1%) applied in each load step of the hybrid MD-FE simulations. The force constant k between polymer beads and anchor points is $1400 \text{ kJ mol}^{-1} \text{ nm}^{-2}$. The thickness of the DPD domain L_{DPD} is 2.0 nm.

System	Young’s modulus E (MPa)	Poisson’s ratio ν	Number of anchor point N
1	876±21.6	$0.3\pm 3.7\times 10^{-3}$	9047
2	989±17.3	$0.3\pm 4.9\times 10^{-3}$	9010
3	1167±35.4	$0.3\pm 4.1\times 10^{-3}$	9009
4	917±12.6	$0.3\pm 2.1\times 10^{-3}$	9051
5	1032±11.8	$0.3\pm 3.8\times 10^{-3}$	9141
6	1223±38.2	$0.3\pm 2.7\times 10^{-3}$	9313
7	869±25.3	$0.3\pm 3.5\times 10^{-3}$	9016
8	903±16.5	$0.3\pm 5.6\times 10^{-3}$	9022
9	968±14.9	$0.3\pm 4.3\times 10^{-3}$	9094
10	815±12.7	$0.3\pm 6.5\times 10^{-3}$	9035

The anchor-point-related parameters k , N and L_{DPD} denote the force constant between an anchor point and a polymer bead, the number of anchor points and the thickness of the DPD domain, respectively. More details on the parameters of the FE part can be found in ref. 55.

4.3.2 Details on the coarse-grained nanocomposite systems

The initial configurations for the inner MD region are prepared as required by the non-periodic MD simulations. Each repeat unit in the polystyrene chains is treated as one bead located at its center of mass^{32,33}. Two different bead types (R and S) are defined to account for the chirality of the chains. The atomistic coordinates of the silica nanoparticles are generated from a lattice of crystalline silica by removing all atoms beyond the predefined nanoparticle radius. Then the coarse-grained beads were placed at the positions of the silicon atoms. To describe the polymer-nanoparticle interaction reasonably, we use different silica beads for the surface (SF) and the core (CR). Note that the surface beads have the dominant contribution to the attractive interaction with the polystyrene beads. In the grafted systems, polystyrene chains are attached to the silica surfaces with a linker segment $(-[\text{H}_2\text{C}(\text{H}(\text{C}_2\text{H}_5)\text{C})]_3(\text{CH}_3)_2\text{Si}-)$. The linker segment in the coarse-grained system is formed by two different beads defined by the $-\text{CH}_2\text{CHCH}_2-$ group (L1 bead) and the $-(\text{CH}_3)_2\text{Si}$ group (L2 bead). To generate the initial configurations of the nanocomposites (Figure 4.2), silica nanoparticles are initially placed randomly in the simulation space; then the polymer chains grow gradually bead-by-bead. The initial structures are equilibrated for 10 ns using a standard periodic MD simulation at 590 K. Afterwards the equilibrated structures are cooled down from 590 K to 100 K at a rate of 10 K ns^{-1} . The glass transition temperature T_g for our coarse-grained model is 170 K ³⁴.

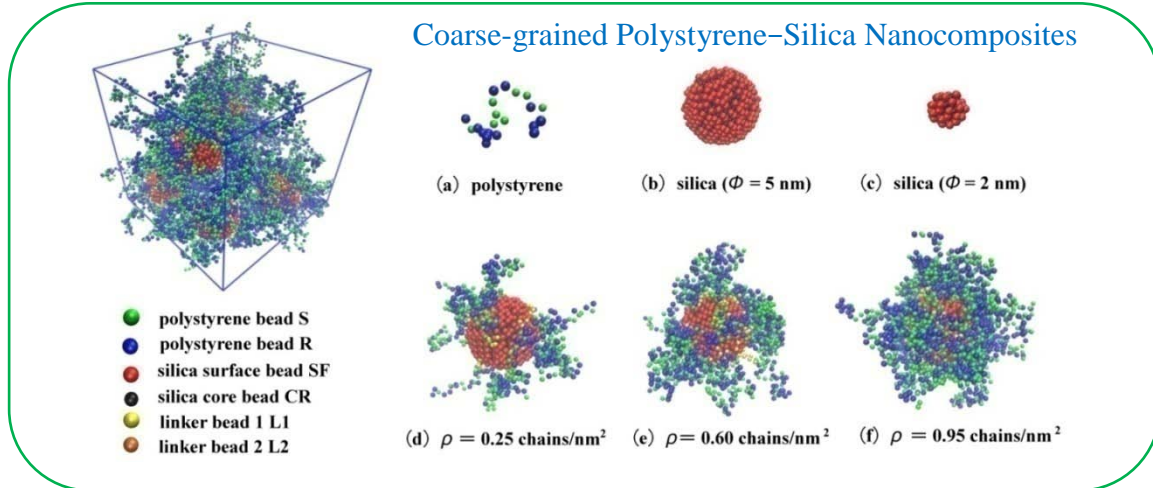


Fig. 4.2 Coarse-grained polystyrene–silica nanocomposite systems with and without grafted polymer chains. Φ and ρ are the diameter and grafting density of the nanoparticles, respectively.

To adopt non-periodic boundary conditions for the hybrid MD-FE simulation, all polymer segments outside the simulation box are then cut and shifted back into it. Note that more than 98.5% of the fragmented beads are from the DPD domain. This means that the chain cutting procedure has a negligibly small influence on the inner MD domain. The particle domain (MD+DPD) has the dimension (21 nm \times 21 nm \times 21 nm). The thickness of the DPD domain is 2 nm. With the final structures after the standard periodic MD simulation, the number and position of anchor points are chosen. The FE region is defined as a mesh structure with an appropriate size (30 nm \times 30 nm \times 30 nm). The effective material properties, i.e. Young's modulus and Poisson's ratio, have been identified from standard periodic MD simulations by applying uniaxial deformations at 100 K under $NLP_{\perp}T$ conditions. Here the MD box is elongated with a constant rate in the y-direction. In addition, the box lengths in the two perpendicular directions are coupled to a pressure bath (1 bar) by the Berendsen method. The relation between the strain ε and the time t follows the equation: $\varepsilon(t) = \frac{\mu t}{L_0} \times 100\%$. Here, μ and L_0 denote the deformation rate and the initial box length in the selected elongation direction. The Young's modulus is calculated within the elastic deformation region (up to 3% strain). MD Simulations have demonstrated that the deformation rate (i.e. 1.5 ~ 45 nm ns⁻¹) has only a small influence on the Young's modulus³⁴. For instance, for deformation rates of 1.5, 15 and 45 nm ns⁻¹ at 100 K, the Young's modulus of pure polystyrene is 823 \pm 27.1, 815 \pm 12.7 and 819 \pm 36.6 MPa,

respectively. For the present deformation simulations we have chosen an elongation rate μ of 15 nm ns⁻¹. It should be mentioned that the strain rate used in the present work to simulate the uniaxial deformation of nanocomposites is similar to the ones used in other investigations⁶¹. It is computationally demanding to use a very low strain rate for MD deformation simulations, because they require an expensive computational effort for large systems.

4.3.3 Geometrical transformation model

A geometrical transformation model is proposed to analyze changes of structural properties of free polymer chains under an external load. This model allows differentiating changes in the polymer structure, which are merely affine to the system deformation, from those, which follow from additional relaxation processes. The components (i.e. R_{ex} , R_{ey} and R_{ez}) of the end-to-end distance R_e of free polymer chains in the three Cartesian directions change by the same ratio as the respective system dimensions (i.e. L_x , L_y and L_z) during the deformation. β denotes the angle between the end-to-end vector of a polymer chain and the deformation direction (i.e. y-axis); θ denotes the angle between the perpendicular direction (i.e. x-axis) and the projection of the end-to-end vector of polymer chains in the xz-plane after deformation. Note that the symbols with a subscript “0” refer to the corresponding variables before deformation. On the basis of the proposed model, Equations (4.1), (4.2), and (4.3) are obtained,

$$1 + \varepsilon_{xx} = \frac{L_x}{L_{x0}} = \frac{R_{ex}}{R_{ex0}} = \frac{R_e \sin \beta \cos \theta}{R_{e0} \sin \beta_0 \cos \theta_0} \quad (4.1)$$

$$1 + \varepsilon_{yy} = \frac{L_y}{L_{y0}} = \frac{R_{ey}}{R_{ey0}} = \frac{R_e \cos \beta}{R_{e0} \cos \beta_0} \quad (4.2)$$

$$1 + \varepsilon_{zz} = \frac{L_z}{L_{z0}} = \frac{R_{ez}}{R_{ez0}} = \frac{R_e \sin \beta \sin \theta}{R_{e0} \sin \beta_0 \sin \theta_0} \quad (4.3)$$

where ε_{xx} , ε_{yy} and ε_{zz} are the strain in the x-, y- and z-directions. Note that here we have $\varepsilon_{xx} = \varepsilon_{zz} = -\nu \varepsilon_{yy}$ (ν is the Poisson's ratio of the considered material). Thus, the squared

projections (R_{ex}^2 , R_{ey}^2 and R_{ez}^2) of R_e of polymer chains correlate with the strain in the respective directions as given by Equations (4.4), (4.5), and (4.6).

$$R_{ex}^2 = R_{ex0}^2 [1 - \nu \varepsilon_{yy}]^2 \quad (4.4)$$

$$R_{ey}^2 = R_{ey0}^2 [1 + \varepsilon_{yy}]^2 \quad (4.5)$$

$$R_{ez}^2 = R_{ez0}^2 [1 - \nu \varepsilon_{yy}]^2 \quad (4.6)$$

Additionally, β can be expressed as in Equation (4.7) by solving Equations (4.1), (4.2), and (4.3).

$$\beta = \tan^{-1} \left(\frac{1 - \nu \varepsilon_{yy}}{1 + \varepsilon_{yy}} \tan \beta_0 \right) \quad (4.7)$$

To characterize the orientation change of free polymer chains during the deformation, the chain orientation has been defined by the second-order Legendre polynomial

$$\langle P_2 \rangle = \frac{3}{2} \langle \cos^2 \beta \rangle - \frac{1}{2}. \quad (4.8)$$

4.4 Results and discussion

4.4.1 Parameter identification from periodic MD simulations

The stress-strain curves for all systems (Figure 4.3) are characterized by an elastic deformation region, in which the stress increases linearly with the strain. Yield occurs at about 5% strain. The elastic region is followed by a stress plateau. Additionally it can be observed that (i) an increase of the nanoparticle mass fraction or (ii) an increase of the grafting density on the nanoparticle surfaces, as well as (iii) a decrease of the nanoparticle size at a constant mass fraction enhances the yield strength of the materials. The Young's modulus has been calculated from the slope of the stress-strain curves in the linear region (up to 3% strain). It increases with the nanoparticle mass fraction (Fig 4.4 (a)) and the grafting density (Fig 4.4 (c)) on the nanoparticle surface, as well as with a decreasing nanoparticle size at the same mass fraction (Fig 4.4 (a)). The Young's

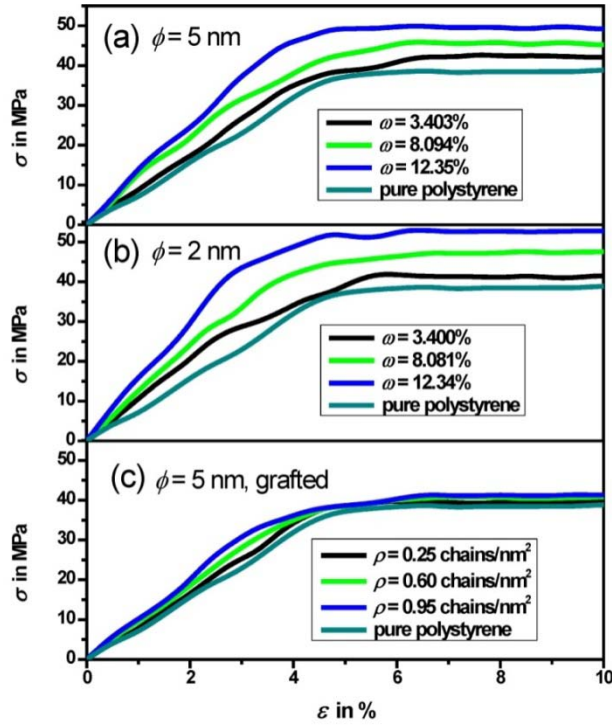


Fig. 4.3 Stress-strain curves for the polystyrene–silica nanocomposite systems from periodic MD simulations. The simulation temperature is 100 K ($T_g = 170$ K). The load is applied in y -direction. (a) $\phi = 5$ nm, ungrafted; (b) $\phi = 2$ nm, ungrafted; (c) $\omega = 1.73\%$, $\phi = 5$ nm and grafted.

modulus of silica nanoparticles ($E_{NP} = 3832 \pm 43$ MPa) has been calculated by deforming a coarse-grained silica crystal at 100 K. A linear relation⁶² between the mass fraction of the nanoparticles and the Young's modulus of the nanocomposites is not obtained in our simulations. This seems to be no surprise since the complex interactions between the polymer matrix and the nanoparticles might cause effects that cannot be captured by such a simple mixing rule. As shown in Figure 4.4 (a), the Young's modulus E_{NC} of the nanocomposites can be expressed approximately as a quadratic function of the nanoparticle mass fraction ω , i.e. $E_{NC}(\omega) = p_1\omega^2 + p_2\omega + p_3$. A quadratic relation between the Young's modulus of nanocomposites and the nanofiller content has been observed by other researchers^{63,64}. Also note that smaller particles (nanoparticle diameter $\phi = 2$ nm) at the same mass fraction lead to a higher E value than larger particles ($\phi = 5$ nm), most likely due to their larger interphase region. Smaller nanoparticles

produce a Young's modulus that is about 4 to 5% higher than in samples with larger nanoparticles (constant nanoparticle mass fraction assumed). An increasing interphase area leads to an increasing interaction between the matrix and the nanofiller, so that a higher fraction of polymer chains in nanocomposites is strongly adsorbed by the nanoparticle surface. This explains that macroscopic mechanical properties of polymer nanocomposites are largely determined by the microscopic interphase structure⁶⁵⁻⁶⁷. As an example, Odegard et al.⁶⁸ have demonstrated by an effective interphase model that the mechanical strength of polyimide–silica nanocomposites is improved when increasing the interphase area. Although extended mixing rules are research areas on their own, influence factors such as e.g. grafting densities which are discussed in this work, are difficult to consider by such approaches. This enhances the need of more accurate, particle-based considerations at a level of atoms and molecules.

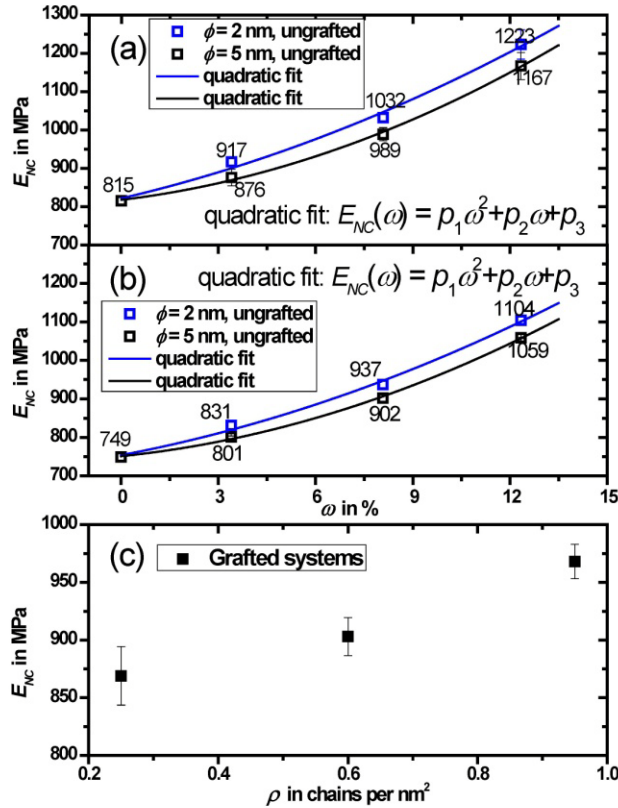


Fig. 4.4 Young's modulus E_{NC} of polymer nanocomposites versus (a, b) nanoparticle mass fraction ω and (c) grafting density ρ . The black and blue lines in Figures 4.4 (a) and 4.4 (b) represent quadratic fits ($E_{NC} = p_1\omega^2 + p_2\omega + p_3$). (a) standard MD simulation, $\Phi = 5$ nm: $p_1 = 1.46$ MPa, $p_2 = 10.1$ MPa, $p_3 = 818$ MPa; $\Phi = 2$ nm: $p_1 = 1.01$ MPa, $p_2 = 19.7$ MPa,

$p_3 = 822 \text{ MPa}$. (b) hybrid MD-FE simulation, $\phi = 5 \text{ nm}$: $p_1 = 1.31 \text{ MPa}$, $p_2 = 8.64 \text{ MPa}$, $p_3 = 751 \text{ MPa}$; $\phi = 2 \text{ nm}$: $p_1 = 0.98 \text{ MPa}$, $p_2 = 16.0 \text{ MPa}$, $p_3 = 754 \text{ MPa}$.

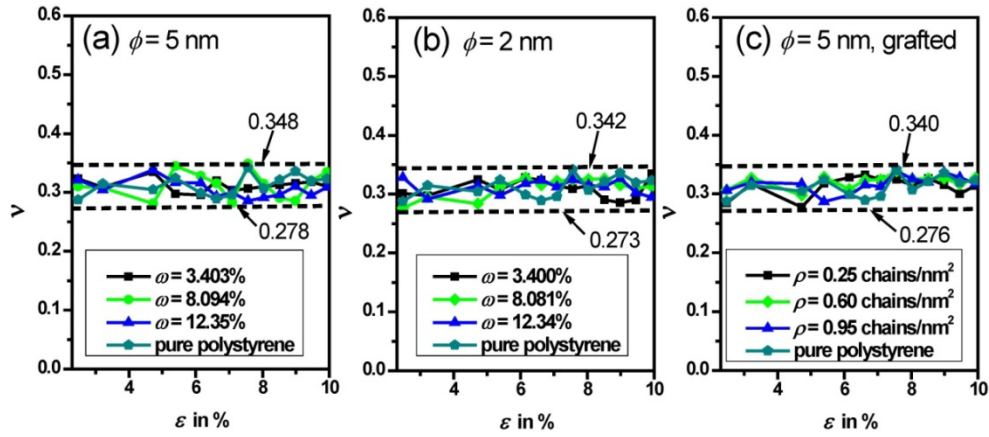


Fig. 4.5 Poisson's ratio ν of all simulated systems as a function of uniaxial strain ε . The simulation temperature is 100 K. The load is applied in the y -direction. The two dashed lines stand for the maximum and minimum calculated value of the Poisson's ratio. (a) $\phi = 5 \text{ nm}$, ungrafted; (b) $\phi = 2 \text{ nm}$, ungrafted; (c) $\omega = 1.73\%$, $\phi = 5 \text{ nm}$ and grafted.

The Poisson's ratio of all simulated nanocomposites has been also calculated by MD simulations under periodic boundary conditions at 100 K (Figure 4.5). The Poisson's ratio depends neither on the mass fraction of the nanoparticles nor on their grafting density. Up to 10% strain, the Poisson's ratio fluctuates around 0.3. This value is close to the Poisson's ratio calculated from a united-atom model⁶¹ (0.33 ± 0.02) and observed by an experimental measurement⁶⁹ ($0.32 \sim 0.33$). Young's moduli and Poisson's ratios obtained by MD simulations under periodic boundary conditions are introduced as material parameters in the FE model of the hybrid computations under external loads (Table 4.3).

4.4.2 Influence of nanoparticles on microscopic structural and dynamic properties of polymer chains as derived by periodic MD simulations

Squared end-to-end distances of the free polymer chains are calculated as a function of the distance of their center of mass from the nanoparticle surface. For this purpose, the nanoparticles are considered as spheres with a known diameter ($\phi = 2$ or 5 nm). The space around the nanoparticles (surface separation between 0 and 3 nm) is divided into 10 spherical shells with a thickness of 0.3 nm. The free polymer chains are allocated to a shell according to their center-of-mass positions. The squared end-to-end distances are averaged over all free polymer chains and nanoparticles in the nanocomposites. As shown in Figure 4.6, at larger distances from the nanoparticle surface (i.e. 2 ~ 3 nm), the squared end-to-end distances of the polymer chains in all systems have a plateau that is close to the squared end-to-end distance (6.26 nm^2) of the pure polymer. The nanoparticles do not influence significantly the structural properties of the bulk polymer chains beyond a distance of about 1.1 nm. The reason is that the interaction between polymer chains and nanoparticles decays gradually to a negligible value when the separation from their surface is enlarged.

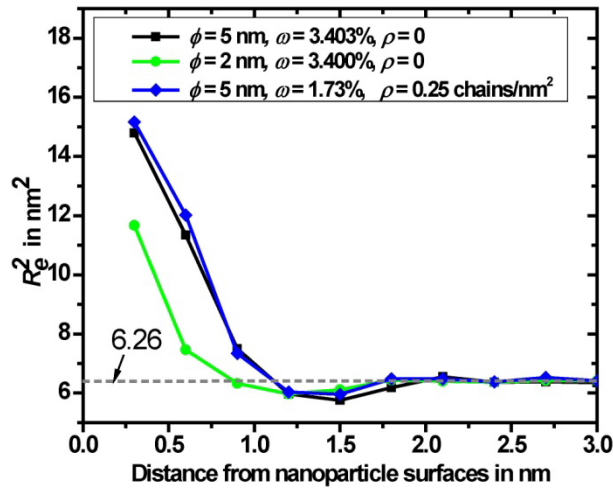


Fig. 4.6 Squared end-to-end distance R_g^2 of polymer chains in the considered nanocomposite systems as a function of the distance from the nanoparticle surface. The dashed line refers to R_g^2 in the pure polystyrene system.

However, at closer separations, the end-to-end distances for all systems increase above the bulk value. This expansion of polymer chains near nanoparticles, which are larger than their radius of gyration, has been observed before in atomistic³⁰ and coarse-grained simulations^{32,33}. For the same reason, the squared end-to-end distances of free polymer chains in the interphase of bigger

nanoparticles ($\sim 15 \text{ nm}^2$) are larger than those with smaller nanoparticles ($\sim 12 \text{ nm}^2$). In the neighborhood of the nanoparticles (e.g. limited to 1.1 nm from the surface), when the first few monomer units of a polymer approach the nanoparticle surface, the polymer chain is compressed in the direction of the surface normal. Those chains located even closer to the nanoparticles, have to swell tangential to the surface. This expansion in the tangential direction overcompensates the compression in the normal direction. Consequently, the chain end-to-end distance first decreases and then increases as the chains approach the nanoparticles. From the profile of the squared end-to-end distances of free polymer chains, it can be concluded that the thickness of the interphase between the polymer matrix and the nanofiller is roughly 1 ~ 1.5 nm.

To characterize the distribution of the nanoparticles in the polymer matrix, the radial distribution function of their centers of mass is calculated as an example (Figure 4.S1 (a), $\phi = 2$ and $\omega = 3.4\%$). The shape of the normalized radial distribution function is characteristic for short-range order via a dense packing (excluded volume) and a lack of long-range order. The positions of the first ($\sim 3.3 \text{ nm}$) and second peaks ($\sim 4.1 \text{ nm}$) indicate that close nanoparticles are separated by 2 or 3 polystyrene beads, pointing to a stronger polymer adsorption onto the particle surfaces. The structural properties of free polymer chains within the interphase regions differ from the behavior of the bulk polymer due to the interaction with the nanoparticles. Figure 4.S1 (b) displays the radial distribution function of polymer beads (i.e. number density of polymer monomers) around the nanoparticles versus the distance from the nanoparticle surfaces ($\phi = 2$ and $\omega = 3.4\%$). The radial distribution function curve shows a layered structure of the polymer beads in the vicinity of the nanoparticles. This has been also observed in other experimental and simulation investigations^{33,70}. The structural behavior of nanoparticles lead to a peak at the distance of about 1 nm where the number density of polymer beads is roughly 1.2 times the bulk value. This indicates that compared with the bulk, a denser packing of the polymer chains is formed in the interphase region due to the polymer-nanoparticle interaction as well as due to excluded volume effects.

Figure 4.S2 shows the center-of-mass mean square displacement (MSD) of the polymer chains and the nanoparticles at 590 K in the ungrafted systems for different nanoparticle mass fractions.

We observe that the center-of-mass MSDs of the polymer chains and the nanoparticles are reduced with an increase of the nanoparticle mass fraction (at constant nanoparticle size). These diagrams also indicate that the MSDs of the polymer chains are slightly larger in the presence of larger nanoparticles (at same nanoparticle mass fraction). The diffusion coefficient D derived from the center-of-mass MSDs describes the global dynamics of polymer chains and nanoparticles. The diffusion coefficient of the free polymer chains D_{ps} (Figure 4.7 (a)) and the nanoparticles D_{np} (Figure 4.7 (b)) is reduced almost linearly with an increasing nanoparticle mass fraction (at constant nanoparticle size). A similar linear relation has been observed by Capaldi et al.⁷¹ in atomistic MD simulations of polyethylene–silsesquioxanes composites. Larger nanoparticles

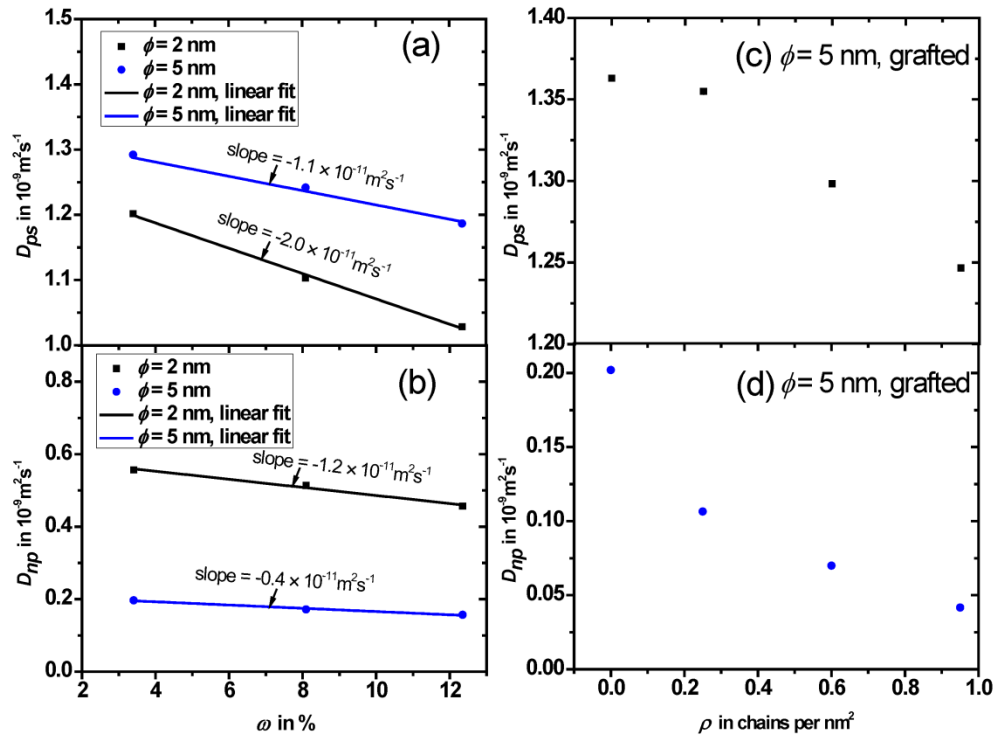


Fig. 4.7 Diffusion coefficient of the polymer (D_{ps}) and the nanoparticle (D_{np}) versus nanoparticle mass fraction ω and grafting density ρ . The simulation temperature is 590 K. The error bars of the diffusion coefficients are not visible in the figures due to their very small values.

diffuse slower than smaller ones. The factor between 0.28 and 0.30 at different nanoparticle concentrations is in line with a simple Stokes-Einstein estimate of 2.5. Correspondingly, the

slope of the 2 nm particles equals three times that of the 5 nm particles. In contrast, the reduction of the diffusion coefficient of free polymer chains as a function of the nanoparticle mass fraction is steeper in the systems with smaller nanoparticles (slope = $-2.0 \times 10^{-11} \text{ m}^2 \text{ s}^{-1}$) than for larger nanoparticles (slope = $-1.1 \times 10^{-11} \text{ m}^2 \text{ s}^{-1}$). This demonstrates that smaller nanoparticles suppress the mobility of free polymer chains more efficiently than larger nanoparticles when their mass fraction is identical.

Furthermore, the dynamics of the free polymer chains in the vicinity of nanoparticles is slower than that of the polymer chains in the pure polymer. To verify this we have calculated the diffusion coefficient of free polymer chains within the sub-shell region (0 ~ 1 nm from the nanoparticle surface) in the systems with large ($\emptyset = 5 \text{ nm}$, $\omega = 3.4\%$) and small nanoparticles ($\emptyset = 2 \text{ nm}$, $\omega = 3.4\%$). They amount to $0.97 \pm 0.002 \text{ nm}^2 \times 10^{-9} \text{ m}^2 \text{ s}^{-1}$ and $1.13 \pm 0.001 \times 10^{-9} \text{ m}^2 \text{ s}^{-1}$, respectively. Both values are smaller than the diffusion coefficient ($1.37 \pm 0.002 \times 10^{-9} \text{ m}^2 \text{ s}^{-1}$) in the pure polymer. This demonstrates that the nanoparticles slow down the dynamics of the free polymer chains in the interphase region. We can conclude that the interaction of the polymer chains with the nanoparticles influences not only their structure (e.g. end-to-end distance, Figure 4.6) but also their dynamics in the interphase. The same observations have been reported by other researchers using either atomistic³¹ or coarse-grained⁷²⁻⁷⁶ MD simulations. Increasing the nanoparticle mass fraction or blending with smaller nanoparticles at the same nanoparticle mass fraction produces a larger interface area. Note that the nanoparticles in all systems do not touch each other. For instance, the interphase area ($\sim 1708 \text{ nm}^2$) in the systems containing smaller nanoparticles ($\emptyset = 2 \text{ nm}$, $\omega = 12.34\%$) is almost three times as large as that ($\sim 628 \text{ nm}^2$) in the systems containing larger nanoparticles ($\emptyset = 5 \text{ nm}$, $\omega = 12.35\%$). The role of the interface area is also emphasized by comparing the systems with $\emptyset = 5 \text{ nm}$, $\omega = 12.35\%$ and $\emptyset = 2 \text{ nm}$, $\omega = 3.4\%$. Both have total interface areas of similar order of magnitude and thus also a similar polymer diffusion coefficient (1.20×10^{-9} and $1.18 \times 10^{-9} \text{ m}^2 \text{ s}^{-1}$, respectively), cf. Fig. 4.7 (a).

The center-of-mass MSDs of the free and grafted polymer chains as well as of the nanoparticles in the grafted systems are presented in Figure 4.S3. The diffusion coefficients of free chains and nanoparticles are shown in Figures 4.7 (c) and 4.7 (d). It can be concluded that an increase of the

grafting density of the nanoparticles hinders the global dynamics of the free and grafted chains as well as of the nanoparticles. We assume that grafting more polymer chains onto the nanoparticles causes an increase of geometric hindrance effects between the free chains and nanoparticles as well as an increase of the congestion of the grafted chains.

4.4.3 Hybrid MD-FE simulations

Prerequisites of hybrid MD-FE simulations. Pre-equilibrium runs have to be performed first at $T = 100$ K to relax the inner MD region. In this relaxation step, the Young's modulus in the FE region of all simulated systems is set to a very low value (i.e. $E = 0.1$ MPa), while the Poisson's ratio is set to zero. The diagonal elements of the stress tensor in the MD domain are calculated by collecting the components of the average forces on the anchor points that are perpendicular to the surface of the MD box. After the relaxation in 500 combined MD-FE iterations (total MD simulation time of 125 ns), all three diagonal elements of the stress tensor converge from their initial values (~ 6.3 kPa) to nearly zero, demonstrating that the systems have been equilibrated. In this step the density of the inner MD domain has been reduced by only about 0.12%. The size of the MD domain remains roughly constant during the relaxation. The equilibrated configurations are then used to start the hybrid simulation. Moreover, we find that the deviations of the mean normal stresses⁵⁵ in each load step converge roughly to zero in about 80 MD-FE iterations. Thus we have employed 80 MD-FE iterations for each load step (increase of the strain by 1%) in the hybrid simulation.

Uniaxial tension. In Figure 4.8 (a), $\bar{\sigma}_{yy}$ denotes the mean normal stress in the deformation direction and is displayed as a function of the number of MD-FE iterations for different nanoparticle mass fractions with a constant diameter of 5 nm. At each load level, $\bar{\sigma}_{yy}$ increases with increasing nanoparticle mass fraction. The same qualitative behavior is obtained for smaller particles of 2 nm diameter and for a higher grafting density, cf. Figure 4.8 (b) and 4.8 (c): again, high nanoparticle mass fractions and grafting densities generate larger mean stresses. The agreement between hybrid MD-FE and standard MD simulations follows from the fact that the Young's modulus required in the FE region is taken from MD. As displayed in Figure 4.4 (b), the stiffness of a nanocomposite increases with an increasing mass content of the nanoparticles.

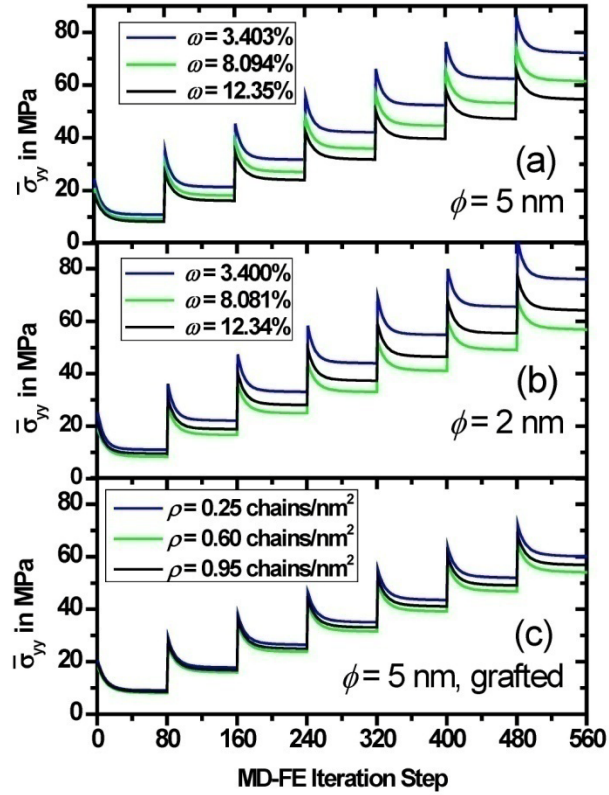


Fig. 4.8 Mean normal stresses $\bar{\sigma}_{yy}$ of polystyrene–silica nanocomposites with different silica concentrations as a function of the number of MD-FE iterations. The nanocomposite systems are elongated along the y direction. The step size $\Delta\varepsilon$ is 1% for each load step and the final strain is 7%, which requires in total 560 MD-FE iterations (80 iterations for each load step). (a) $\phi = 5$ nm, ungrafted; (b) $\phi = 2$ nm, ungrafted; (c) $\phi = 5$ nm, grafted.

Similar to standard MD simulations we compute the Young's modulus of the nanocomposites by the hybrid MD-FE formalism. The data are derived via the mean normal stress at 3% strain. Additionally, we investigate the relation between the Young's modulus and the nanoparticle mass fraction, cf. Figure 4.4 (b). Within both simulation methods we obtain the similar qualitative behavior. This is valid for the influence of the nanoparticle radius and the nanoparticle mass fraction. Both sets of data are consistent with experimental investigations^{62,77-80}; they only differ in the absolute values of the Young's moduli which are shifted to lower values in the hybrid case. This is most likely due to certain computational approximations in the coupling scheme (i.e. chain cutting procedure described in Section 4.2) which causes a decreased

stiffness in the overlapping region between the MD and FE domains. The described issue is an additional subject of ongoing investigations. To deal with it, we currently investigate strategies how the hybrid simulations may be realized without cutting chains or how the finite elements may be chosen properly such that all anchor points are surely contained in the finite elements of the overlapping region. Additionally, as a possible remedial strategy, simulations with an enlarged overlapping region would increase the stability of the coupling approach. Under these conditions the ratio of cut chains becomes smaller, which leads to an attenuated influence on the stiffness of the considered nanocomposites. Nevertheless, even at lower absolute values, our coupling scheme is able to reproduce qualitatively the impact of the nanoparticles at different mass fractions and diameters. Thus, we are convinced that the observed trends enable us already at the current state to treat larger systems which are barely accessible by pure MD approaches.

Structural properties of polymer chains during the uniaxial deformation. Figure 4.9 presents the MD-FE based chain orientation parameter $\langle P_2 \rangle$ averaged over all free chains as a function of the strain. It is nearly zero before deformation and increases almost linearly with the strain. Thus it can be concluded that free polymer chains adjust their conformations from a random orientation to align gradually with the deformation direction under an external load. The $\langle P_2 \rangle$ values in Figure 4.9 have been fitted to straight lines. The polymer orientation toward the elongation direction becomes weaker with an increasing nanoparticle mass fraction. The presence of nanoparticles hinders the rotation of the polymer chains probably by adsorbing parts of them. Comparing Figures 4.9 (a) and (b), smaller nanoparticles hinder the orientation adjustment of free polymer chains during the deformation more efficiently than larger nanoparticles when the nanoparticle mass fraction is identical. The observation emphasizes again the role of the interface area. Figure 4.9 (c) shows the rather small influence of surface grafting on the chain orientation. In particular, the slopes of the $\langle P_2 \rangle$ curves are only slightly affected.

How much of the polymer reorientation follows merely from an affine deformation of the sample, and how much is owed to the molecular relaxation processes? To clarify this point, we introduce the ratio Ψ which measures the deviation between Ψ chain orientation parameters (see Figure 4.10),

i.e. $\Psi = \frac{\langle P_2 \rangle_h - \langle P_2 \rangle_0}{\langle P_2 \rangle_g - \langle P_2 \rangle_0}$. $\langle P_2 \rangle_h$ and $\langle P_2 \rangle_g$ represent the orientation parameter of free

polymer chains as determined by the hybrid MD-FE simulations and the geometrical transformation model, respectively; $\langle P_2 \rangle_0$ denotes the orientation parameter of free polymer chains before deformation. For pure polystyrene the ratio Ψ amounts to nearly 1.0 throughout the deformation process. This demonstrates little relaxation of polymer chains, as expected for a polymer glass. In the nanocomposite systems, the ratios Ψ are smaller than 1.0, which means that the polymer chains in the hybrid system change their orientation less than those of a pure polymer matrix. This effect becomes even stronger with increasing nanoparticle mass fraction as well as with increasing grafting density. Both dependencies are reasonable since interfacial adsorption restricts the orientation adjustment of a fraction of polymer chains in the nanocomposite such that they cannot fully follow the overall deformation.

Figure 4.11 presents the squared average of the projection of the end-to-end distance R_e of free polymer chains $R_{\parallel}^2 = \langle R_{ey} \rangle^2$ in the tensile direction (solid symbols) and the mean of the associated quantities $R_{\perp}^2 = \frac{1}{2}(\langle R_{ex} \rangle^2 + \langle R_{ez} \rangle^2)$ in perpendicular direction (hollow symbols). Note that the bracket $\langle \dots \rangle$ denotes the average over all free polymer chains in the MD domain. R_{\parallel}^2 increases with the strain for all nanoparticle mass fractions and grafting densities. The opposite tendency is observed in the perpendicular direction. In other words, the polymer chains in the materials elongate in the tensile direction and shrink in the perpendicular direction during the uniaxial stretching. The fact that the data sets do not share the same values at zero elongation is due to the small system size which might lead to an excess of chain orientation in the same direction. Nevertheless, we have also found that R_{\parallel}^2 increases, depending on the strain, to approximately 15% to 20% higher values than the associated quantity R_{\perp}^2 in the perpendicular direction. The geometrical model, which describes the behavior of an ideal, undisturbed system, would render approximately 5% to 10% higher values in the perpendicular direction for the same strain applied in the nanocomposite systems. This shows that the presence of nanoparticles has an impact on the structural properties of the polymer chains which cannot be captured by simple models.

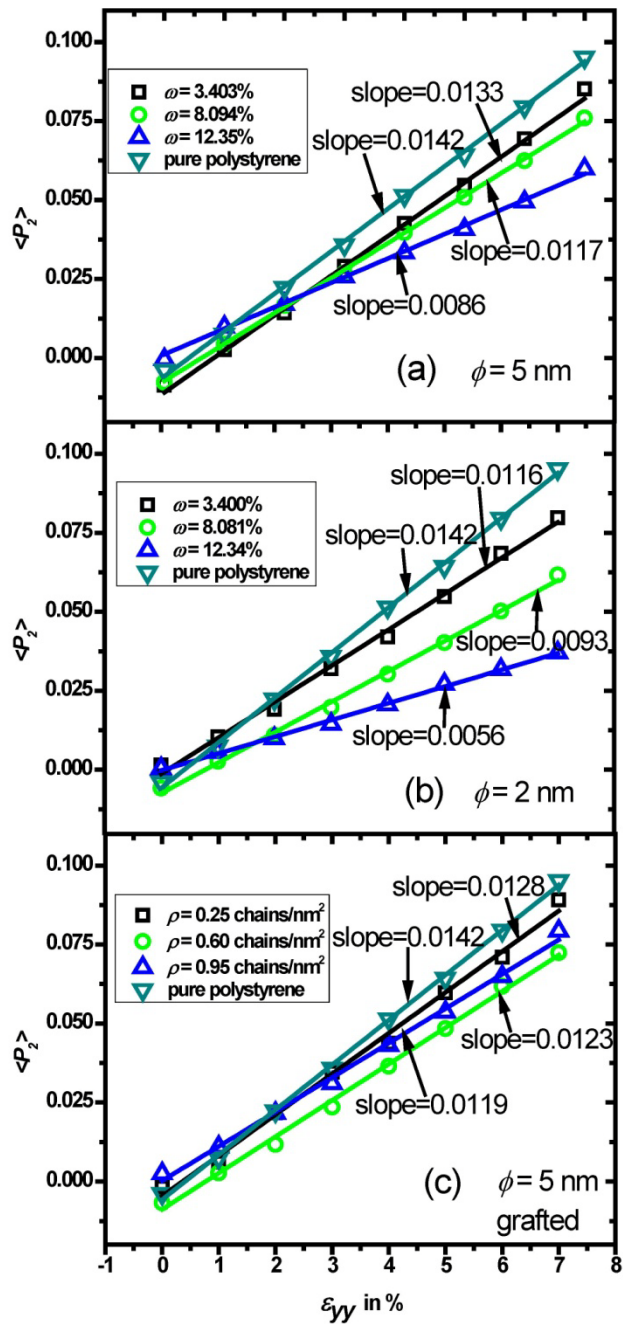


Fig. 4.9 Chain orientation parameter $\langle P_2 \rangle$ of free polymer chains in the considered systems versus the strain ϵ_{yy} during hybrid MD-FE simulations. (a) $\Phi = 5$ nm, ungrafted; (b) $\Phi = 2$ nm, ungrafted; (c) $\omega = 1.73\%$, $\Phi = 5$ nm and grafted. Also shown are linear fits to the data points.

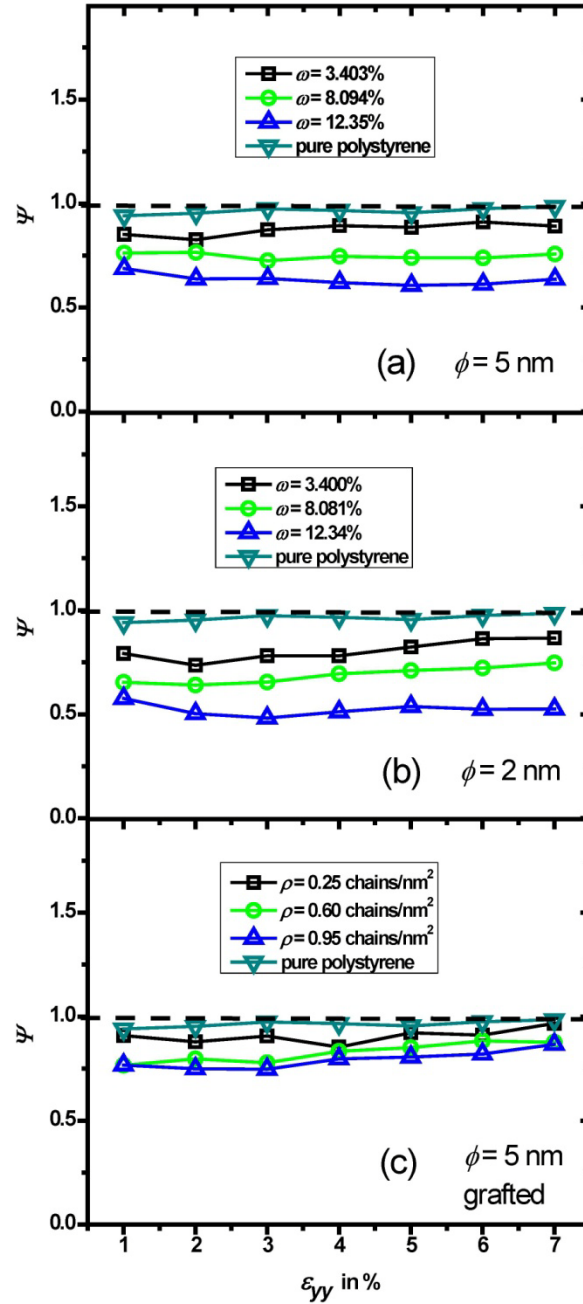


Fig. 4.10 Ratio of the orientation parameter deviation $\Psi = \frac{\langle P_2 \rangle_h - \langle P_2 \rangle_0}{\langle P_2 \rangle_g - \langle P_2 \rangle_0}$ of free polymer chains in the considered systems versus the strain ϵ_{yy} . $\langle P_2 \rangle_h$ and $\langle P_2 \rangle_g$ are derived by hybrid MD-FE simulations and the geometrical transformation method, respectively. (a) $\phi = 5$ nm, ungrafted; (b) $\phi = 2$ nm, ungrafted; (c) $\omega = 1.73\%$, $\phi = 5$ nm and grafted.

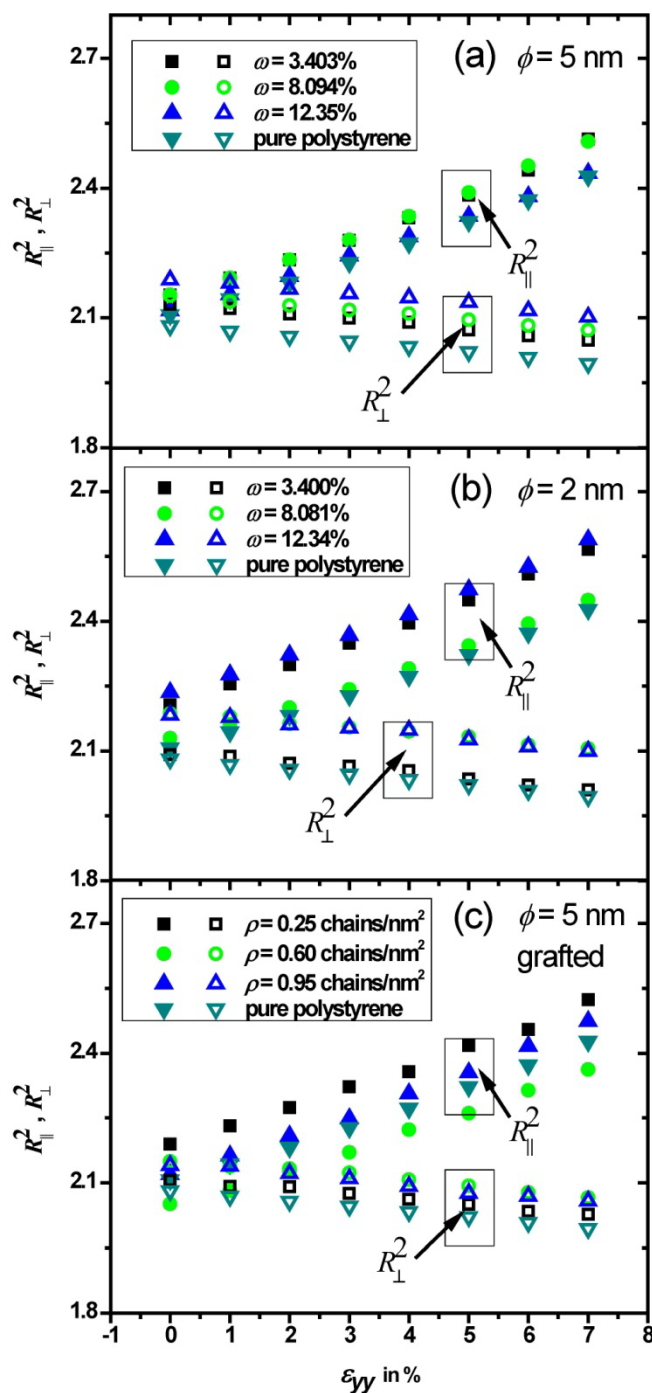


Fig. 4.11 Squared average of the projection of the end-to-end distance of free polymer chains in tensile direction (R_{\parallel}^2 , solid symbols) and the mean of the associated quantities in the perpendicular direction (R_{\perp}^2 , hollow symbols) versus the strain ϵ_{yy} . (a) $\phi = 5$ nm, ungrafted; (b) $\phi = 2$ nm, ungrafted; (c) $\omega = 1.73\%$, $\phi = 5$ nm and grafted.

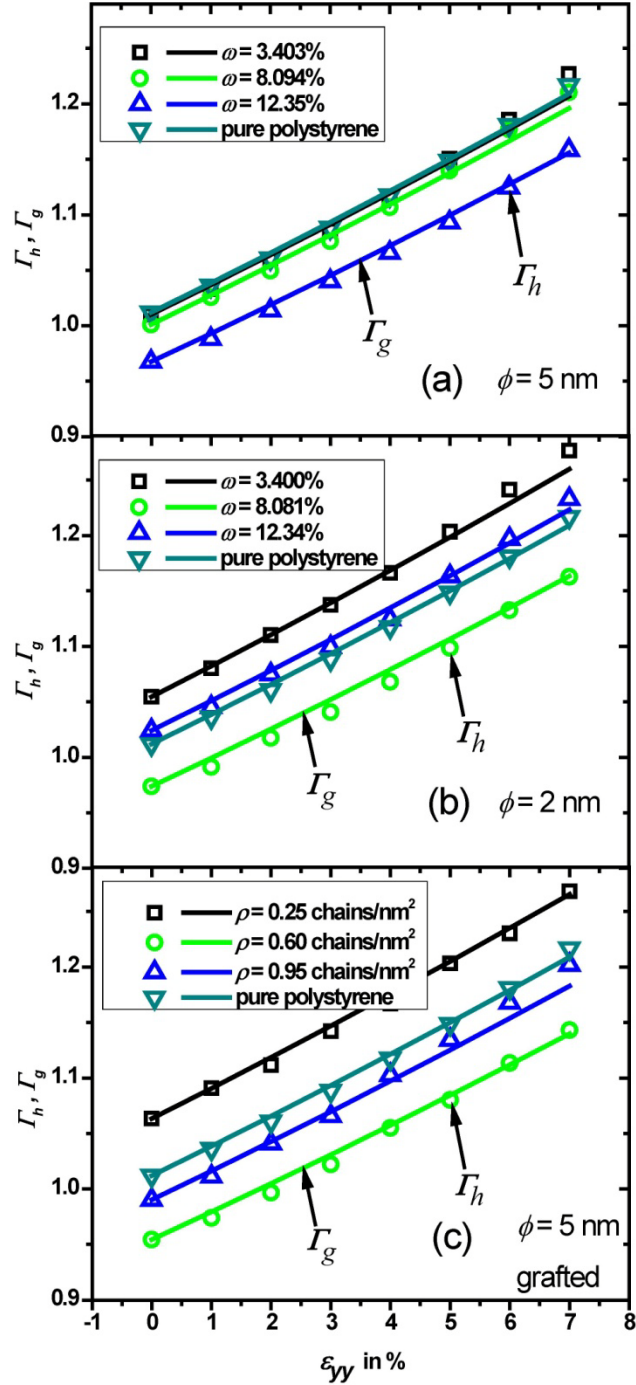


Fig. 4.12 Anisotropy parameter $\Gamma = \langle \frac{2R_{ey}^2}{R_{ex}^2 + R_{ez}^2} \rangle$ identified from the hybrid MD-FE simulations (Γ_h , hollow symbols) and from the geometrical transformation model (Γ_g , solid lines) as a function of the strain ε_{yy} during deformation. (a) $\phi = 5$ nm, ungrafted; (b) $\phi = 2$ nm, ungrafted; (c) $\omega = 1.73\%$, $\phi = 5$ nm and grafted.

An anisotropy parameter $\Gamma = \langle \frac{2R_{ey}^2}{R_{ex}^2 + R_{ez}^2} \rangle$ is employed to quantify the relation between the squared projection of the end-to-end distance in the tensile direction and the averaged squared projection in the perpendicular direction. The bracket $\langle \dots \rangle$ denotes that Γ is the average over all free polymer chains in the MD domain. It has to be mentioned that Γ captures the deformation-induced molecular anisotropy and provides deeper insight into the molecular configuration under a tensile loading. In an undeformed amorphous system $\Gamma = 1$ holds, whereas for uniaxial tension one expects increasing Γ with increasing strain. In Figure 4.12, a comparison is given between the anisotropy parameter obtained from the hybrid system Γ_h (hollow symbols) and from the geometrical transformation model Γ_g (solid lines). Both quantities behave as expected and render almost the same dependency on the applied strain. This indicates that the polymer chains mostly follow the macroscopic deformation. In contrast to the quantities discussed in Figure 4.10, the anisotropy parameter seems not to be as sensitive to the presence of nanoparticles. Due to the small system size and the limited statistical quality, the anisotropy parameters Γ_h and Γ_g are only approximately 1.0 when the strain is zero. This inherent molecular anisotropy persists at elongations and causes the ordinate offsets of the curves, see the discussion above.


4.5 Conclusions

In this contribution, both standard periodic molecular dynamics (MD) and hybrid molecular dynamics–finite element (MD-FE) methods have been applied to simulate the uniaxial deformation of polystyrene nanocomposites containing up to 136 silica nanoparticles. Mechanical properties (Young’s modulus and Poisson’s ratio) have been calculated by the standard MD simulations under periodic boundary conditions and then used as material parameters of the hybrid MD-FE simulations. It has been found that the Young’s moduli of polymer nanocomposites follow approximately a quadratic relation with the nanoparticle mass fraction. The hybrid simulations give similar results, with slightly lower overall moduli due to a technical feature of the method. Both pure MD and hybrid MD-FE simulations demonstrate that an increase of the nanoparticle mass fraction, a reduction of the particle size or a grafting polymer chains on nanoparticle surfaces enhances the yield strengths and Young’s moduli of

nanocomposites. This indicates that both the fraction of high-modulus fillers and their total interfacial area contribute to a general stiffening of polymer nanocomposites. Specifically, smaller nanoparticles have a more significant impact on the mechanical properties of nanocomposites than larger ones, when the nanoparticle mass fraction is constant.

The structural and dynamic properties of polymer chains in nanocomposites below and above the glass transition temperature have been calculated, too. The squared end-to-end distances of free polymer chains are larger in the vicinity of nanoparticles than in the polymer bulk due to the polymer-nanoparticle interaction. Larger nanoparticles have a stronger influence on the squared end-to-end distances of polymer chains in their neighborhood than smaller nanoparticles, as the interaction of larger nanoparticles with polymer chains is stronger when polymer chains are located at the same distance from nanoparticle surfaces. In addition, the mobility of polymer chains and nanoparticles in the melt are reduced with an increase of the nanoparticle mass fraction, a reduction of the nanoparticle size or an increase of the grafting density of polymer chains on the nanoparticle surface. As we have found that smaller nanoparticles slow down the dynamics of polymer chains more efficiently than larger nanoparticles at the same mass fraction, we regard the interphase area as the most influential parameter for global dynamics. From the profiles of the structural and dynamic properties of free polymer chains measured relative to the distance from the nanoparticle surface, we conclude that the interphase thickness is roughly 1 ~ 1.5 nm.

Furthermore, the changes of the molecular structure of free polymer chains with the strain have been investigated by hybrid MD-FE simulations. We have found that the alignment parameter of free polymer chains in nanocomposites increases almost linearly with the strain during the deformation. The addition of the nanoparticles hinders the alignment of polymer chains in the deformation process to some extent. Also here, smaller nanoparticles are more efficient than larger nanoparticles. The grafting state of nanoparticle surfaces has a much smaller effect at a low nanoparticle mass fraction. In addition, monitoring of individual components of the chain end-to-end vectors (parallel and perpendicular to the elongation direction) and the resulting anisotropy parameters exposed almost the same chain behavior upon elongation.



The deformations of individual polymer chains upon elongation have been analyzed in terms of a simple geometrical transformation model which assumes that all atoms in the material translate affinely with the deformation of the whole system. The analysis shows that most of the observed molecular changes in the linear deformation region can be explained simply by an affine translation, as is expected for a polymer glass. The addition of nanoparticles, however, restricts the polymer mobility, so that the polymer conformations deviate more from affine translations than in neat polystyrene.

As an outlook, the hybrid method can be used to perform additional loading-unloading tests. They allow us to analyze the changes in the polymer structure during deformation cycles. Additionally, the deformation mechanism of polymer nanocomposites at larger strains (i.e. chain slid, plastic flow and cavity formation) will be accessible by the hybrid method with some necessary extensions. Both research directions are in progress.

References

- [1] J. Jordan, K.I. Jacob, R. Tannenbaum, M.A. Sharaf, and I. Jasiuk, *Mater. Sci. Eng. A* 393, 1 (2005).
- [2] D.R. Paul and L.M. Robeson, *Polymer* 49, 3187 (2008).
- [3] M.M.M. Gudrun Schmidt, *Curr. Opin. Colloid Interface Sci.* 8, 103 (2003).
- [4] S. Sinha Ray and M. Okamoto, *Prog. Polym. Sci.* 28, 1539 (2003).
- [5] H. Zou, S. Wu, and J. Shen, *Chem. Rev.* 108, 3893 (2008).
- [6] X. Ji, J.E. Hampsey, Q. Hu, J. He, Z. Yang, and Y. Lu, *Chem. Mater.* 15, 3656 (2003).
- [7] E.T. Thostenson, Z. Ren, and T.-W. Chou, *Compos. Sci. Technol.* 61, 1899 (2001).
- [8] R. Andrews and M.C. Weisenberger, *Curr. Opin. Solid State Mater. Sci.* 8, 31 (2004).
- [9] J.N. Coleman, U. Khan, W.J. Blau, and Y.K. Gun'ko, *Carbon* 44, 1624 (2006).
- [10] F. Gao, *Mater. Today* 7, 50 (2004).
- [11] A. Okada and A. Usuki, *Macromol. Mater. Eng.* 291, 1449 (2006).
- [12] G. Choudalakis and A.D. Gotsis, *Eur. Polym. J.* 45, 967 (2009).
- [13] A. Okada and A. Usuki, *Mater. Sci. Eng. C* 3, 109 (1995).
- [14] M.A. Rafiee, J. Rafiee, Z. Wang, H. Song, Z.Z. Yu, and N. Koratkar, *ACS Nano* 3, 3884 (2009).
- [15] J.C. Huang, C. Bin He, Y. Xiao, K.Y. Mya, J. Dai, and Y.P. Siow, *Polymer* 44, 4491 (2003).
- [16] S.C. Tjong, *Mater. Sci. Eng. R Reports* 53, 73 (2006).
- [17] X.L. Xie, Y.W. Mai, and X.P. Zhou, *Mater. Sci. Eng. R Reports* 49, 89 (2005).
- [18] P.C. Ma, N.A. Siddiqui, G. Marom, and J.K. Kim, *Compos. Part A Appl. Sci. Manuf.* 41, 1345 (2010).
- [19] S. Mishra, S.H. Sonawane, and R.P. Singh, *J. Polym. Sci. Part B Polym. Phys.* 43, 107 (2005).
- [20] E. Reynaud, T. Jouen, C. Gauthier, G. Vigier, and J. Varlet, *Polymer* 42, 8759 (2001).
- [21] M.Z. Rong, M.Q. Zhang, Y.X. Zheng, H.M. Zeng, and K. Friedrich, *Polymer* 42, 3301 (2001).
- [22] M.Z. Rong, M.Q. Zhang, Y.X. Zheng, H.M. Zeng, R. Walter, and K. Friedrich, *Polymer* 42, 167 (2001).

- [23] D.N. Bikiaris, G.Z. Papageorgiou, E. Pavlidou, N. Vouroutzis, P. Palatzoglou, and G.P. Karayannidis, *J. Appl. Polym. Sci.* 100, 2684 (2006).
- [24] G.J. Papakonstantopoulos, M. Doxastakis, P.F. Nealey, J.L. Barrat, and J.J. De Pablo, *Phys. Rev. E - Stat. Nonlinear, Soft Matter Phys.* 75, 031803 (2007).
- [25] G.J. Papakonstantopoulos, K. Yoshimoto, M. Doxastakis, P.F. Nealey, and J.J. De Pablo, *Phys. Rev. E - Stat. Nonlinear, Soft Matter Phys.* 72, 031801 (2005).
- [26] G. Raos, M. Moreno, and S. Elli, *Macromolecules* 39, 6744 (2006).
- [27] G.N. Toepperwein and J.J. De Pablo, *Macromolecules* 44, 5498 (2011).
- [28] R.A. Riggleman, G. Toepperwein, G.J. Papakonstantopoulos, J.L. Barrat, and J.J. De Pablo, *J. Chem. Phys.* 130, (2009).
- [29] D. Gersappe, *Phys. Rev. Lett.* 89, 058301 (2002).
- [30] T.V.M. Nodoro, E. Voyiatzis, A. Ghanbari, D.N. Theodorou, M.C. Böhm, and F. Müller-Plathe, *Macromolecules* 44, 2316 (2011).
- [31] T.V.M. Nodoro, M.C. Böhm, and F. Müller-Plathe, *Macromolecules* 45, 171 (2012).
- [32] A. Ghanbari, M. Rahimi, and J. Dehghany, *J. Phys. Chem. C* 117, 25069–25076 (2013).
- [33] A. Ghanbari, T.V.M. Nodoro, M. Rahimi, M.C. Böhm, and F. Müller-Plathe, *Macromolecules* 45, 572 (2012).
- [34] M. Rahimi, I. Iriarte-Carretero, A. Ghanbari, M.C. Böhm, and F. Müller-Plathe, *Nanotechnology* 23, 305702 (2012).
- [35] C.L. Tucker and E. Liang, *Compos. Sci. Technol.* 59, 655 (1999).
- [36] R.E. Rudd and J.Q. Broughton, *Phys. Status Solidi* 217, 251 (2000).
- [37] T.D. Fornes and D.R. Paul, *Polymer* 44, 4993 (2003).
- [38] B. Mortazavi, J. Bardon, and S. Ahzi, *Comput. Mater. Sci.* 69, 100 (2013).
- [39] Q.H. Zeng, A.B. Yu, and G.Q. Lu, *Prog. Polym. Sci.* 33, 191 (2008).
- [40] D. Raabe, *Adv. Mater.* 14, 709 (2002).
- [41] W.A. Curtin and R.E. Miller, *Model. Simul. Mater. Sci. Eng.* 11, R33 (2003).
- [42] A. Nakano, M.E. Bachlechner, R.K. Kalia, E. Lidorikis, P. Vashishta, G.Z. Voyiadjis, T.J. Campbell, S. Ogata, and F. Shimajo, *Comput. Sci. Eng.* 3, 56 (2001).
- [43] L. Mishnaevsky and E. Levashov, *Comput. Mater. Sci.* 96, 365 (2015).
- [44] B.J. Yang, H. Shin, H.K. Lee, and H. Kim, *Appl. Phys. Lett.* 103, (2013).

- [45] J. Broughton, F. Abraham, N. Bernstein, and E. Kaxiras, *Phys. Rev. B* 60, 2391 (1999).
- [46] S.P. Xiao and T. Belytschko, *Comput. Methods Appl. Mech. Eng.* 193, 1645 (2004).
- [47] S. Zhang, R. Khare, Q. Lu, *Int. J. Numer. Methods Eng.* 70, 913 (2007).
- [48] R. Khare, S.L. Mielke, J.T. Paci, S. Zhang, R. Ballarini, G.C. Schatz, and T. Belytschko, *Phys. Rev. B* 75, 1 (2007).
- [49] D. Davydov, J.-P. Pelteret, and P. Steinmann, *Comput. Methods Appl. Mech. Eng.* 277, 260 (2014).
- [50] H. Ben Dhia and G. Rateau, *Int. J. Numer. Methods Eng.* 62, 1442 (2005).
- [51] H. Ben Dhia and O. Jamond, *Comput. Methods Appl. Mech. Eng.* 199, 1403 (2010).
- [52] P.T. Bauman, J.T. Oden, and S. Prudhomme, *Comput. Methods Appl. Mech. Eng.* 198, 799 (2009).
- [53] L. Chamoin, J.T. Oden, and S. Prudhomme, *Comput. Methods Appl. Mech. Eng.* 197, 3530 (2008).
- [54] M. Rahimi, H.A. Karimi-Varzaneh, M.C. Böhm, F. Müller-Plathe, S. Pfaller, G. Possart, and P. Steinmann, *J. Chem. Phys.* 134, 154108 (2011).
- [55] S. Pfaller, M. Rahimi, G. Possart, P. Steinmann, F. Müller-Plathe, and M.C. Böhm, *Comput. Methods Appl. Mech. Eng.* 260, 109 (2013).
- [56] S. Liu, A. Gerisch, M. Rahimi, J. Lang, M.C. Böhm, and F. Müller-Plathe, *J. Chem. Phys.* 142, 104105 (2015).
- [57] D. Reith, M. Pütz, and F. Müller-Plathe, *J. Comput. Chem.* 24, 1624 (2003).
- [58] S. Liu, M.C. Böhm, and F. Müller-Plathe, *Mater. Res. Express* 3, 105301 (2016).
- [59] S. Pfaller, G. Possart, P. Steinmann, M. Rahimi, F. Müller-Plathe, and M.C. Böhm, *Comput. Mech.* 49, 565 (2012).
- [60] R. Delgado-Buscalioni, K. Kremer, and M. Praprotnik, *J. Chem. Phys.* 131, 244107 (2009).
- [61] A. V. Lyulin, N.K. Balabaev, M.A. Mazo, and M.A.J. Michels, *Macromolecules* 37, 8785 (2004).
- [62] Z.K. Zhu, Y. Yang, J. Yin, and Z.N. Qi, *J. Appl. Polym. Sci.* 73, 2977 (1999).
- [63] S.Y. Fu, X.Q. Feng, B. Lauke, and Y.W. Mai, *Compos. Part B Eng.* 39, 933 (2008).
- [64] X.L. Ji, J.K. Jing, W. Jiang, and B.Z. Jiang, *Polym. Eng. Sci.* 42, 983 (2002).
- [65] B.J. Ash, D.F. Rogers, C.J. Wiegand, L.S. Schadler, R.W. Siegel, B.C.

- Benicewicz, and T. Apple, *Polym. Compos.* 23, 1014 (2002).
- [66] R. Tannenbaum, M. Zubris, K. David, D. Ciprari, K. Jacob, I. Jasiuk, and N. Dan, *J. Phys. Chem. B* 110, 2227 (2006).
- [67] D. Ciprari, K. Jacob, and R. Tannenbaum, *Macromolecules* 39, 6565 (2006).
- [68] G.M. Odegard, T.C. Clancy, and T.S. Gates, *Polymer* 46, 553 (2005).
- [69] D.W. Ward, I.M.; Hadley, *Macromolecules* 35, 9595 (2002).
- [70] D. Barbier, D. Brown, A.C. Grillet, and S. Neyertz, *Macromolecules* 37, 4695 (2004).
- [71] F.M. Capaldi, G.C. Rutledge, and M.C. Boyce, *Macromolecules* 38, 6700 (2005).
- [72] G.D. Smith, D. Bedrov, L. Li, and O. Byutner, *J. Chem. Phys.* 117, 9478 (2002).
- [73] T. Desai, P. Keblinski, and S.K. Kumar, *J. Chem. Phys.* 122, (2005).
- [74] M. Goswami and B.G. Sumpter, 2008 8th IEEE Conf. Nanotechnology, IEEE-NANO 748 (2008).
- [75] J. Liu, Y. Gao, D. Cao, L. Zhang, and Z. Guo, *Langmuir* 27, 7926 (2011).
- [76] Y. Gao, J. Liu, J. Shen, L. Zhang, Z. Guo, and D. Cao, *Phys. Chem. Chem. Phys.* 16, 16039 (2014).
- [77] J. Cho, M.S. Joshi, and C.T. Sun, *Compos. Sci. Technol.* 66, 1941 (2006).
- [78] B. Fragneaud, K. Masenelli-Varlot, A. Gonzalez-Montiel, M. Terrones, and J.Y. Cavallé, *Compos. Sci. Technol.* 68, 3265 (2008).
- [79] C. Guo, L. Zhou, and J. Lv, *Polym. Polym. Compos.* 21, 449 (2013).
- [80] J. Gao, M.E. Itkis, A. Yu, E. Bekyarova, B. Zhao, and R.C. Haddon, *J. Am. Chem. Soc.* 127, 3847 (2005).

Supporting Information

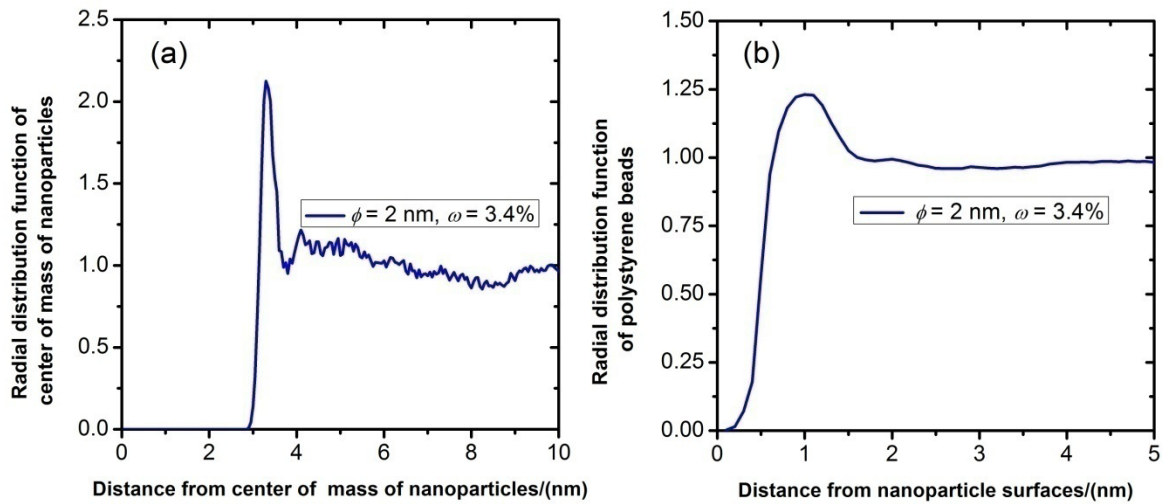


Fig.4.S1 (a) Radial distribution function of the mass center of nanoparticles in the nanocomposite system. (b) Radial distribution function of polystyrene beads (i.e. number density of polymer monomers) around the nanoparticles versus the distance from the nanoparticle surface. $\phi = 2$ nm, $\omega = 3.4\%$.

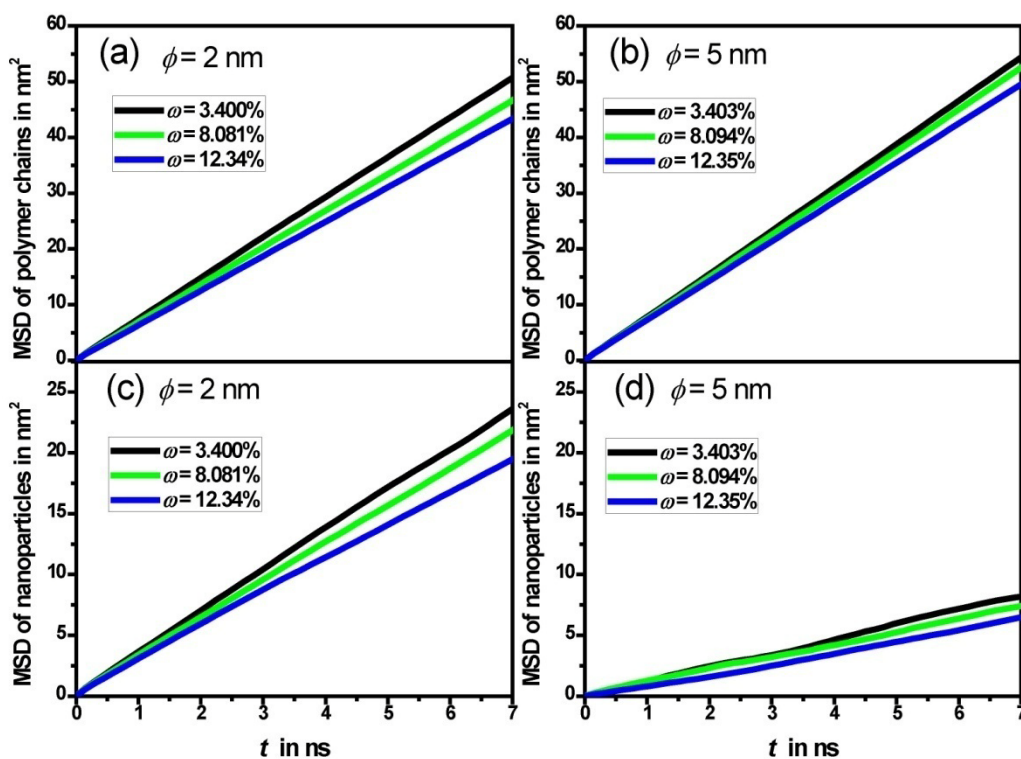


Fig. 4.S2 Center-of-mass mean square displacements (MSDs) of polymer chains and nanoparticles versus the simulation time t in ungrafted nanocomposite systems ($\phi = 5$ or 2 nm). The simulation temperature is 590 K.

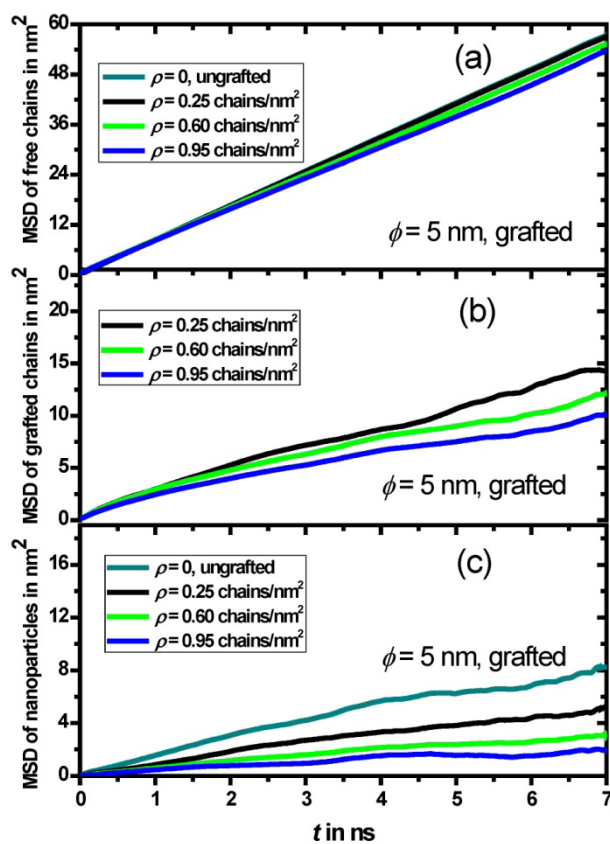


Fig. 4.S3 Center-of-mass mean square displacements (MSDs) of polymer chains and nanoparticles versus the simulation time t in grafted nanocomposite systems ($\phi = 5$ nm). The simulation temperature is 590 K. The mass fraction of the nanoparticles ω amounts to 1.73%.

5. Concluding Remarks and Outlook

Polymer nanocomposites are typical heterogeneous materials that contain a polymer matrix and a certain fraction of nanoparticles¹⁻³. Due to a high surface-to-volume ratio of nanoparticles, a large interphase area between the polymer and the nanoparticles is formed. Mechanical enhancement of polymer nanocomposites relative to the neat polymer is fundamentally attributed to the presence of the interphase⁴. Understanding structural details of the interphase and their correlation with the mechanical properties of polymer nanocomposites at a molecular scale is helpful to design improved materials in a bottom-to-up way. Polymer nanocomposites have been investigated extensively in the past decades. Nevertheless, there are still several questions that cannot be addressed properly by experimental methods⁵. Some unsolved problems are as follows: (i) what are the microscopic details of the interfacial structure of polymer nanocomposites and why does the interfacial structure largely influence the mechanical properties of polymer nanocomposites? (ii) how is the global and interfacial chain behavior of polymer nanocomposites influenced by nanoparticle characteristics (mass fraction, size, geometry and grafting state)? (iii) how is the structure of polymer chains in nanocomposites changed under an external load, and to what extent are the structural properties of the polymer chains influenced by the presence of nanoparticles during a deformation process? To answer these questions, different simulation techniques⁶ such as standard MD and hybrid MD-FE methods have been used to investigate the interphase structure and mechanical behavior of polystyrene nanocomposites containing a certain amount of silica nanoparticles.

The simulation space of the hybrid MD-FE method contains a particle-based region in which molecular details are analyzed and a continuum-based region where external load steps are applied to deform the material. To exchange the information between the MD and FE region, a large number of anchor points (e.g. several thousand) are introduced into the DPD shell which is located between the MD and FE region. Anchor-point-related key parameters include the force constant between the anchor points and the polymer beads, the number of anchor points and the thickness of the DPD shell. The influence of variations of these input parameters on the polymer properties is still not known explicitly. Nevertheless, reasonable values of these input parameters have to be chosen for physically realistic runs of the hybrid MD-FE deformation simulations. An

uncertainty quantification (UQ) method⁷ has been used to analyze systematically the influence of different parameter combinations on the quantities of interest (QoI) of a model polystyrene. The studied polymer properties include the mass density, chain dimension, radial distribution function and diffusion coefficient. Simulation results have shown that the variations of the polymer properties as a function of the input parameters are small when the thickness of the DPD shell and the MD region are chosen large enough. This indicates that the hybrid method is robust provided that the input parameters are chosen within a reasonable range.

Following extensive related investigations of our former colleagues (i.e. Tinashe V.M. Ndoro^{8,9}, Azadeh Ghanbari^{10,11} and Evangelos Voyiatzis¹²), the influence of the interphase area of nanocomposites on global and local properties of polymer chains has been further investigated quantitatively. It has been found that structural and dynamic properties of polymer chains in the interphase differ from the ones in the bulk. Nanoparticle characteristics such as the size, mass fraction, grafting state and geometrical shape influence the global and local properties of polymer chains in nanocomposites¹³. Compared with polymer chains in neat polystyrene, the global dimension (averaged over all chains) of polymer chains in nanocomposites is reduced with an increase of the nanoparticle mass fraction when the nanoparticle size is comparable to the gyration radii of the polymer chains in a coiled configuration. However, the local dimension of polymer chains in the interphase increases with a decrease of their distance from the nanoparticle center of mass due to polymer-nanoparticle interactions. Specifically, the polymer chains in the vicinity of large nanoparticles experience a stronger expansion in their local dimensions than in the vicinity of small nanoparticles. In addition, the polymer chains in the interphase are perpendicularly orientated to the radial directions of the nanoparticles, whereas the polymer chains far from the nanoparticles are randomly orientated. The molecular anisotropy of the polymer chains in the interphase becomes stronger when they are closer to the nanoparticles. The layering arrangement of polymer chains in the vicinity of nanoparticles confines to some extent the chain orientation during a deformation process.

Furthermore, both the global and local dynamic behavior of polymer chains such as molecular diffusion and chain relaxation are suppressed by the presence of either grafted or ungrafted nanoparticles due to interfacial adsorption effects. The global center of mass diffusion coefficient

of polymer chains is reduced almost linearly with an increase of the total surface area of the nanoparticles, whereas the relaxation time of the chain end-to-end vector exhibits the opposite tendency. The local dynamics of polymer chains in the interphase is suppressed stronger than the global dynamics. Specifically, the relaxation time of the chain end-to-end vector in the interphase increases monotonically with an increase of the surface area of an individual nanoparticle. The suppression of the chain dynamics by tetrahedral nanoparticles is stronger than in the case of cubic nanoparticles, followed by spherical nanoparticles (constant nanoparticle mass fraction assumed). According to the profiles of the structural and dynamic properties of polymer chains as a function of the distance from the nanoparticle center of mass¹⁴, the interphase thickness is in general equal to about one radius of gyration (1~1.5 nm) of the polymer in coil.


Mechanical properties such as Young's modulus and Poisson's ratio are derived by standard MD simulations. The observed results have demonstrated that both the Young's moduli and yield stresses of polymer nanocomposites increase with (i) an increase of the nanoparticle mass fraction or (ii) with an increase of the grafting density on the nanoparticle surfaces, as well as (iii) with a decrease of the nanoparticle size at a constant mass fraction. The Poisson's ratio of polystyrene nanocomposites is more or less unaffected by the addition of nanoparticles. They have the same Poisson's ratio (~0.3) as the neat polystyrene. In addition, the Young's moduli of polymer nanocomposites are more or less quadratically correlated with the nanoparticle mass fraction. This has been also indicated by hybrid simulations of deformations. The obtained Young's moduli and Poisson's ratios are then used as material parameters in the hybrid deformation simulations. It can be concluded that the mechanical enhancement of nanocomposites is mainly contributed to the total surface area of the nanoparticles.

The convergence behavior of the mean normal stress is examined prior to productive hybrid simulations. The mean normal stress derived from the hybrid simulation is increased linearly with the applied strain. As in agreement with standard MD simulations, the mean normal stresses of polymer nanocomposites for identical strain levels are also increased with an increase of the nanoparticle mass fraction, with a reduction of the nanoparticle size at the same mass fraction or when grafting the polymer chains on nanoparticle surfaces. In the hybrid simulations, the

orientation parameter of polymer chains is enlarged almost linearly with the applied strain. In contrast to neat polystyrene, the presence of nanoparticles hinders the rotation of polymer conformations along the deformation direction. The hindrance effect of smaller nanoparticles is stronger than the one of larger nanoparticles. In addition, the global dimension of free polymer chains swells in the deformation direction, while it shrinks in the perpendicular direction. The molecular anisotropy of free polymer chains becomes increasingly larger upon the elongation. Changes of polymer structural properties under an external load are also analyzed by a simple geometrical transformation model. All atoms of the studied materials in the model are assumed to move affinely as the deformation of the whole system. The quantitative analyses have indicated that the changes of chain structures can be described predominantly by a simple affine translation, as expected for a polymer glass.

As summarized above, correlations between macroscopic mechanical properties of polymer nanocomposites and their microscopic interfacial structures have been investigated systematically by standard MD and hybrid MD-FE simulations. The present work has demonstrated that the MD-FE hybrid framework is a promising method for deformation simulations of different polymer materials. It can be used for future investigations of the mechanical deformations of other crystalline or semicrystalline polymer materials¹⁵. However, many challenging problems in the deformation behavior of polymer nanocomposites still have to be solved. For instance, up to now it is at a molecular level not clearly known, how the presence of nanoparticles influence the changes in the structure and dynamics of polymer chains during a plastic deformation. It has been shown that the addition of nanoparticles often leads to a higher modulus, but to a shorter elongation at break. This phenomenon cannot be explained simply by experimental methods. To address these problems, further efforts in the direction of multiscale simulations are needed.

Additionally, the post-yield deformation behavior of polymer nanocomposites is more complicated than the elastic deformation at small strains. Beyond the yield point, the deformation-induced stress is not increased linearly with the applied strain. Subsequently, for larger strains, the stress stays at a plateau where the slip motion and plastic flow of the polymer chains are awakened. The stress-hardening in association with bond stretching ultimately takes



place beyond a long stress plateau. The crazes and cavities extend gradually to a macro size. The fractures of polymer nanocomposites are often observed in this final phase^{16,17}. The molecular mechanism of the craze formation and material fracture has still not been explained by systematic investigations at a microscopic level^{18,19}. Furthermore, other scientific topics²⁰⁻²⁴ such as loading-unloading tests, the rate dependence of the stress-strain behavior and energetic conversion of the mechanical work during the deformation process also can be investigated by the hybrid MD-FE method.

Reference

- [1] M. Martin-Gallego, M.M. Bernal, M. Hernandez, R. Verdejo, and M.A. Lopez-Manchado, *Eur. Polym. J.* 49, 1347 (2013).
- [2] D. Ciprai, K. Jacob, and R. Tannenbaum, *Macromolecules* 39, 6565 (2006).
- [3] G. Mittal, V. Dhand, K.Y. Rhee, S.-J. Park, and W.R. Lee, *J. Ind. Eng. Chem.* 21, 11 (2015).
- [4] T. Kuilla, S. Bhadra, D. Yao, N.H. Kim, S. Bose, and J.H. Lee, *Prog. Polym. Sci.* 35, 1350 (2010).
- [5] M. Liu, Z. Jia, D. Jia, and C. Zhou, *Prog. Polym. Sci.* 39, 1498 (2014).
- [6] B. Mortazavi, O. Benzerara, H. Meyer, J. Bardon, and S. Ahzi, *Carbon* 60, 356 (2013).
- [7] N. Vu-Bac, R. Rafiee, X. Zhuang, T. Lahmer, and T. Rabczuk, *Compos. Part B Eng.* 68, 446 (2015).
- [8] T.V.M. Nodoro, M.C. Böhm, and F. Müller-Plathe, *Macromolecules* 45, 171 (2012).
- [9] T.V.M. Nodoro, E. Voyiatzis, A. Ghanbari, D.N. Theodorou, M.C. Böhm, and F. Müller-Plathe, *Macromolecules* 44, 2316 (2011).
- [10] A. Ghanbari, T.V.M. Nodoro, M. Rahimi, M.C. Böhm, and F. Müller-Plathe, *Macromolecules* 45, 572 (2012).
- [11] A. Ghanbari, M. Rahimi, and J. Dehghany, *J. Phys. Chem. C* 117, 25069 (2013).
- [12] E. Voyiatzis, M. Rahimi, F. Müller-Plathe, and M.C. Böhm, *Macromolecules* 47, 7878 (2014).
- [13] N. Jouault, J.F. Moll, D. Meng, K. Windsor, S. Ramcharan, C. Kearney, and S.K. Kumar, *ACS Macro Lett.* 2, 371 (2013).
- [14] A.P. Holt, P.J. Griffin, V. Bocharova, A.L. Agapov, A.E. Imel, M.D. Dadmun, J.R. Sangoro, and A.P. Sokolov, *Macromolecules* 47, 1837 (2014).
- [15] A. Sedighiamiri, D.J.A. Senden, D. Tranchida, L.E. Govaert, and J.A.W. Van Dommelen, *Comput. Mater. Sci.* 82, 415 (2014).
- [16] A. Pawlak, A. Galeski, and A. Rozanski, *Prog. Polym. Sci.* 39, 921 (2014).
- [17] M. Nie, D.M. Kalyon, and F.T. Fisher, *ACS Appl. Mater. Interfaces* 6, 14886 (2014).
- [18] S. Chandrasekaran, N. Sato, F. Tölle, R. Mülhaupt, B. Fiedler, and K. Schulte, *Compos. Sci. Technol.* 97, 90 (2014).
- [19] M.A.N. Dewapriya, R.K.N.D. Rajapakse, and N. Nigam, *Carbon* 93, 830 (2015).

[20] T. Sain, J. Meaud, B. Yeom, A.M. Waas, and E.M. Arruda, *Int. J. Solids Struct.* 54, 147 (2015).

[21] S. Yang, S. Yu, J. Ryu, J.M. Cho, W. Kyoung, D.S. Han, and M. Cho, *Int. J. Plast.* 41, 124 (2013).

[22] C. Li, E. Jaramillo, and A. Strachan, *Polymer* 54, 881 (2013).

[23] E. Senses and P. Akcora, *Macromolecules* 46, 1868 (2013).

[24] R.J. Young, I.A. Kinloch, L. Gong, and K.S. Novoselov, *Compos. Sci. Technol.* 72, 1459 (2012).

Simulation Tools and Supercomputing Resources

The IBIsCO package used in the present work is originally developed by Dr. Hossein Ali Karimi Varzaneh¹ and is then extended by Dr. Mohammad Rahimi² with an application of stochastic boundary conditions. The finite element code is developed by Dr. Sebastian Pfaller³ in the Chair of Applied Mechanics at Erlangen University. The mathematic tool for uncertainty quantification analysis⁴ is provided by the group of Prof. Jens Lang in the Department of Mathematics at Technical University Darmstadt. Additional open-sourced tools (i.e. Visual Molecular Dynamics (VMD)⁵ and LAMMPS^{6,7}) are used in the present work, too. Hereby I would like to thank all contributors of these aforementioned tools. Most of simulations in the present work have been accomplished by the supercomputing clusters of the group of Prof. Florian Müller-Plathe. A minority of them have been performed at Hochschul-rechenzentrum der Technischen Universität Darmstadt⁸ and at the Jülich Supercomputing Center⁹.

References

- [1] H.A. Karimi-Varzaneh, H.J. Qian, X.Y. Chen, P. Carbone and F. Müller-Plathe. *J. Comput. Chem.*, 32, 1475 (2011).
- [2] M. Rahimi, H.A. Karimi-Varzaneh, M.C. Böhm, F. Müller-Plathe, S. Pfaller, G. Possart and P. Steinmann. (2011). *J. Chem. Phys.*, 134, 154108 (2011).
- [3] S. Pfaller, M. Rahimi, G. Possart, P. Steinmann, F. Müller-Plathe, and M.C. Böhm, *Comput. Methods Appl. Mech. Eng.*, 260, 109 (2013).
- [4] B. Schieche. Unsteady adaptive stochastic collocation methods in Uncertainty Quantification. PhD thesis, TU Darmstadt, 2012.
- [5] W. Humphrey, A. Dalke, and K. Schulten. *J. Mol. Graph.*, 14, 33 (1996).
- [6] <http://lammps.sandia.gov>
- [7] S. Plimpton, *J. Comp. Phys.*, 117, 1 (1995).
- [8] <http://www.hrz.tu-darmstadt.de/home/index.de.jsp>
- [9] http://www.fz-juelich.de/ias/jsc/DE/Home/home_node.htm

Publications

- [1] S.Y. Liu, S. Pfaller, M. Rahimi, G. Possart, P. Steinmann, M.C. Böhm, F. Müller-Plathe, *Comput. Mater. Sci.*, 129 (2017) 1.
- [2] S.Y. Liu, M.C. Böhm, F. Müller-Plathe, *Mater. Res. Express*, 3 (2016) 105301.
- [3] S.Y. Liu, A. Gerisch, M. Rahimi, J. Lang, M.C. Böhm, F. Müller-Plathe, *J. Chem. Phys.*, 142 (2015) 104105.
- [4] F. Leroy, S.Y. Liu, J.G. Zhang, *J Phys. Chem. Part C*, 119 (2015) 28470.
- [5] D. Davydov, E. Voyiatzis, G. Chatzigeorgiou, S.Y. Liu, P. Steinmann, M.C. Böhm, F. Müller-Plathe, *Soft Materials*, 12.sup1 (2014) S142-S151.
- [6] S.Y. Liu, Z.Y. Jiang, X.H. He, *J. Memb. Sci.*, 442 (2013) 97.
- [7] G. X. Hou, S. Y. Liu, X. M. Sang, *Adv. Mater. Res.*, Vols 163-167 (2010) 1991.

Financial Support

I am grateful to the Deutsche Forschungsgemeinschaft (DFG) that has supported financially the present Ph.D. project within the Priority Program 1369 *Polymer-Solid Contacts: Interfaces and Interphases*.



Acknowledgments

Doing a Ph.D. is a tough thing. Doing a Ph.D. abroad with a very difficult project is even tougher. To be honest, I did not realize this point when I newly came to Germany. After going through all the past thousand days, I finally understood all the stories in Dr. Phillip Gao's book "The Ph.D. grind". A Ph.D. training is just like a life journey full of ups and downs. I like the simple word "GRIND", as it summarizes properly all the sufferings and happiness I have experienced in this long journey. When looking back, I am happy with what I have done in this period. Although I have ever felt helpless and hopeless for numerous times, I am still very lucky to receive kind favors from the people around me. By taking this chance, I would sincerely express my heartfelt gratitude to all of them.

My first biggest gratitude goes to my supervisor Prof. Florian Müller-Plathe. He not only offered me an opportunity to pursue a Ph.D. in his group but also guided me directly or imperceptibly to reach a good Ph.D.. During three years, I have learnt a lot from his passion on science, his optimism in life and his generosity to people. There is a very famous Chinese proverb that says: a teacher in one day is like a father all the life. I will remember his advices on my professional and personal life and will bring them together to face new challenges in my future career.

I am sincerely grateful to my co-supervisor Prof. Michael C. Böhm who gave me many useful instructions about my research work. I appreciate his time to consider my projects, to check my results and to revise my manuscripts. Additionally, He was always patient to listen to my doubts, to answer my questions and to teach me in details how to make things better. His strong encouragements played an irreplaceable role in my recoveries from several tough periods in my Ph.D. time. I will keep his kindness in my heart for the whole life.

My next acknowledgement is addressed to my project collaborators Dr. Mohammed Rahimi, Dr. Sebastian Pfaller, Dr. Alf Gerisch, Dr. Gunnar Possart, Prof. Paul Steinmann and Prof. Jens Lang for their supports on my projects. I would like to offer my special thanks to Dr. Mohammed

Rahimi and Dr. Sebastian Pfaller for fruitful discussions and suggestions. Additionally, I am thankful to our former group member Dr. Azadeh Ghanbari for her kind help.

My sincere thanks then come to our secretary Ms. Dana Voss who helped me a lot to deal with the administrative things throughout the whole period of my study in Darmstadt. Without her help, I could not get used to the life in Germany so smoothly. In addition, her continuous efforts to maintain a very comfortable atmosphere in our group are highly appreciated.

I would also thank other colleagues in our group. They are: Andreas Kalogirou, Dr. Donatas Surblys, Dr. Evangelos Voyiatzis, Prof. Frédéric Leroy, Prof. Hong Liu, Gustavo Garcia Rondina, Dr.-Ing. Hans-Jürgen Bär, Dr. Haoxue Han, Prof. Hossein Eslami, Dr. Jianguo Zhang, Jurek Schneider, Kenkoh Endoh, Dr. Michael Langeloth, Dr. Mahshid Rahimi, Dr. Sarah Katherine Fegan, Vikram Reddy Ardham, Dr. Yongbiao Yang and Yangyang Gao. Specifically, kind help of Jurek Schneider in correcting the German abstract of my thesis is highly appreciated. It is my pleasure to work with these nice people in the same group. Some of them have already left Darmstadt and have opened their new stage of life in other places. I wish they all live happily and smoothly wherever they are or whatever they do.

Last but most importantly, family is always a pillar of my inner soul. I dedicate my deepest thankfulness to my mother, father, sister and brother-in-law as well as my little cute niece for their loves. Their supports and encouragements are the most important source of my strengths and confidences to overcome most of difficulties. I felt warm and relaxed in each time after I talked with them. Especially, the shiniest smiles of my niece made me believe firmly that my efforts are worth it. All glories in my life are established not only by me but also by them.



Curriculum Vita

Name: Shengyuan
Last Name: Liu
Place of Birth: Hengyang (P.R. China)
Date of Birth: 20th November, 1987 (Chinese Lunar Calendar)
Nationality: Chinese

Education

2006-2010 Hebei Polytechnic University (P.R. China), (B.Sc. of Materials Chemistry)
2010-2013 Tianjin University (P.R. China), (M.Eng. of Materials Chemical Engineering)
2013-2016 Ph.D. student in the Department of Chemistry, Technical University Darmstadt

(Shengyuan Liu)



Shengyuan Liu
Teichhausstraße 53
64287 Darmstadt
Germany

Darmstadt, 15 of December, 2016

Erklärung

Ich erkläre hiermit, noch keinen Promotionsversuch unternommen zu haben.

(Shengyuan Liu)



Shengyuan Liu
Teichhausstraße 53
64287 Darmstadt
Germany

Darmstadt, 15 of December, 2016

Eidesstattliche Erklärung

Ich erkläre hiermit, dass ich meine Dissertation selbstständig und nur mit den angegebenen Hilfsmitteln angefertigt habe.

(Shengyuan Liu)